ANALYTICAL INVESTIGATION OF INTERNALLY RESONANT SECOND HARMONIC LAMB WAVES IN NONLINEAR ELASTIC ISOTROPIC PLATES

A Thesis
Presented to
The Academic Faculty

by

Martin F. Mueller

In Partial Fulfillment
of the Requirements for the Degree
Master of Science in the
School of Civil and Environmental Engineering

Georgia Institute of Technology
December 2009

ANALYTICAL INVESTIGATION OF INTERNALLY RESONANT SECOND HARMONIC LAMB WAVES IN NONLINEAR ELASTIC ISOTROPIC PLATES

Approved by:

Dr. Laurence J. Jacobs, Advisor
School of Civil and Environmental Engineering
Georgia Institute of Technology

Dr. Jin-Yeon Kim
School of Civil and Environmental Engineering
Georgia Institute of Technology

Dr. Jianmin Qu
George W. Woodruff School of Mechanical Engineering
Georgia Institute of Technology

Date Approved: August 14, 2009

ACKNOWLEDGEMENTS

First, I would like to thank my tutor and commitee member Dr. Jin-Yeon Kim, whose meetings I experienced as exceedingly fruitful for my scientific education. This work would not have been possible without his consolidated knowledge and professional guidance. My special thanks go to my advisor, Dr. Laurence Jacobs, for all his support and effort to make not only this thesis but also my stay at the Georgia Institute of Technology happen. Thanks also to the committee member Dr. Jianmin Qu for reviewing this work.

For the daily and pleasant life together in "Larry's lab", I would like to thank all my lab mates. Also, thanks to Mike and the IT-helpdesk of Mason building for quick support with numerous requests.

At the University of Stuttgart, Germany, I would like to express my gratitude to Prof. Lothar Gaul and Dipl.-Ing. Helge Sprenger from the Institute of Applied and Experimental Mechanics for their efforts to offer the exchange program I benefit from. In this context, thanks to the German Academic Exchange Service (DAAD) for supporting the transatlantic partnership. Also, Katja Striegel from the Office of International Affairs of the University of Stuttgart deserves special thanks for her commitment.

Finally, I am deeply grateful for my dear family Ingrid, Eberhard and Simone, who have never ceased to show their love to me. And many thanks to all my friends both in Atlanta and in Germany for countless conversations and experiences that led to where we are today.

SUMMARY

This research deals with the second harmonic generation of Lamb waves in nonlinear elastic, homogeneous, isotropic plates. These waves find current applications in the field of ultrasonic, nondestructive testing and evaluation of materials. The second harmonic Lamb wave generation is investigated analytically in order to provide information on suitable excitation modes maximizing the second harmonic amplitude.

Using an existing solution for the problem of second harmonic generation in wave guides, the solution is explained for the plate and examined as to the symmetry properties of the second harmonic wave, since published results are contradictory. It is shown that the cross-modal generation of a symmetric secondary mode by an antisymmetric primary mode is possible.

Modes showing internal resonance, whose conditions are nonzero power flux from the primary wave and phase velocity matching, are shown to be most useful for measurements. In addition, group velocity matching is required. A material-independent analysis of the linear Lamb mode theory provides mode types satisfying all three requirements.

Using the example of an aluminum plate, the found internally resonant modes are evaluated with regard to the rate of second harmonic generation and practical issues such as excitability and ease of measurement. Pros and cons of each mode type are presented.

TABLE OF CONTENTS

LIST OF TABLES

LIST OF FIGURES

LIST OF SYMBOLS

a_i	generalized coordinates in the reference configuration
$A_n(z)$	amplitude coefficient of the nth secondary mode
c_{ph}	phase velocity
c_{g}	group velocity
c_{L}	longitudinal wave speed
c_{R}	Rayleigh surface wave speed
c_{T}	shear wave speed
d	plate thickness
$\boldsymbol{E}$	Lagrangian strain tensor
f	frequency
f_n^{vol}	power flux from the primary to the nth secondary mode via volume
f_n^{surf}	power flux from the primary to the nth secondary mode via surface
$\bar{\boldsymbol{f}}^{2\omega}$	complex second harmonic body force due to nonlinearities
$\boldsymbol{F}$	deformation gradient tensor
h	half plate thickness
$\boldsymbol{I}$	second-order identity tensor
i	imaginary unit
L_n	dispersion length of the nth secondary mode
$\boldsymbol{n}_y$	unit normal vector in y-direction
$\boldsymbol{n}_z$	unit normal vector in z-direction
r_s	rate of second harmonic generation
$\boldsymbol{S}$	second Piola-Kirchhoff stress tensor
$\bar{\boldsymbol{S}}^{2\omega}$	complex second harmonic stress due to nonlinearities
t	time
$\boldsymbol{u}$	particle displacement vector

$\tilde{\boldsymbol{u}}$	particle displacement mode vector
$\boldsymbol{u}^{(1)}$	particle displacement vector of the primary wave
$\boldsymbol{u}^{(2)}$	particle displacement vector of the secondary wave
$\boldsymbol{v}$	particle velocity vector
$\tilde{\boldsymbol{v}}$	particle velocity mode vector
$\boldsymbol{v}^{(1)}$	particle velocity vector of the primary wave
$\boldsymbol{v}^{(2)}$	particle velocity vector of the secondary wave
x, y, z	Cartesian coordinates in the reference configuration
α, β	wave number quantities from linear Lamb wave theory
$\boldsymbol{\varepsilon}$	linear strain tensor
κ	wave number
κ_n	wave number of the nth secondary mode
κ_d	wave number difference from exact phase matching
λ	Lamé's first parameter
μ	shear modulus
$\phi, \boldsymbol{\psi}$	Helmholtz potentials
ρ_0	mass density in reference configuration
$\boldsymbol{\sigma}$	linear Cauchy stress tensor
$\tilde{\boldsymbol{\sigma}}$	linear Cauchy stress mode tensor
ω	angular frequency
$\mathcal{A}, \mathcal{B}, \mathcal{C}$	third-order elastic constants of Landau and Lifshitz
$\mathcal{A}(y)$	generic antisymmetric function in y
$\mathcal{P}_{nn}$	power flux of the nth secondary mode
$\mathcal{S}(y)$	generic symmetric function in y

CHAPTER I

INTRODUCTION

Since its early stages in the late 19th century, the field of nondestructive evaluation (NDE) of materials has undergone a long process of development and innovation. To these days, most methods focus on detection of flaws and defects, which then need to be evaluated as to the probability of a fatal failure of the structure. Bray et al. [4] provide an extensive background on this topic. While these methods come into action when the risk of material failure might be fairly high already – since the detection of cracks requires their existence – recent approaches attempt to monitor the material's properties and draw conclusions on the material's state of fatigue, even before visible cracks arise. Thereby, fatigue damage can be detected at an early stage.

Previous research has shown that the nonlinear material properties are much more sensitive to changes in the microstructure, as for example due to plastic strain [19] or fatigue damage [20, 12], than the linear properties. Therefore, recent attention is drawn on experiments employing the nonlinear behavior of wave motion in order to characterize the nonlinear acoustic properties of a material. These nonlinear acoustic properties can then be related to the material microstructure properties such as plasticity.

Measurement of the second harmonic amplitude is the goal of many of these methods. Second harmonics are waves that contain components at twice the frequency of the excitation wave. These waves at the double frequency arise due to the structure's material nonlinearity when considering the quadratic approximation of the nonlinear problem, as opposed to the linear approximation in linear elastic theory. The intensity of the second harmonic amplitude is shown to be related to the nonlinear material

constants, so that measurement of the former is a direct measure of the degree of the material's nonlinearity. The use of second harmonics as opposed to higher harmonics is justified by the fact that the higher ones have much smaller amplitudes than the second harmonic, whose amplitude itself is already very small when compared to the linear portion of the wave at excitation frequency.

In order to facilitate measurements of second harmonics, and to back out the measured data physically, theories on nonlinear wave motion are needed. While theoretical publications on the nonlinear behavior of elastic bulk and surface waves [16, 24] appeared early, the development of an applicable theory for Lamb waves in plates turned out to be more difficult because of the dispersive behavior of these guided waves. De Lima et al. [5, 6] developed an analytical solution for the second harmonic generation in wave guides using perturbation theory and a modal expansion method. Shortly after, Deng [8] followed, using the same approach. Both solutions employ perturbation to obtain a primary wave, associated with the wave launched into the plate, which causes a secondary wave, associated with the second harmonic wave, due to body forces and surface tractions driven by nonlinearities at twice the excitation frequency. A modal expansion expresses the secondary wave as a sum of modes at twice the excitation frequency.

For practical applications, the excitation of certain modes is more advantageous than others. Modes satisfying phase velocity matching, i.e. the phase velocity of the primary mode equals the phase velocity of the secondary mode, are favorable for measurements because the second harmonic mode shows a linear increase of the amplitude in this case. In this context, several questions arise concerning practical applications.

First, De Lima et al. [6] and Deng [8] contradict each other with regard to the symmetry properties of the second harmonic wave. Specifically, De Lima's conclusion allows for the excitation of an antisymmetric secondary mode, while Deng's conclusion

does not. Moreover, Deng does not mention explicitly which type of symmetry of the primary mode will generate a symmetric secondary mode. In short, the question is whether the cross-modal generation from an antisymmetric primary to a symmetric secondary mode is possible. This is crucial as to the choice of excitation frequencies and modes.

This research will demonstrate that there are several modes which satisfy phase velocity matching. This leads to another question: Which mode should be selected in order to obtain a strong second harmonic amplitude, which is most easily excitable and measurable? In addition to the rate of second harmonic generation, other practical issues include what are the displacements at the surface, or what is the symmetry of the modes involved?

Thus, the objective of this work, is to understand the process of second harmonic Lamb wave generation by means of the solution derived by De Lima [5]. This goal is approached in Chapter 2, where not only De Lima's solution is presented and customized for this work, but also physical interpretation and explanation is provided. This chapter also presents a proof about the symmetry properties, which shows that both a symmetric and an antisymmetric primary mode can generate a symmetric secondary mode, but neither a symmetric nor an antisymmetric secondary mode can generate an antisymmetric secondary mode.

Chapter 3 presents an analytical investigation of the linear dispersion relationship of Lamb modes with regard to phase velocity and group velocity matching. The latter concept, that the group velocity of the primary and the secondary mode should be equal, is introduced because finite signals, as opposed to infinite harmonic signals are considered in practice. The analysis of this chapter yields five types of modes satisfying phase and group velocity matching, which are then evaluated further in Chapter 4 for the example of an aluminum plate. Features as to the rate of second harmonic generation and other practical issues such as excitability and ease of measurement

are presented and compared, which is followed by conclusions on which modes are favorable to practical applications.

CHAPTER II

SECOND HARMONIC LAMB WAVE GENERATION

Early work on nonlinear Lamb wave propagation such as Deng [7] was based on the concept of partial bulk waves comprising the effective Lamb wave. By reflection at the surface, each partial wave produces new partial waves and so on. While this approach appears to be complicated, the concept of modes simplifies the analysis significantly. The mode solution to the linear problem is well known and established long ago. Yet, there was no way to apply it to the nonlinear problem until recently. De Lima [5] and later Deng [8] developed an analysis employing the linear mode solution for the nonlinear problem via a modal expansion approach. Not only has the analysis of the problem become less cumbersome, but it also provides greater physical insight into the process of second harmonic generation.

This chapter presents a concise derivation following De Lima's notation. First, the nonlinear boundary value problem is derived. A pertubation method transforms the nonlinear problem into two linear boundary value problems. The first one is associated with the wave launched into the plate, which is called the primary wave, while the other one represents the governing equation for the second harmonic wave due to nonlinearities, called the secondary wave. The perturbation condition that the secondary wave must be much smaller in amplitude than the primary wave is crucial for the validity of this solution. Solving for the primary wave leads to the well known linear Lamb mode solution. The secondary boundary value problem is forced by the primary wave and is approached via a modal expansion method. Power fluxes from the primary wave to the secondary modes in the expansion are calculated, which determine the rate of second harmonic generation for each of the secondary modes.

Section 2.2 then discusses features of the solution more thoroughly, beginning with a physical interpretation. A proof follows that antisymmetric secondary modes cannot exist and that both symmetric and antisymmetric primary modes can generate symmetric secondary modes. Finally, two types of solutions are discussed and their implications on methods for the characterization of materials are presented.

2.1 Derivation

The subject under consideration is an isotropic, homogeneous, nonlinear elastic, infinite plate with thickness $d = 2h$. Nonlinearities arise due to both finite deformation and nonlinear material behavior. The coordinate system is chosen to be Cartesian $\{x, y, z\}$ with its origin at $y = 0$ as shown in Figure 2.1. At the surface $y = \pm h$, the plate is assumed to be stress free.

For the wave motion, only time-harmonic plane waves propagating in the positive z-direction are considered, assuming plane strain in the x-direction. Motions are restricted to the y-z-plane, representing Lamb waves in the linear theory. That is, shear horizontal (SH) waves are beyond the scope of this work.

2.1.1 Nonlinear Boundary Value Problem and Perturbation

In the first step, the set of equations describing nonlinear wave propagation needs to be obtained. Details on the underlying basics of continuum mechanics can be found in Malvern [15]. The starting point is the balance of linear momentum for a continuous

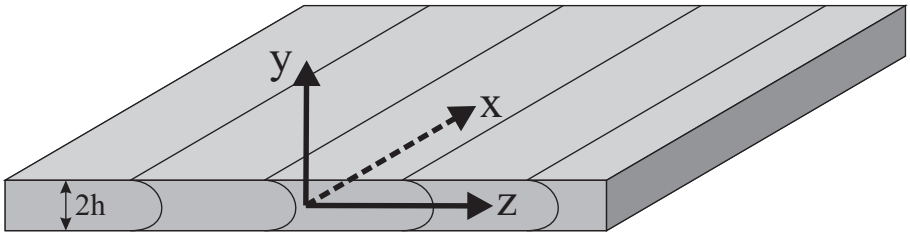

Figure 2.1: Coordinate Sysyem of the Infinite Plate

medium neglecting body forces

$$\boldsymbol{\nabla} \cdot (\boldsymbol{S} \cdot \boldsymbol{F}^T) = \rho_0 \frac{\partial^2 \boldsymbol{u}}{\partial t^2}, \tag{2.1}$$

using the second Piola-Kirchhoff stress $\boldsymbol{S}$, the density in the reference configuration ρ_0, and the deformation gradient

$$\boldsymbol{F} = \boldsymbol{I} + \boldsymbol{\nabla} \boldsymbol{u} \tag{2.2}$$

in terms of the displacement vector $\boldsymbol{u}$, and the second-order identity tensor $\boldsymbol{I}$. In order to obtain a displacement description of Eq.(2.1), the second order elastic constitutive law for an isotropic medium derived by Renton [21]

$$\begin{aligned} \boldsymbol{S} &= \lambda \operatorname{tr}(\boldsymbol{E})\, \boldsymbol{I} + 2\mu\, \boldsymbol{E} + \\ &\quad \left(\mathcal{C} \operatorname{tr}(\boldsymbol{E})^2 + \mathcal{B} \operatorname{tr}(\boldsymbol{E}^2)\right) \boldsymbol{I} + 2\mathcal{B} \operatorname{tr}(\boldsymbol{E})\, \boldsymbol{E} + \mathcal{A}\, (\boldsymbol{E}^2)^T \end{aligned} \tag{2.3}$$

is applied, where λ is Lamé's constant, μ the shear modulus, $\mathcal{A}$, $\mathcal{B}$, $\mathcal{C}$ the third-order elastic constants as proposed by Landau and Lifshitz [13], and

$$\boldsymbol{E} = \frac{1}{2}(\boldsymbol{F}^T \cdot \boldsymbol{F} - \boldsymbol{I}) \tag{2.4}$$

the Lagrangian strain tensor. Combining Eqs.(2.1) to (2.4), the equations of motion become

$$(\lambda + 2\mu)\boldsymbol{\nabla}(\boldsymbol{\nabla} \cdot \boldsymbol{u}) - \mu \boldsymbol{\nabla} \times (\boldsymbol{\nabla} \times \boldsymbol{u}) + \boldsymbol{\nabla} \cdot \bar{\boldsymbol{S}} = \rho_0 \frac{\partial^2 \boldsymbol{u}}{\partial t^2}, \tag{2.5}$$

where $\bar{\boldsymbol{S}}$ contains all nonlinear terms of $\boldsymbol{S} \cdot \boldsymbol{F}^T$, i.e.

$$\boldsymbol{S} \cdot \boldsymbol{F}^T = \boldsymbol{S}^L + \bar{\boldsymbol{S}}, \tag{2.6}$$

with $\boldsymbol{S}^L$ being the linear portion of the second Piola-Kirchhoff stress.

Since the plate is assumed to be stress free on its surface, the boundary condition for Eq.(2.5) is stated as

$$\boldsymbol{n}_y \cdot (\boldsymbol{S} \cdot \boldsymbol{F}^T) = 0 \quad \text{at} \quad y = \pm h, \tag{2.7}$$

or using Eq.(2.6)

$$\boldsymbol{n}_y \cdot \boldsymbol{S}^L = -\boldsymbol{n}_y \cdot \bar{\boldsymbol{S}} \quad \text{at} \quad y = \pm h, \tag{2.8}$$

where $\boldsymbol{n}_y$ is the outward unit normal vector to the surface in the reference configuration.

In order to solve the nonlinear boundary value problem (BVP) represented by Eqs.(2.5) and (2.8), a perturbation approach is chosen, which assumes that the total displacement field can be written as

$$\boldsymbol{u} = \boldsymbol{u}^{(1)} + \boldsymbol{u}^{(2)}, \tag{2.9}$$

where $\boldsymbol{u}^{(1)}$ is called the primary solution associated with the linear BVP, while the secondary solution $\boldsymbol{u}^{(2)}$ arises due to nonlinearities. If it is assumed that

$$|\boldsymbol{u}^{(2)}| \ll |\boldsymbol{u}^{(1)}|, \tag{2.10}$$

which is referred to as the perturbation condition, the nonlinear BVP can be broken down to two linear BVPs. It is noted explicitly that the solution presented here cannot be applied if the perturbation condition is not satisfied. Measurements have shown, however, that second harmonic amplitudes are usually much smaller than the primary wave's amplitude.

As contributions from the nonlinearities are small, $\boldsymbol{u}^{(1)}$ is the solution to the homogeneous linear BVP

$$(\lambda + 2\mu)\boldsymbol{\nabla}(\boldsymbol{\nabla} \cdot \boldsymbol{u}^{(1)}) - \mu\boldsymbol{\nabla} \times (\boldsymbol{\nabla} \times \boldsymbol{u}^{(1)}) = \rho_0 \frac{\partial^2 \boldsymbol{u}^{(1)}}{\partial t^2}, \tag{2.11a}$$

$$\boldsymbol{n}_y \cdot \boldsymbol{S}^L(\boldsymbol{u}^{(1)}) = 0 \quad \text{at} \quad y = \pm h. \tag{2.11b}$$

By substituting Eq.(2.9) into the nonlinear BVP from Eq.(2.5) one obtains the BVP for the secondary solution as

$$(\lambda + 2\mu)\boldsymbol{\nabla}(\boldsymbol{\nabla} \cdot \boldsymbol{u}^{(2)}) - \mu\boldsymbol{\nabla} \times (\boldsymbol{\nabla} \times \boldsymbol{u}^{(2)}) + \boldsymbol{\nabla} \cdot \bar{\boldsymbol{S}}^{(1)} = \rho_0 \frac{\partial^2 \boldsymbol{u}^{(2)}}{\partial t^2} \tag{2.12a}$$

$$\boldsymbol{n}_y \cdot \boldsymbol{S}^L(\boldsymbol{u}^{(2)}) = -\boldsymbol{n}_y \cdot \bar{\boldsymbol{S}}^{(1)} \quad \text{at} \quad y = \pm h. \tag{2.12b}$$

The term $\bar{\boldsymbol{S}}^{(1)}$ depends only on quadratic terms of the primary solution $\boldsymbol{u}^{(1)}$. Higher order terms of $\boldsymbol{u}^{(2)}$ and cross terms can be neglected due to the perturbation condition Eq.(2.10). Third and higher order terms of $\boldsymbol{u}^{(1)}$ are not taken into account because all displacements are still assumed to be small. With $\bar{\boldsymbol{S}}^{(1)}$ known, Eqs.(2.12) may be regarded as a linear, forced BVP with nonzero stress boundary conditions. For convenience, the definition

$$\bar{\boldsymbol{f}} = \boldsymbol{\nabla} \cdot \bar{\boldsymbol{S}} \tag{2.13}$$

is introduced. Eqs.(2.2) to (2.4) yield the forcing terms given in index notation

$$\begin{aligned}
\bar{f}_i = {} & \big(\mu + \frac{\mathcal{A}}{4}\big)\Big(\frac{\partial^2 u_l}{\partial a_k^2}\frac{\partial u_l}{\partial a_i} + \frac{\partial^2 u_l}{\partial a_k^2}\frac{\partial u_i}{\partial a_l} + 2\frac{\partial^2 u_i}{\partial a_l \partial a_k}\frac{\partial u_l}{\partial a_k}\Big) \\
& + \big(\lambda + \mu + \frac{\mathcal{A}}{4} + \mathcal{B}\big)\Big(\frac{\partial^2 u_l}{\partial a_i \partial a_k}\frac{\partial u_l}{\partial a_k} + \frac{\partial^2 u_k}{\partial a_l \partial a_k}\frac{\partial u_i}{\partial a_l}\Big) \\
& + (\lambda + \mathcal{B})\Big(\frac{\partial^2 u_i}{\partial a_k^2}\frac{\partial u_l}{\partial a_l}\Big) + (\mathcal{B} + 2\mathcal{C})\Big(\frac{\partial^2 u_k}{\partial a_i \partial a_k}\frac{\partial u_l}{\partial a_l}\Big) \\
& + \big(\frac{\mathcal{A}}{4} + \mathcal{B}\big)\Big(\frac{\partial^2 u_k}{\partial a_l \partial a_k}\frac{\partial u_l}{\partial a_i} + \frac{\partial^2 u_l}{\partial a_i \partial a_k}\frac{\partial u_k}{\partial a_l}\Big)
\end{aligned} \tag{2.14a}$$

and

$$\begin{aligned}
\bar{S}_{ij} = {} & \Big(\frac{\lambda}{2}\frac{\partial u_k}{\partial a_l}\frac{\partial u_k}{\partial a_l} + \mathcal{C}\frac{\partial u_k}{\partial a_k}\frac{\partial u_l}{\partial a_l}\Big)\delta_{ij} + \mathcal{B}\frac{\partial u_k}{\partial a_k}\frac{\partial u_i}{\partial a_j} + \frac{\mathcal{A}}{4}\frac{\partial u_i}{\partial a_k}\frac{\partial u_k}{\partial a_j} \\
& + \frac{\mathcal{B}}{2}\Big(\frac{\partial u_k}{\partial a_l}\frac{\partial u_k}{\partial a_l} + \frac{\partial u_k}{\partial a_l}\frac{\partial u_l}{\partial a_k}\Big)\delta_{ij} + (\lambda + \mathcal{B})\frac{\partial u_k}{\partial a_k}\frac{\partial u_j}{\partial a_i} \\
& + \big(\mu + \frac{\mathcal{A}}{4}\big)\Big(\frac{\partial u_j}{\partial a_k}\frac{\partial u_i}{\partial a_k} + \frac{\partial u_k}{\partial a_j}\frac{\partial u_k}{\partial a_i} + \frac{\partial u_j}{\partial a_k}\frac{\partial u_k}{\partial a_i}\Big),
\end{aligned} \tag{2.14b}$$

where a_i represents the coordinate basis in the reference configuration, i.e.

$$\{a_1, a_2, a_3\} = \{x, y, z\}. \tag{2.15}$$

The following section shows the solution to the primary and secondary BVP using a modal expansion technique.

2.1.2 Solution of the Linear Boundary Value Problems

2.1.2.1 Primary Solution

In order to obtain the forcing terms $\bar{\boldsymbol{f}}$ and $\bar{\boldsymbol{S}}$ for the secondary BVP, the primary solution of Eqs.(2.11) must be known, as Eqs.(2.14) need to be evaluated for the primary wave solution. The primary BVP displays a homogeneous, linear problem for a stress free plate, whose solution is given, for example, in Graff [10]. A review of the established solution can be found in Appendix A. For future reference, the main results are stated shortly.

There exist four different types of modes which are characterized by their frequency relations and their displacement fields. The latter ones have the common form

$$\boldsymbol{u}(x,y,z,t) = \tilde{\boldsymbol{u}}(x,y)\, e^{i(\kappa z - \omega t)}, \tag{2.16}$$

where κ is the wave number and ω the angular frequency of the mode $\tilde{\boldsymbol{u}}(x,y)$. Two types – symmetric and antisymmetric shear horizontal (SH) modes – are not considered in this research because of the plane strain assumptions, which means there can be no dependency in the x-direction. The other two types are the symmetric and antisymmetric Lamb modes. Symmetric Lamb modes follow the frequency equation

$$\frac{\tan\beta h}{\tan\alpha h} = -\frac{4\alpha\beta\kappa^2}{(\kappa^2-\beta^2)^2}, \tag{2.17}$$

and their displacement field reads as

$$\tilde{u}_x = 0, \tag{2.18a}$$

$$\tilde{u}_y = iD\Big(-\frac{(\kappa^2-\beta^2)\sin\beta h}{2\kappa\sin\alpha h}\sin\alpha y + \kappa\sin\beta y\Big), \tag{2.18b}$$

$$\tilde{u}_z = -D\Big(\frac{(\kappa^2-\beta^2)\sin\beta h}{2\alpha\sin\alpha h}\cos\alpha y + \beta\cos\beta y\Big). \tag{2.18c}$$

Antisymmetric Lamb modes satisfy the frequency equation

$$\frac{\tan\beta h}{\tan\alpha h} = -\frac{(\kappa^2-\beta^2)^2}{4\alpha\beta\kappa^2} \tag{2.19}$$

and show the displacement field

$$\tilde{u}_x = 0, \tag{2.20a}$$

$$\tilde{u}_y = iC\Big(-\frac{(\kappa^2-\beta^2)\cos\beta h}{2\kappa\cos\alpha h}\cos\alpha y + \kappa\cos\beta y\Big), \tag{2.20b}$$

$$\tilde{u}_z = C\Big(\frac{(\kappa^2-\beta^2)\cos\beta h}{2\alpha\cos\alpha h}\sin\alpha y + \beta\sin\beta y\Big). \tag{2.20c}$$

The wave numbers α and β are defined as

$$\alpha = \sqrt{(\omega/c_{\mathrm{L}})^2-\kappa^2}, \quad \beta = \sqrt{(\omega/c_{\mathrm{T}})^2-\kappa^2}, \tag{2.21}$$

where the material constants c_{L} and c_{T} are the longitudinal and shear velocities in an infinite medium, respectively. The complex constants C and D determine the amplitude of the respective mode and depend on the actual excitation.

The symmetry of a mode is defined by the y-symmetry of the in-plane displacement component $\tilde{u}_z(y)$, i.e. for symmetric modes, the in-plane component $\tilde{u}_z(y)$ is symmetric in y, while the out-of-plane component $\tilde{u}_y(y)$ is antisymmetric in y. For antisymmetric modes, the in-plane component $\tilde{u}_z(y)$ is antisymmetric in y, while the out-of-plane component $\tilde{u}_y(y)$ is symmetric in y.

An important implication of the frequency equations is dispersivity of the modes,

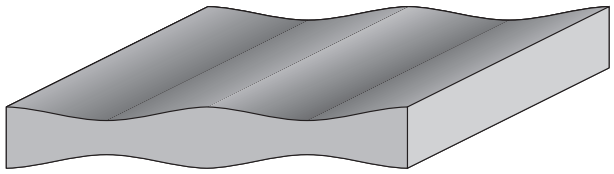

Symmetric Lamb Mode

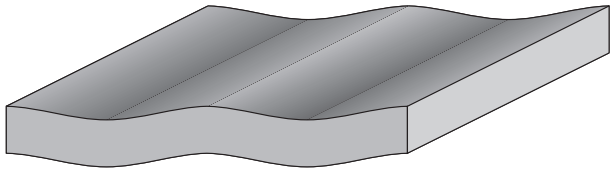

Antisymmetric Lamb Mode

Figure 2.2: Deformed Plate for Symmetric and Antisymmetric Lamb Mode

which means that the phase velocity

$$c_{\text{ph}} = \frac{\omega}{\kappa} \tag{2.22}$$

depends on frequency according to the frequency equations. Dispersion curves such as the one shown in Figure 2.3 for an aluminum plate, whose material properties are presented in Chapter 4, display the solutions to the transcendental frequency equations graphically. It is observed that for a given excitation frequency ω, there exist only a finite number of propagating modes for which the wave number κ and the phase velocity c_{ph} are real. Modes showing a complex wave number are called evanescent as they decay exponentially with propagation distance, being detectable only in the near field.

Other field variables such as the linear strain tensor $\boldsymbol{\varepsilon}$ or the Cauchy stress tensor

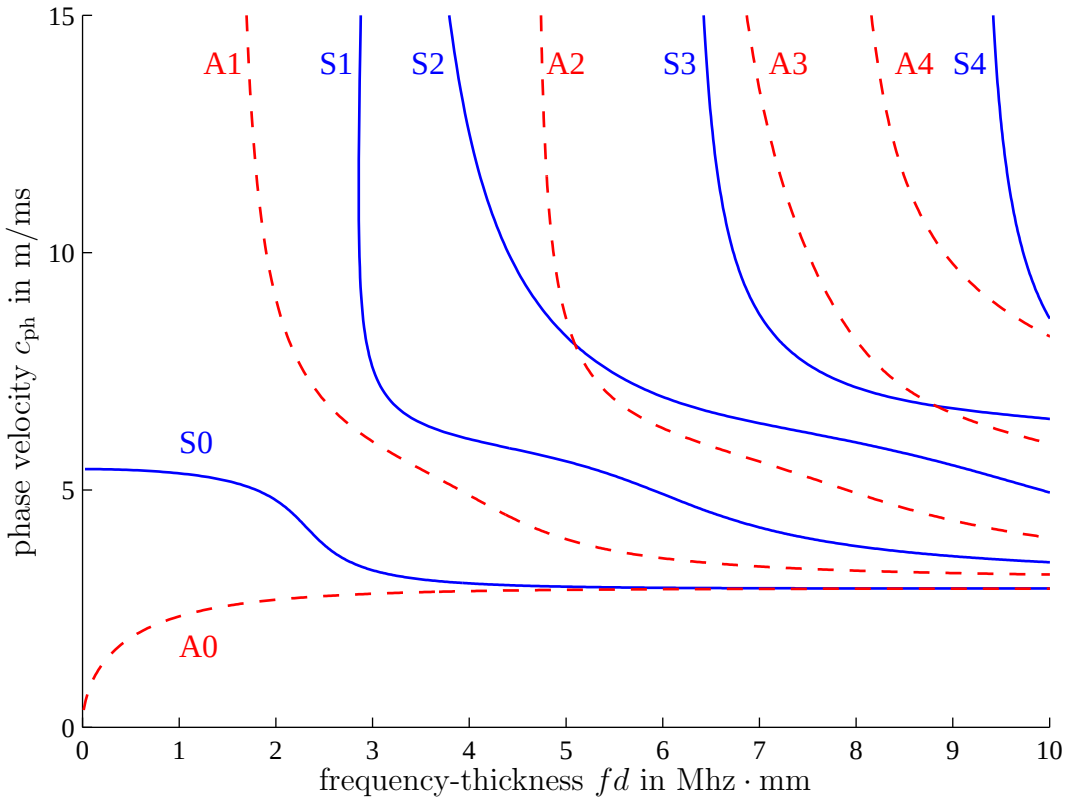

Figure 2.3: Lamb Mode Dispersion Curve for an Aluminum Plate. S – Symmetric modes, A – Antisymmetric Modes.

$\boldsymbol{\sigma}$ can be obtained from the displacement field $\boldsymbol{u}$ using Eqs.(A.14) and (A.13) in Appendix A.

2.1.2.2 Secondary Solution

The final step is to solve the secondary problem of Eqs.(2.12), which represents a linear BVP that is forced by the second harmonic body force term $\bar{\boldsymbol{f}}$ and second harmonic tractions on the surface due to the stress tensor $\bar{\boldsymbol{S}}$. By substitution of the primary solution into Eqs.(2.14), the forcing terms $\bar{\boldsymbol{f}}$ and $\bar{\boldsymbol{S}}$ for the secondary BVP are obtained. It should be pointed out, however, that one has to use real displacements since products of displacements are involved. Thus, substituting

$$\boldsymbol{u}^{(1)}_{\text{real}} = \frac{1}{2}\tilde{\boldsymbol{u}}^{(1)}(y)e^{i(\kappa z-\omega t)} + c.c.\,, \tag{2.23}$$

– where *c.c.* stands for conjugate complex – in Eqs.(2.14) yields the real forcing terms

$$\bar{\boldsymbol{f}}^{(1)}_{\text{real}} = \frac{1}{2}\bar{\boldsymbol{f}}^{2\omega}(y)e^{2i(\kappa z-\omega t)} + c.c. + \text{const}, \tag{2.24a}$$

$$\bar{\boldsymbol{S}}^{(1)}_{\text{real}} = \frac{1}{2}\bar{\boldsymbol{S}}^{2\omega}(y)e^{2i(\kappa z-\omega t)} + c.c. + \text{const}. \tag{2.24b}$$

It is noted that the term 'const' signifies a real constant, which leads to a static deformation of the plate. However, this phenomenon is not investigated in this work. Further manipulations are carried out in the harmonic complex domain again, for which reason the harmonic complex portions of Eqs.(2.24) are absorbed as

$$\bar{\boldsymbol{f}}^{(1)} = \bar{\boldsymbol{f}}^{2\omega}(y)e^{2i(\kappa z-\omega t)}, \tag{2.25a}$$

$$\bar{\boldsymbol{S}}^{(1)} = \bar{\boldsymbol{S}}^{2\omega}(y)e^{2i(\kappa z-\omega t)}. \tag{2.25b}$$

Note that the forcing terms are harmonic at twice the primary frequency, from which the term *second harmonic* originates. This is due to the fact that in the second-order approximation of the constitutive law, quadratic terms of displacements enter the equations, resulting in forcing terms at twice the primary frequency.

Having obtained the forcing terms, the secondary BVP is defined completely, constituting a forced linear problem. Before the final solution is derived, some preliminary results from linear elastic theory need to be reviewed. These results can be applied because the secondary BVP presents a linear problem.

First, the complex reciprocity relation is derived by Auld [2] and customized by De Lima [5]. Given two solutions m and n for the linear BVP with body forces $\boldsymbol{b}_m$ and $\boldsymbol{b}_n$, respectively,

$$\boldsymbol{v}_m = \tilde{\boldsymbol{v}}_m(y)\, e^{i(\kappa_m z - \omega t)}, \quad \boldsymbol{\sigma}_m = \tilde{\boldsymbol{\sigma}}_m(y) e^{i(\kappa_m z - \omega t)} \tag{2.26}$$

$$\boldsymbol{v}_n = \tilde{\boldsymbol{v}}_n(y)\, e^{i(\kappa_n z - \omega t)}, \quad \boldsymbol{\sigma}_n = \tilde{\boldsymbol{\sigma}}_n(y) e^{i(\kappa_n z - \omega t)} \tag{2.27}$$

where the complex particle velocity $\boldsymbol{v} = \dot{\boldsymbol{u}}$, the linear stress tensor $\boldsymbol{\sigma}$ and the body forces $\boldsymbol{b}$ are all complex variables, the complex reciprocity relation reads as

$$\boldsymbol{\nabla} \cdot (\boldsymbol{v}_n^* \cdot \boldsymbol{\sigma}_m + \boldsymbol{v}_m \cdot \boldsymbol{\sigma}_n^*) = -\boldsymbol{v}_n^* \cdot \boldsymbol{b}_m - \boldsymbol{v}_m \cdot \boldsymbol{b}_n^*, \tag{2.28}$$

where the superscript * means conjugate complex. Based on this relation, Auld [2] concludes orthogonality of the linear plate modes, which is defined via the power flux between two modes. The power flux per unit depth in x between two modes m and n is defined as

$$\mathcal{P}_{mn} = \frac{1}{4} \int_{-h}^{h} (-\tilde{\boldsymbol{v}}_n^* \cdot \tilde{\boldsymbol{\sigma}}_m - \tilde{\boldsymbol{v}}_m \cdot \tilde{\boldsymbol{\sigma}}_n^*) \cdot \boldsymbol{n}_z \, \mathrm{d}y, \tag{2.29}$$

with the unit normal vector $\boldsymbol{n}_z$ in propagation direction z. Mode orthogonality means that for two propagating modes at the same frequency, the power flux is nonzero only if the two modes are equal, or

$$\mathcal{P}_{mn} = \begin{cases} 0 & \text{if} \quad n \neq m \\ -\frac{1}{2}\, \Re e \int_{-h}^{h} \tilde{\boldsymbol{v}}_n^* \cdot \tilde{\boldsymbol{\sigma}}_n \cdot \boldsymbol{n}_z \, \mathrm{d}y & \text{if} \quad n = m\,. \end{cases} \tag{2.30}$$

This statement is interpreted physically in such that in linear theory, two different modes do not interfere by transferring energy to each other, while $\mathcal{P}_{nn}$ quantifies how

much energy is transported by mode n over the cross section unit area per unit time and unit depth.

Having introduced these concepts from linear elastic theory, the secondary BVP can be approached. The pair $\{\boldsymbol{v}^{(2)}, \boldsymbol{S}^{(2)}\}$ is the unknown solution under body force $\bar{\boldsymbol{f}}^{(1)}$, where the short notation $\boldsymbol{S}^{(2)} = \boldsymbol{S}^{L}(\boldsymbol{u}^{(2)})$ is used. Substituting the unknown solution and an arbitrary known mode under zero body force

$$\boldsymbol{v}_n = \tilde{\boldsymbol{v}}_n(y)\, e^{i(\kappa_n z - \omega t)}, \quad \boldsymbol{\sigma}_n = \tilde{\boldsymbol{\sigma}}_n(y) e^{i(\kappa_n z - \omega t)}, \quad \boldsymbol{b}_n = 0 \tag{2.31}$$

into the reciprocity relation Eq.(2.28), one obtains

$$\begin{aligned} &-\frac{\partial}{\partial z}\big((\tilde{\boldsymbol{v}}_n^* \cdot \boldsymbol{S}^{(2)} + \boldsymbol{v}^{(2)} \cdot \tilde{\boldsymbol{\sigma}}_n^*) \cdot \boldsymbol{n}_z\, e^{-i\kappa_n^* z}\big) - \frac{\partial}{\partial y}\big((\tilde{\boldsymbol{v}}_n^* \cdot \boldsymbol{S}^{(2)} + \boldsymbol{v}^{(2)} \cdot \tilde{\boldsymbol{\sigma}}_n^*) \cdot \boldsymbol{n}_y\, e^{-i\kappa_n^* z}\big) \\ &= \tilde{\boldsymbol{v}}_n^* \cdot \bar{\boldsymbol{f}}^{(1)}\, e^{-i\kappa_n^* z} \end{aligned} \tag{2.32}$$

since $\partial/\partial x \equiv 0$ and $e^{i\omega t}$ cancels.

The key step in the derivation of the secondary solution is the expansion of the secondary solution to a series of secondary modes. For a fixed frequency, there exist an infinite number of modes (propagating and evanescent), so that the unknown secondary field variables may be expressed as modal expansions of all these modes, i.e.

$$\boldsymbol{u}^{(2)} = \sum_{m=1}^{\infty} A_m(z)\, \tilde{\boldsymbol{u}}_m^{(2)}(y)\, e^{-2i\omega t}, \tag{2.33a}$$

$$\boldsymbol{v}^{(2)} = \sum_{m=1}^{\infty} A_m(z)\, \tilde{\boldsymbol{v}}_m^{(2)}(y)\, e^{-2i\omega t}, \tag{2.33b}$$

$$\boldsymbol{S}^{(2)} = \sum_{m=1}^{\infty} A_m(z)\, \tilde{\boldsymbol{\sigma}}_m^{(2)}(y)\, e^{-2i\omega t}, \tag{2.33c}$$

acting at frequency 2ω, since the body force and surface tractions act at the second harmonic frequency. Each mode m in the expansion enters the secondary solution with its own amplitude coefficient $A_m(z)$. Therefore, the amplitude coefficient $A_m(z)$ expresses how strong the secondary mode m in the expansion is generated by the

primary wave. The final goal consists of finding an analytical expression for the amplitude coefficient $A_m(z)$ of each secondary mode m.

To achieve this, one substitutes Eqs.(2.33) in the first term of Eq.(2.32) and integrates the result over the plate thickness to obtain

$$-\frac{\partial}{\partial z}\int_{-h}^{h}\left[\sum_{m=1}^{\infty}A_m(z)(\tilde{\boldsymbol{v}}_n^*\cdot\tilde{\boldsymbol{\sigma}}_m^{(2)}+\tilde{\boldsymbol{v}}_m^{(2)}\cdot\tilde{\boldsymbol{\sigma}}_n^*)\cdot\boldsymbol{n}_z e^{-i(\kappa_n^* z+2\omega t)}\right]\mathrm{d}y$$
$$-(\tilde{\boldsymbol{v}}_n^*\cdot\boldsymbol{S}^{(2)}+\boldsymbol{v}^{(2)}\cdot\tilde{\boldsymbol{\sigma}}_n^*)\cdot\boldsymbol{n}_y\, e^{-i\kappa_n^* z}\Big|_{-h}^{h}=\int_{-h}^{h}\tilde{\boldsymbol{v}}_n^*\cdot\bar{\boldsymbol{f}}^{(1)}\, e^{-i\kappa_n^* z}\,\mathrm{d}y. \tag{2.34}$$

Using the definition of the power flux Eq.(2.29) and regarding the fact that the mode n is stress free at the surface, i.e. $\tilde{\boldsymbol{\sigma}}_n(\pm h)=0$, Eq.(2.34) is rewritten as

$$\frac{\partial}{\partial z}\Big[\sum_{m=1}^{\infty}4A_m(z)\mathcal{P}_{mn}e^{-i(\kappa_n^* z+2\omega t)}\Big]-\tilde{\boldsymbol{v}}_n^*\cdot\boldsymbol{S}^{(2)}\cdot\boldsymbol{n}_y\, e^{-i\kappa_n^* z}\Big|_{-h}^{h}$$
$$=\int_{-h}^{h}\tilde{\boldsymbol{v}}_n^*\cdot\bar{\boldsymbol{f}}^{(1)}\, e^{-i\kappa_n^* z}\,\mathrm{d}y. \tag{2.35}$$

Furthermore, the boundary condition Eq.(2.12b) for the secondary BVP and the orthogonality condition Eq.(2.30) yield

$$\frac{\partial}{\partial z}\Big(4A_n(z)\mathcal{P}_{nn}\, e^{-i(\kappa_n^* z+2\omega t)}\Big)+\boldsymbol{n}_y\cdot\bar{\boldsymbol{S}}^{(1)}\cdot\tilde{\boldsymbol{v}}_n^*\, e^{-i\kappa_n^* z}\Big|_{-h}^{h}$$
$$=\int_{-h}^{h}\tilde{\boldsymbol{v}}_n^*\cdot\bar{\boldsymbol{f}}^{(1)}\, e^{-i\kappa_n^* z}\,\mathrm{d}y, \tag{2.36}$$

since $\boldsymbol{S}^{(2)}$ is a symmetric tensor. The power fluxes from the primary wave to the nth mode in the expansion of the secondary wave via body forces f_n^{vol} and surface tractions f_n^{surf}, respectively,

$$f_n^{\mathrm{vol}}=\int_{-h}^{h}\tilde{\boldsymbol{v}}_n^*\cdot\bar{\boldsymbol{f}}^{2\omega}\,\mathrm{d}y, \tag{2.37a}$$

$$f_n^{\mathrm{surf}}=-\boldsymbol{n}_y\cdot\bar{\boldsymbol{S}}^{2\omega}\cdot\tilde{\boldsymbol{v}}_n^*\Big|_{-h}^{h}, \tag{2.37b}$$

are not only defined to make some expressions shorter, but more importantly, because they provide much physical insight into the solution. This notation will enable the observation that the amplitude coefficient $A_n(z)$ is proportional to f_n^{vol} and f_n^{surf},

meaning that the second harmonic generation of a mode is caused and characterized by the magnitude of the power flux from the primary wave to the respective second harmonic mode.

Using the definitions of Eqs.(2.37) in combination with Eqs.(2.25) and Eq.(2.36), one arrives at the first order, linear, ordinary differential equation

$$4\mathcal{P}_{nn}\Big(\frac{\mathrm{d}}{\mathrm{d}z} - i\kappa_n^*\Big)A_n(z) = (f_n^{\mathrm{surf}} + f_n^{\mathrm{vol}})e^{2i\kappa z}. \tag{2.38}$$

for $A_n(z)$. To come up with an initial condition, it is assumed that the primary wave is excited at $z = 0$ where the secondary solution has to be zero due to causality, since the secondary wave is forced by the primary wave. Thus,

$$\boldsymbol{u}^{(2)} = \boldsymbol{v}^{(2)} = 0 \quad \text{at} \quad z = 0, \tag{2.39}$$

and from Eqs.(2.33)

$$A_n(z) = 0 \quad \text{at} \quad z = 0. \tag{2.40}$$

The solution to Eq.(2.38) with the initial condition Eq.(2.40) is given by

$$A_n(z) = \frac{f_n^{\mathrm{vol}} + f_n^{\mathrm{surf}}}{4\mathcal{P}_{nn}} \begin{cases} \frac{i}{\kappa_n^* - 2\kappa}\big(e^{2i\kappa z} - e^{i\kappa_n^* z}\big) & \text{if} \quad \kappa_n^* \neq 2\kappa \\ z\, e^{2i\kappa z} & \text{if} \quad \kappa_n^* = 2\kappa, \end{cases} \tag{2.41}$$

which – in combination with Eqs.(2.33) – provides an analytical solution for the second harmonic wave, when small secondary amplitudes compared to the primary wave's amplitude are assumed. Table 2.1 summarizes the essential equations that yield the solution for the secondary wave.

Having achieved the solution for the secondary wave, subsequent sections will draw conclusions from the results and explain the physical interpretation of the solution in a more detailed way.

Table 2.1: Overview – Essential Equations for the Second Harmonic Solution

Modal Expansion (Eq.(2.33))

$$\boldsymbol{u}^{(2)} = \sum_{n=1}^{\infty} A_n(z)\, \tilde{\boldsymbol{u}}_n^{(2)}(y)\, e^{-2i\omega t},$$

with amplitude coefficient $A_n(z)$ for the nth mode in the expansion (Eq.(2.41))

$$A_n(z) = \frac{f_n^{\mathrm{vol}} + f_n^{\mathrm{surf}}}{4\mathcal{P}_{nn}} \begin{cases} \frac{i}{\kappa_n^* - 2\kappa}\left(e^{2i\kappa z} - e^{i\kappa_n^* z}\right) & \text{if} \quad \kappa_n^* \neq 2\kappa \\ z\, e^{2i\kappa z} & \text{if} \quad \kappa_n^* = 2\kappa, \end{cases},$$

where f_n^{vol} and f_n^{surf} are power fluxes from the primary to secondary mode n

$$f_n^{\mathrm{vol}} = \int_{-h}^{h} \tilde{\boldsymbol{v}}_n^* \cdot \bar{\boldsymbol{f}}^{2\omega}\, \mathrm{d}y \;\ldots\; \text{via volume body force (Eq.(2.37a))},$$
$$f_n^{\mathrm{surf}} = -\boldsymbol{n}_y \cdot \bar{\boldsymbol{S}}^{2\omega} \cdot \tilde{\boldsymbol{v}}_n^* \Big|_{-h}^{h} \;\ldots\; \text{via surface tractions (Eq.(2.37b))},$$

and $\mathcal{P}_{nn}$ is the power flux of secondary mode n (Eq.(2.29))

$$\mathcal{P}_{nn} = -\tfrac{1}{2}\, \Re e \int_{-h}^{h} \tilde{\boldsymbol{v}}_n^* \cdot \tilde{\boldsymbol{\sigma}}_n \cdot \boldsymbol{n}_z\, \mathrm{d}y.$$

Body force $\bar{\boldsymbol{f}}^{2\omega}$ and stress $\bar{\boldsymbol{S}}^{2\omega}$ are obtained from Eqs.(2.14) and Eqs.(2.24) applied for the real primary mode $\boldsymbol{u}^{(1)}$. Secondary field quantities $\tilde{\boldsymbol{u}}_n$, $\tilde{\boldsymbol{v}}_n$ and $\tilde{\boldsymbol{\sigma}}_n$ are solutions of the linear plate theory as in Appendix A evaluated for frequency 2ω and wave number κ_n.

2.2 Discussion

2.2.1 Physical Interpretation

The obtained solution can be understood most easily by looking at a simple, ideal thought experiment: A transducer excites the infinte plate with the primary frequency ω. Even though several modes can propagate at frequency ω, a single mode can be selected by adjusting the angle between the transducer and the plate in the correct fashion. As this primary mode $\tilde{\boldsymbol{u}}^{(1)}$ propagates along the plate, nonlinearities in the plate lead to body forces $\bar{\boldsymbol{f}}^{(1)}$ and surface tractions $\boldsymbol{n}_y \cdot \bar{\boldsymbol{S}}^{(1)}$ that act harmonically at twice the primary frequency, 2ω, as shown by Eqs.(2.25), and thus, excite modes at twice the primary frequency. Figure 2.4 shows an arbitrary example of this process in the dispersion curve: the mode S1 is excited at the primary frequency $fd^{(1)} = 3.6\,\mathrm{MHz\,mm}$ and generates all the modes at twice the primary frequency $fd^{(2)} = 7.2\,\mathrm{MHz\,mm}$, whose sum displays the secondary wave as described by Eqs.(2.33). In this example, only symmetric secondary modes are marked because it will be proven in the following section that antisymmetric Lamb modes are not excited in the process of second harmonic generation.

As mentioned before, the sum of the secondary modes is represented by Eqs.(2.33) and constitutes the secondary wave $\boldsymbol{u}^{(2)}$. Note that in many cases, only propagating modes are of interest, so that the evanescent modes may be disregarded in the modal expansion. Then, the expansion is comprised of N propagating modes

$$\boldsymbol{u}^{(2)} = \sum_{n=1}^{N} A_n(z)\, \tilde{\boldsymbol{u}}_n^{(2)}(y)\, e^{-2i\omega t}, \tag{2.42a}$$

$$\boldsymbol{v}^{(2)} = \sum_{n=1}^{N} A_n(z)\, \tilde{\boldsymbol{v}}_n^{(2)}(y)\, e^{-2i\omega t}, \tag{2.42b}$$

$$\boldsymbol{S}^{(2)} = \sum_{n=1}^{N} A_n(z)\, \tilde{\boldsymbol{\sigma}}_n^{(2)}(y)\, e^{-2i\omega t}. \tag{2.42c}$$

Each mode n enters the sum with its own amplitude coefficient $A_n(z)$ making certain second harmonic modes more or less excitable by the primary mode. Thus, the

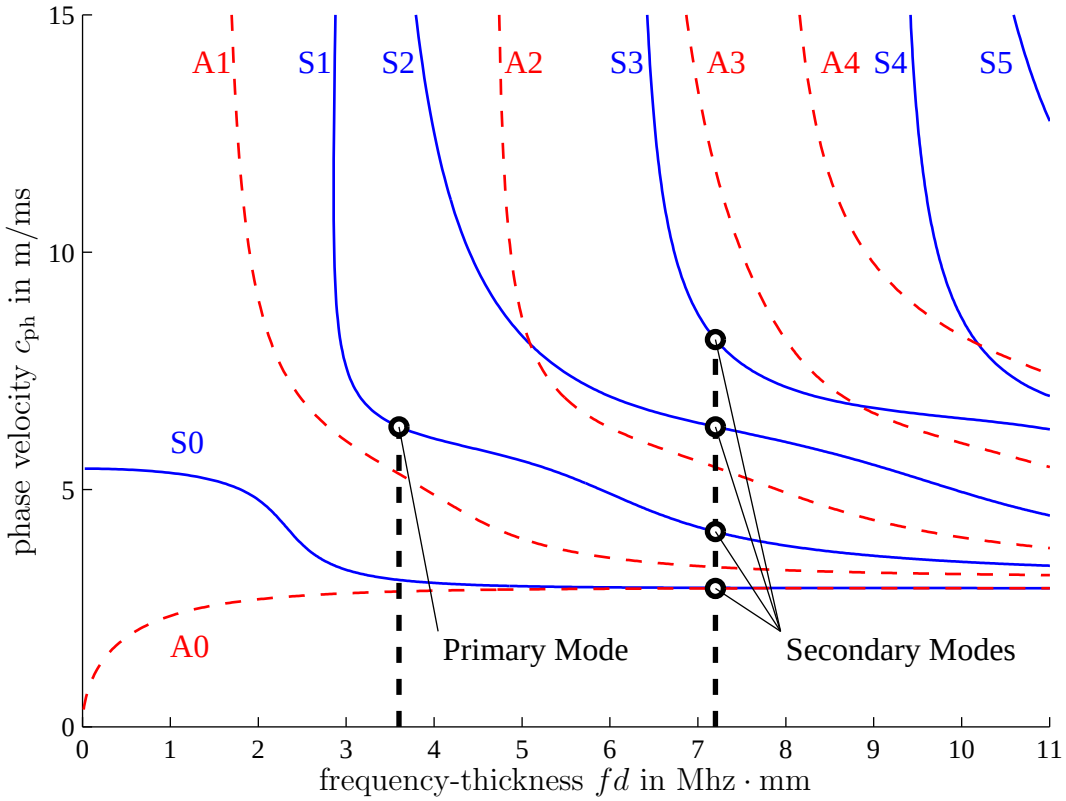

Figure 2.4: Lamb Mode Dispersion Curve for Aluminum with Example for Second Harmonic Generation. S – Symmetric Modes, A – Antisymmetric Modes.

amplitude coefficients for the secondary modes provide significant information about the secondary wave.

The amplitude coefficient $A_n(z)$ for mode n depends on various factors. First, regarding Eq.(2.41) the wave number of a respective second harmonic mode n determines whether case one ($\kappa_n \neq 2\kappa$) or case two ($\kappa_n = 2\kappa$) applies for this mode. Note that all wave numbers are real and $\kappa_n^* = \kappa_n$, since only propagating modes are considered. The second case in Eq.(2.41) is referred to as phase velocity matching – or short, phase matching – as the condition on the wave numbers implies that the phase velocities of the primary and the secondary mode are the same. The result is a linear increase of the second harmonic amplitude, while the first case leads to a sinusoidal behavior of the secondary amplitude. Both cases are discussed in more detail in Section 2.2.3 and Section 2.2.4, respectively.

The possiblity of a secondary mode to be excited in general, however, is independent of the condition on the wave numbers. Eq.(2.41) shows that the quantity

$$a_n = \frac{f_n^{\mathrm{vol}} + f_n^{\mathrm{surf}}}{4\mathcal{P}_{nn}} \tag{2.43}$$

needs to be nonzero for a secondary mode n to enter the modal expansion. Eqs.(2.37) for f_n^{vol} and f_n^{surf} may be interpreted as power fluxes from the primary mode to the secondary mode n via body forces and surface tractions, respectively. That is, the quantity a_n is zero if there is no power flux from the primary mode to the respective secondary mode n. If the power flux is nonzero, the values of f_n^{vol} and f_n^{surf} indicate the intensity of coupling between the primary and the secondary mode n due to nonlinearities, i.e. a high absolute value indicates that the secondary mode n is easily excited by the primary mode. With regard to practical methods measuring the secondary amplitude, high energy coupling between the primary and the secondary wave is desirable, since it leads to higher measurable amplitudes.

The term $\mathcal{P}_{nn}$ displays the power flux of the secondary mode n and is nonzero for propagating modes. It serves as a normalization factor to compensate for the degree of freedom in the choice of the secondary mode in the expansion, as Eqs.(2.18) and (2.20) leave the value for D or C, respectively, open.

Extension of the problem to several primary modes traveling at different frequencies is easily achieved by performing the discussed analysis for each primary mode and adding the obtained secondary solution sums. This procedure is justified by the fact that the perturbation analysis transforms the nonlinear problem into linear problems so that the superposition principle may be applied.

2.2.2 Symmetry Properties of the Secondary Wave

Based on the modal solution presented above, both De Lima [5] and Deng [8] conclude symmetry properties of the secondary wave. Surprisingly, their conclusions are contradictory. De Lima states that a primary mode can generate a secondary mode

only of the same symmetry, e.g. an antisymmetric primary mode can excite an antisymmetric but not a symmetric secondary mode, and vice versa. In contrast, Deng states that the secondary wave must be purely symmetric, thus contradicting De Lima who allows second harmonic generation from an antisymmetric to an antisymmetric mode. While it seems to be common sense that a symmetric primary can generate a symmetric secondary mode, Deng does not conclude explicitly that a symmetric secondary mode can be generated by an antisymmetric primary mode. This question is of practical importance in experiments since antisymmetric modes are easier to excite and therefore preferred to symmetric modes.

This section intends to clarify the issues mentioned above using the modal solution presented in Section 2.1. As discussed in Section 2.2.1, nonzero power flux from the primary to the secondary mode is necessary for a secondary mode to be generated. That is to say, $f_n^{\text{vol}} + f_n^{\text{surf}} \neq 0$ means that mode n is generated by the primary wave, while for $f_n^{\text{vol}} + f_n^{\text{surf}} = 0$, mode n is not generated by the primary mode. In general, f_n^{vol} and f_n^{surf} are very complicated to compute, being comprised of many terms that need to be multiplied, simplified and integrated. This task is approached later on in Chapter 4 using the symbolic toolbox of Matlab. Conclusions on symmetries can be achieved, however, by utilizing simple symmetry properties of functions.

2.2.2.1 Symmetric Primary Mode

First, let the primary mode be a symmetric Lamb mode whose displacement field is given in Eqs.(2.18). Also recalling Figure 2.1, it is observed that the displacement field is independent of x and its x-component is zero, which results in a two-dimensional description in the y-z-plane. The same holds for antisymmetric Lamb modes.

In order to investigate symmetries along the y-axis, the following notation is introduced: $\mathcal{S}(y)$ is a generic, unspecified element of the set of symmetric functions in y, while $\mathcal{A}(y)$ is a generic, unspecified element of the set of antisymmetric functions in

y. As discussed in Section 2.1.2.1 on the primary solution, $u_y = \mathcal{A}(y)$ and $u_z = \mathcal{S}(y)$ hold for a symmetric mode. Further, it is seen that a derivative of u_i with respect to y changes the type symmetry in y, while a derivative with respect to z does not change the type of symmetry in y. Moreover, the following rules are known:

1. $\mathcal{S}(y) \cdot \mathcal{S}(y) = \mathcal{S}(y)$ and $\mathcal{A}(y) \cdot \mathcal{A}(y) = \mathcal{S}(y)$,
2. $\mathcal{A}(y) \cdot \mathcal{S}(y) = \mathcal{A}(y)$ and $\mathcal{S}(y) \cdot \mathcal{A}(y) = \mathcal{A}(y)$,
3. $\mathcal{S}(y) + \mathcal{S}(y) = \mathcal{S}(y)$ and $\mathcal{A}(y) + \mathcal{A}(y) = \mathcal{A}(y)$.

Using these results, each term in Eq.(2.14b) can be investigated in the same way as it is shown exemplarily for the first term as follows

$$\begin{aligned}\frac{\partial u_k}{\partial a_l}\frac{\partial u_k}{\partial a_l} &= \frac{\partial u_y}{\partial y}\frac{\partial u_y}{\partial y} + \frac{\partial u_y}{\partial z}\frac{\partial u_y}{\partial z} + \frac{\partial u_z}{\partial y}\frac{\partial u_z}{\partial y} + \frac{\partial u_z}{\partial z}\frac{\partial u_z}{\partial z} = \\ &= \mathcal{S}^2(y) + \mathcal{A}^2(y) + \mathcal{A}^2(y) + \mathcal{S}^2(y) = \\ &= \mathcal{S}(y) + \mathcal{S}(y) + \mathcal{S}(y) + \mathcal{S}(y) = \mathcal{S}(y). \end{aligned} \tag{2.44}$$

For completeness, Appendix B shows the calculation for all terms in Eq.(2.14b), which yields

$$\bar{\boldsymbol{S}}_{\text{sym}} = \begin{pmatrix} \mathcal{S}(y) & \mathcal{A}(y) \\ \mathcal{A}(y) & \mathcal{S}(y) \end{pmatrix}. \tag{2.45a}$$

Furthermore, by the definition of $\bar{\boldsymbol{f}}$ in Eq.(2.13),

$$\bar{\boldsymbol{f}}_{\text{sym}} = \begin{pmatrix} \frac{\partial}{\partial y} & \frac{\partial}{\partial z} \end{pmatrix} \cdot \begin{pmatrix} \mathcal{S}(y) & \mathcal{A}(y) \\ \mathcal{A}(y) & \mathcal{S}(y) \end{pmatrix} = \begin{pmatrix} \mathcal{A}(y) \\ \mathcal{S}(y) \end{pmatrix}, \tag{2.45b}$$

where the subscript stands for the type of symmetry of the primary mode.

2.2.2.2 Antisymmetric Primary Mode

Before attention is drawn on the conclusions, the same preparatory work is perfomed for the case of an antisymmetric primary mode. Given the displacement field for antisymmetric modes in Eqs.(2.20), it is seen that $u_y = \mathcal{S}(y)$ and $u_z = \mathcal{A}(y)$. Application

to the same exemplary term as in the section above

$$\frac{\partial u_k}{\partial a_l}\frac{\partial u_k}{\partial a_l} = \frac{\partial u_y}{\partial y}\frac{\partial u_y}{\partial y} + \frac{\partial u_y}{\partial z}\frac{\partial u_y}{\partial z} + \frac{\partial u_z}{\partial y}\frac{\partial u_z}{\partial y} + \frac{\partial u_z}{\partial z}\frac{\partial u_z}{\partial z} =$$
$$= \mathcal{A}^2(y) + \mathcal{S}^2(y) + \mathcal{S}^2(y) + \mathcal{A}^2(y) =$$
$$= \mathcal{S}(y) + \mathcal{S}(y) + \mathcal{S}(y) + \mathcal{S}(y) = \mathcal{S}(y) \tag{2.46}$$

shows that – although each single term changes its symmetry – the result is the same in terms of symmetry as for the symmetric primary mode above. This is due to the fact that products of displacements are involved. Again, by carrying out this manipulation for all the terms of Eq.(2.14b) in Appendix B, one obtains

$$\bar{\boldsymbol{S}}_{\text{asym}} = \begin{pmatrix} \mathcal{S}(y) & \mathcal{A}(y) \\ \mathcal{A}(y) & \mathcal{S}(y) \end{pmatrix}, \tag{2.47a}$$

and thus,

$$\bar{\boldsymbol{f}}_{\text{asym}} = \begin{pmatrix} \mathcal{A}(y) \\ \mathcal{S}(y) \end{pmatrix}, \tag{2.47b}$$

as above. Hence, the forcing terms show the same symmetry properties for the cases when the primary mode is either symmetric or antisymmetric.

2.2.2.3 Conclusion

Eqs.(2.25) show that the y-coordinate symmetry properties of $\bar{\boldsymbol{f}}$ and $\bar{\boldsymbol{S}}$ are identical to those of $\bar{\boldsymbol{f}}^{2\omega}$ and $\bar{\boldsymbol{S}}^{2\omega}$, since only the dependency on $\exp(2i(\kappa z - \omega t))$ is removed. Hence, the final conclusion on the power fluxes f_n^{vol} or f_n^{surf} in Eqs.(2.37) depends on the symmetry of the secondary mode n considered in the expansion. Since

$$\boldsymbol{v}(y,z,t) = -i\omega\,\boldsymbol{u}(y,z,t), \tag{2.48}$$

the symmetry properties of the particle velocity equal those of the displacements, i.e.

$$\tilde{\boldsymbol{v}}_{\text{sym}} = \begin{pmatrix} \mathcal{A}(y) \\ \mathcal{S}(y) \end{pmatrix} \tag{2.49a}$$

for a symmetric mode, and

$$\tilde{\boldsymbol{v}}_{\text{asym}} = \begin{pmatrix} \mathcal{S}(y) \\ \mathcal{A}(y) \end{pmatrix} \tag{2.49b}$$

for an antisymmetric mode. Finally, with $\mathbf{n}_y = (1,\ 0)$ and the secondary mode being symmetric, Eqs.(2.37) read as

$$\begin{aligned} f_n^{\text{surf}} &= \begin{pmatrix} 1, & 0 \end{pmatrix} \cdot \begin{pmatrix} \mathcal{S}(y) & \mathcal{A}(y) \\ \mathcal{A}(y) & \mathcal{S}(y) \end{pmatrix} \cdot \begin{pmatrix} \mathcal{A}(y) \\ \mathcal{S}(y) \end{pmatrix} \Big|_{y=-h}^{h} \\ &= \mathcal{A}(y) \Big|_{y=-h}^{h} \neq 0, \end{aligned} \tag{2.50a}$$

$$\begin{aligned} f_n^{\text{vol}} &= \int_{y=-h}^{h} \begin{pmatrix} \mathcal{A}(y) \\ \mathcal{S}(y) \end{pmatrix}^T \cdot \begin{pmatrix} \mathcal{A}(y) \\ \mathcal{S}(y) \end{pmatrix} \mathrm{d}y \\ &= \int_{y=-h}^{h} \mathcal{S}(y)\, \mathrm{d}y \neq 0. \end{aligned} \tag{2.50b}$$

It is noted that the inequality from zero holds in general, but there might be special frequencies and pairs of primary and secondary modes, for which at least one of these terms or their sum can be zero. Thus, if the secondary mode is symmetric, $A_n(z) \neq 0$ holds generally.

For the secondary mode being antisymmetric, one obtains

$$\begin{aligned} f_n^{\text{surf}} &= \begin{pmatrix} 1, & 0 \end{pmatrix} \cdot \begin{pmatrix} \mathcal{S}(y) & \mathcal{A}(y) \\ \mathcal{A}(y) & \mathcal{S}(y) \end{pmatrix} \cdot \begin{pmatrix} \mathcal{S}(y) \\ \mathcal{A}(y) \end{pmatrix} \Big|_{y=-h}^{h} \\ &= \mathcal{S}(y) \Big|_{y=-h}^{h} = 0, \end{aligned} \tag{2.51a}$$

$$\begin{aligned} f_n^{\text{vol}} &= \int_{y=-h}^{h} \begin{pmatrix} \mathcal{S}(y) \\ \mathcal{A}(y) \end{pmatrix}^T \cdot \begin{pmatrix} \mathcal{A}(y) \\ \mathcal{S}(y) \end{pmatrix} \mathrm{d}y \\ &= \int_{y=-h}^{h} \mathcal{A}(y)\, \mathrm{d}y = 0, \end{aligned} \tag{2.51b}$$

implying that $A_n(z) = 0$ according to Eq.(2.41).

Summarizing these results, it is concluded that both a symmetric and an antisymmetric primary mode can excite a symmetric mode at twice the primary frequency.

In contrast, neither a symmetric nor an antisymmetric primary mode can excite an antisymmetric mode at twice the primary frequency. Figure 2.5 displays this result graphically.

Other authors [7, 8, 25] have declared that the secondary wave is purely symmetric at the double frequency. However, they do not prove explicitly that the cross-modal excitation from an antisymmetric primary mode to a symmetric secondary mode is possible.

2.2.3 Internal Resonance

Recalling the modal solution of Section 2.1.2, it was observed that the amplitude coefficient $A_n(z)$ in Eq.(2.41) shows two fundamentally different behaviors depending on the relation between the wave numbers of the primary mode and the nth secondary mode. The second case in Eq.(2.41) is referred to as phase velocity matching or phase matching, since

$$\kappa^{(2)} = 2\kappa \quad \text{and} \quad \omega^{(2)} = 2\omega \tag{2.52}$$

imply with Eq.(2.22) that

$$c_{\mathrm{ph}}^{(2)} = \frac{\omega^{(2)}}{\kappa^{(2)}} = \frac{\omega}{\kappa} = c_{\mathrm{ph}}^{(1)}, \tag{2.53}$$

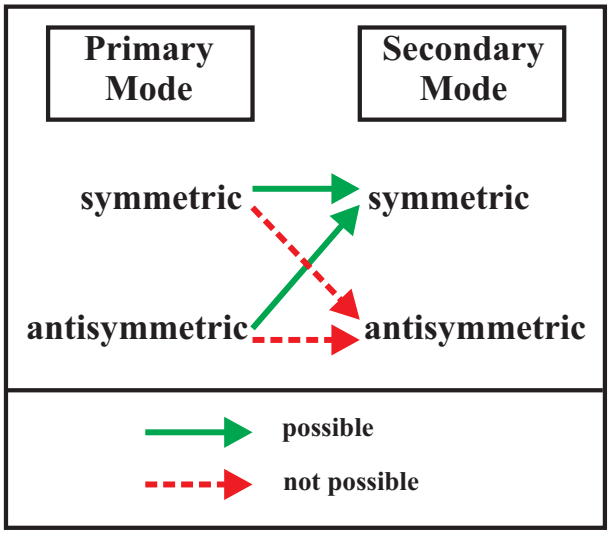

Figure 2.5: Symmetry Scheme of Second Harmonic Lamb Wave Generation

where the superscript (1) stands for the primary and (2) for the secondary mode. That is, the primary and the secondary mode match phase velocity. Recalling Figure 2.4, a case of phase velocity matching is observed between the S1 mode and the S2 mode. Further investigations on phase matching are performed in Chapter 3.

If in addition to phase matching, nonzero power flux from the primary to the secondary wave is assumed, the mode is called to show internal resonance. In this case, the solution for mode n in the expansion takes the form

$$\boldsymbol{u}_n^{(2)} = a_n \, z \, \tilde{\boldsymbol{u}}_n^{(2)}(y) \, e^{2i(\kappa z - \omega t)}, \tag{2.54}$$

where $a_n \neq 0$ is defined in Eq.(2.43). The terminology *internal resonance* is motivated by the linearly growing amplitude with propagation distance z. The proportionality between amplitude and propagation distance suggests that the secondary mode can grow without any bounds. This obviously unrealistic behavior is prohibited by the perturbation condition Eq.(2.10). Once Eq.(2.10) is violated, this perturbation solution is no longer valid. That is, conclusions can only be drawn up to a certain propagation distance, which must be determined in the specific application.

For material's characterization applications in NDE, internal resonance has several important advantages. Firstly, the growing amplitude results in large displacements after some propagation distance, making the signal-to-noise ratio better for measurements. Secondly, the proportionality between amplitude and propagation distance makes it straightforward to calculate the power flux from the primary wave, as the slope in an amplitude-distance-diagram. And finally, after some distance, other modes that are not in internal resonance, as discussed in the following section, may be disregarded as small when compared to the mode in resonance, so they do not disturb measurements of the resonant mode under consideration. In the following discussion of non-resonant modes, the advantages to require internal resonance for practical applications become even clearer.

2.2.4 Non-Resonant Solution

The non-resonant solution represents the usual case. If $\kappa^{(2)} \neq 2\kappa$ the solution for the respective secondary mode n is written as

$$\boldsymbol{u}_n^{(2)} = \frac{a_n i}{\kappa_\mathrm{d}} \, \tilde{\boldsymbol{u}}_n^{(2)}(y) \, \left(e^{2i\kappa z} - e^{i\kappa^{(2)} z} \right) \, e^{-2i\omega t}, \tag{2.55}$$

according to Eq.(2.41), where

$$\kappa_\mathrm{d} = \kappa^{(2)} - 2\kappa \tag{2.56}$$

is interpreted as the deviance from phase matching. Using complex algebra, Eq.(2.55) can be rewritten as

$$\boldsymbol{u}_n^{(2)} = \frac{2a_n}{\kappa_\mathrm{d}} \sin(\tfrac{1}{2}\kappa_\mathrm{d} z) \, \tilde{\boldsymbol{u}}_n^{(2)}(y) \, e^{i\left(\frac{1}{2}(2\kappa+\kappa^{(2)})z - 2\omega t\right)}. \tag{2.57}$$

A few observations are noted. First, the maximum amplitude varies sinusoidally with propagation distance. At distances z, where the sine term becomes zero, the displacements are identically zero for all times. The distance between those points is called the dispersion length and defined by

$$L_n = \frac{2\pi}{\kappa_\mathrm{d}}. \tag{2.58}$$

Also, the maximum amplitude is bounded by the term $2a_n/\kappa_\mathrm{d}$. These features reveal the infeasibility of these modes for experimental use.

If, however, κ_d is small, the solution behaves approximately like internal resonance. That is, for some propagation distance the amplitude grows almost linearly. The valid distance of this approximation can be assessed intuitively as one fourth of the dispersion length, i.e.

$$L_n^{\mathrm{use}} = \frac{1}{4} L_n. \tag{2.59}$$

Thus, not only phase matching modes are of interest for application methods, but also modes that deviate only slightly from exact phase matching. Figure 2.6 shows the qualitative behavior of the second harmonic amplitude depending on phase matching. An example of the application of this concept is given in Chapter 4.

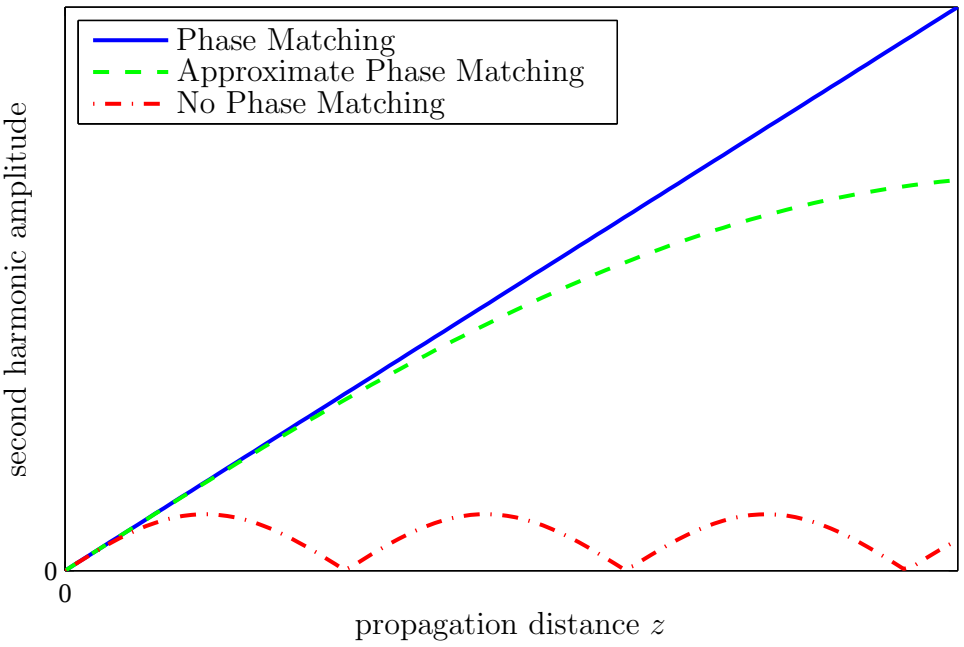

Figure 2.6: Qualitative Behavior of the Second Harmonic Amplitude

CHAPTER III

CHARACTERIZATION OF MODES WITH INTERNAL RESONANCE

Having shown in Section 2.2 that exact or approximate internal resonance is a desirable feature for practical methods, the next step is to analyze the theory of Lamb waves with respect to modes satisfying internal resonance. Apart from phase velocity matching and nonzero powerflux, which were stated as necessary conditions for internal resonance already, the condition of group velocity matching will be required, meaning that the primary and the secondary mode have the same group velocity. Furthermore, using the existing theory of Lamb modes as summarized in Appendix A, conclusions on the displacements at the surface can be drawn, which are critical as to measurements of motions in the plate.

The following section introduces the concepts of phase velocity matching and group velocity matching mentioned above in a more detailed way and shows preliminary manipulations for subsequent sections, where different categories of modes showing internal resonance are analyzed.

The calculus of this chapter is independent of the material's properties and, therefore, employs a large number of analytical relations. In Section 3.2, summaries at the end of each subsection present the results concisely. Also, Chapter 4 presents these results applied for the example of an aluminum plate, which might be more useful for the more practically oriented reader.

3.1 Preliminary

3.1.1 Phase Velocity Matching

Nonzero power flux from the primary mode and phase velocity matching are the conditions for internal resonance. The symmetry analysis in Section 2.2.2 shows that nonzero power flux can be satisfied in general, if and only if the secondary mode is symmetric. The major effort in this chapter, therefore, is to find modes satisfying phase velocity matching. For further manipulations, the normalization

$$\bar{\omega} = \omega h, \quad \bar{\kappa} = \kappa h, \quad \bar{\alpha} = \alpha h, \quad \bar{\beta} = \beta h, \tag{3.1}$$

is found to be useful. Note that $\bar{\omega}$ is not dimensionless but has the unit of an angular frequency-thickness product. Then, phase velocity matching is defined as follows.

Definition. *(Phase Velocity Matching) Let X and Y be Lamb modes, $c_{ph,X}$ the phase velocity of X at frequency $\bar{\omega}$ and $c_{ph,Y}^{(2\omega)}$ the phase velocity of Y at frequency $2\bar{\omega}$. Phase velocity matching from X to Y is defined as the fact that $c_{ph,X} = c_{ph,Y}^{(2\omega)}$. By the definition of the phase velocity in Eq.(2.22), this also implies, if X has the values $\bar{\kappa}$, $\bar{\alpha}$ and $\bar{\beta}$ at frequency $\bar{\omega}$, then Y has the values*

$$\bar{\omega}^{(2\omega)} = 2\bar{\omega}, \quad \bar{\kappa}^{(2\omega)} = 2\bar{\kappa}, \quad \bar{\alpha}^{(2\omega)} = 2\bar{\alpha}, \quad \bar{\beta}^{(2\omega)} = 2\bar{\beta}. \tag{3.2}$$

at frequency $2\bar{\omega}$. The terminology 'phase matching' is equivalent to 'phase velocity matching' in this work.

3.1.2 Group Velocity Matching

In practical applications, where signals are neither pure harmonics nor infinitely long in time, as assumed by the solution presented in Chapter 2, the group velocity of the signal plays an important role. Rose [22] states that the "group velocity is associated with the propagation velocity of a group of waves of similar frequency," and is defined as

$$c_{\mathrm{g}} = \frac{\mathrm{d}\omega}{\mathrm{d}\kappa} = \frac{\mathrm{d}\bar{\omega}}{\mathrm{d}\bar{\kappa}}. \tag{3.3}$$

Achenbach [1] shows that the velocity of energy equals group velocity, meaning that the speed of a finite "wave packet" is given by the group velocity, not by the phase velocity. For finite signals in the time domain, it follows that signals at different group velocities shift relative to each other with propagation distance. If the primary and the secondary mode have different group velocities, the secondary mode generated at the beginning and the primary mode separate locally, making the power flux from the primary to the initial secondary mode zero. Thus, a bounded secondary wave arises, whose amplitude does not show linear increase. Therefore, for practical applications, in which only finite wave packets are used, group velocity matching is required. The definition of group velocity matching follows.

Definition. *(Group Velocity Matching) Let X and Y be Lamb modes, $c_{g,X}$ the group velocity of X at frequency $\bar{\omega}$ and $c_{g,Y}^{(2\omega)}$ the group velocity of Y at frequency $2\bar{\omega}$. Group velocity matching from X to Y is defined as the fact that $c_{g,X} = c_{g,Y}^{(2\omega)}$. The terminology 'group matching' is equivalent to 'group velocity matching' in this work.*

While it is commonly agreed on that phase velocity matching is a necessary condition, the concept of group velocity matching is more controversial. Deng et al. [9], for instance, deny group matching as a necessary condition, while Lee et al. [14] support the argumentation given above. The analytical complexity to describe the influence of the group velocity on time domain signals makes analytical arguments to prove one or the other statement difficult. The physical interpretation given above suggests group velocity matching at least as an adjuvant condition, if not necessary. The following paragraphs show some preliminary analysis on group velocity.

There are different ways to express group velocity in terms of the variables $\bar{\omega}$, $\bar{\kappa}$ and c_{ph}. Note that according to Eq.(2.22), only two of these values are independent. First, an expression in terms of $\bar{\omega}$ and $\bar{\kappa}$ is derived. By rewriting the frequency equation for symmetric modes in Eq.(2.17) and for antisymmetric modes in Eq.(2.19), respectively,

as

$$\Phi_{\mathrm{sym}}(\bar{\omega},\bar{\kappa}) = \cos\bar{\alpha}\sin\bar{\beta}\ (\bar{\kappa}^2-\bar{\beta}^2)^2 + \sin\bar{\alpha}\cos\bar{\beta}\ 4\bar{\alpha}\bar{\beta}\bar{\kappa}^2 = 0 \tag{3.4}$$

and

$$\Phi_{\mathrm{asym}}(\bar{\omega},\bar{\kappa}) = \sin\bar{\alpha}\cos\bar{\beta}\ (\bar{\kappa}^2-\bar{\beta}^2)^2 + \cos\bar{\alpha}\sin\bar{\beta}\ 4\bar{\alpha}\bar{\beta}\bar{\kappa}^2 = 0, \tag{3.5}$$

the frequency equations are expressed as implicit functions of $\bar{\omega}$ and $\bar{\kappa}$. If $\bar{\omega}$ is regarded as $\bar{\omega} = \bar{\omega}(\bar{\kappa})$, the group velocity reads as

$$c_{\mathrm{g,sym}} = -\frac{\partial\Phi_{\mathrm{sym}}/\partial\bar{\kappa}}{\partial\Phi_{\mathrm{sym}}/\partial\bar{\omega}} = \frac{N_{\mathrm{sym}}}{D_{\mathrm{sym}}} \tag{3.6}$$

and

$$c_{\mathrm{g,asym}} = -\frac{\partial\Phi_{\mathrm{asym}}/\partial\bar{\kappa}}{\partial\Phi_{\mathrm{asym}}/\partial\bar{\omega}} = \frac{N_{\mathrm{asym}}}{D_{\mathrm{asym}}}, \tag{3.7}$$

according to Eq.(3.3) and the rules of derivatives of implicit functions. By carrying out these derivatives, one obtains

$$\begin{aligned} N_{\mathrm{sym}} = {} & \cos\bar{\alpha}\cos\bar{\beta}\left[\bar{\alpha}\bar{\kappa}(\bar{\kappa}^2-\bar{\beta}^2)^2 + 4\bar{\alpha}\bar{\beta}^2\bar{\kappa}^3\right] \\ & - \sin\bar{\alpha}\sin\bar{\beta}\left[\bar{\beta}\bar{\kappa}(\bar{\kappa}^2-\bar{\beta}^2)^2 + 4\bar{\alpha}^2\bar{\beta}\bar{\kappa}^3\right] \\ & + \sin\bar{\alpha}\cos\bar{\beta}\left[4\bar{\beta}^2\bar{\kappa}^3 + 4\bar{\alpha}^2\bar{\kappa}^3 - 8\bar{\alpha}^2\bar{\beta}^2\bar{\kappa}\right] \\ & - \cos\bar{\alpha}\sin\bar{\beta}\ 8\bar{\alpha}\bar{\beta}\bar{\kappa}(\bar{\kappa}^2-\bar{\beta}^2), \end{aligned} \tag{3.8a}$$

$$\begin{aligned} D_{\mathrm{sym}} = {} & \cos\bar{\alpha}\cos\bar{\beta}\left[\bar{\alpha}(\bar{\omega}/c_{\mathrm{T}}^2)(\bar{\kappa}^2-\bar{\beta}^2)^2 + 4\bar{\alpha}\bar{\beta}^2\bar{\kappa}^2(\bar{\omega}/c_{\mathrm{L}}^2)\right] \\ & - \sin\bar{\alpha}\sin\bar{\beta}\left[\bar{\beta}(\bar{\omega}/c_{\mathrm{L}}^2)(\bar{\kappa}^2-\bar{\beta}^2)^2 + 4\bar{\alpha}^2\bar{\beta}\bar{\kappa}^2(\bar{\omega}/c_{\mathrm{T}}^2)\right] \\ & + \sin\bar{\alpha}\cos\bar{\beta}\left[4\bar{\beta}^2\bar{\kappa}^2(\bar{\omega}/c_{\mathrm{L}}^2) + 4\bar{\alpha}^2\bar{\kappa}^2(\bar{\omega}/c_{\mathrm{T}}^2)\right] \\ & - \cos\bar{\alpha}\sin\bar{\beta}\ 4\bar{\alpha}\bar{\beta}(\bar{\omega}/c_{\mathrm{T}}^2)(\bar{\kappa}^2-\bar{\beta}^2), \end{aligned} \tag{3.8b}$$

for symmetric modes and

$$\begin{aligned} N_{\text{asym}} = &\cos\bar{\alpha}\cos\bar{\beta}\left[\bar{\beta}\bar{\kappa}(\bar{\kappa}^2-\bar{\beta}^2)^2+4\bar{\alpha}^2\bar{\beta}\bar{\kappa}^3\right] \\ &-\sin\bar{\alpha}\sin\bar{\beta}\left[\bar{\alpha}\bar{\kappa}(\bar{\kappa}^2-\bar{\beta}^2)^2+4\bar{\alpha}\bar{\beta}^2\bar{\kappa}^3\right] \\ &-\sin\bar{\alpha}\cos\bar{\beta}\ 8\bar{\alpha}\bar{\beta}\bar{\kappa}(\bar{\kappa}^2-\bar{\beta}^2) \\ &+\cos\bar{\alpha}\sin\bar{\beta}\left[4\bar{\beta}^2\bar{\kappa}^3+4\bar{\alpha}^2\bar{\kappa}^3-8\bar{\alpha}^2\bar{\beta}^2\bar{\kappa}\right], \end{aligned} \tag{3.9a}$$

$$\begin{aligned} D_{\text{asym}} = &\cos\bar{\alpha}\cos\bar{\beta}\left[\bar{\beta}(\bar{\omega}/c_{\text{L}}^2)(\bar{\kappa}^2-\bar{\beta}^2)^2+4\bar{\alpha}^2\bar{\beta}\bar{\kappa}^2(\bar{\omega}/c_{\text{T}}^2)\right] \\ &-\sin\bar{\alpha}\sin\bar{\beta}\left[\bar{\alpha}(\bar{\omega}/c_{\text{T}}^2)(\bar{\kappa}^2-\bar{\beta}^2)^2+4\bar{\alpha}\bar{\beta}^2\bar{\kappa}^2(\bar{\omega}/c_{\text{L}}^2)\right] \\ &-\sin\bar{\alpha}\cos\bar{\beta}\ 4\bar{\alpha}\bar{\beta}(\bar{\omega}/c_{\text{T}}^2)(\bar{\kappa}^2-\bar{\beta}^2) \\ &+\cos\bar{\alpha}\sin\bar{\beta}\left[4\bar{\beta}^2\bar{\kappa}^2(\bar{\omega}/c_{\text{L}}^2)+4\bar{\alpha}^2\bar{\kappa}^2(\bar{\omega}/c_{\text{T}}^2)\right], \end{aligned} \tag{3.9b}$$

for antisymmetric modes. Keep in mind that both $\bar{\alpha}$ and $\bar{\beta}$ are functions of $\bar{\omega}$ and $\bar{\kappa}$. A description of the group velocity in terms of $\bar{\omega}$ and c_{ph}

$$c_{\text{g}} = c_{\text{ph}}^2\left(c_{\text{ph}}-\bar{\omega}\frac{\mathrm{d}c_{\text{ph}}}{\mathrm{d}\bar{\omega}}\right)^{-1}. \tag{3.10}$$

is presented by Rose [22].

3.2 Matching Pairs

In this section, linear Lamb mode pairs satisfying phase matching, as the principal condition, and group matching, as a subordinate condition, are presented and analyzed. Due to the demonstrated nonexistence of antisymmetric secondary modes, the focus is on symmetric modes at the double frequency. Each subsection about the different types of modes provides general information and conditions, a proof of phase velocity matching and group velocity matching, respectively, and an investigation of the displacement field, especially at the surface.

3.2.1 Crossing Points of Symmetric and Antisymmetric Modes

In the region $c_{\mathrm{ph}} > c_{\mathrm{L}}$, it is possible for symmetric and antisymmetric modes to cross, as will be shown. These distinctive points of crossing, called crossing points from now on, have already found applications in experiments as for example in Deng et al. [9].

3.2.1.1 General Conditions

First, it is noted that both $\bar{\alpha}$ and $\bar{\beta}$ are real and positive in the region $c_{\mathrm{ph}} > c_{\mathrm{L}}$. A crossing point is characterized by the fact that both Eqs.(3.4) and (3.5) need to be satisfied simultaneously. By subtraction of Eq.(3.4) from Eq.(3.5) one obtains

$$\left(\sin\bar{\alpha}\cos\bar{\beta} - \cos\bar{\alpha}\sin\bar{\beta}\right)\left((\bar{\kappa}^2 - \bar{\beta}^2)^2 - 4\bar{\alpha}\bar{\beta}\bar{\kappa}^2\right) = 0. \tag{3.11}$$

Solving for

$$(\bar{\kappa}^2 - \bar{\beta}^2)^2 - 4\bar{\alpha}\bar{\beta}\bar{\kappa}^2 = 0 \tag{3.12}$$

reduces to the solution of the Rayleigh equation (see Graff [10] for reference), which is not the solution sought after. Hence, from Eq.(3.11)

$$\sin\bar{\alpha}\cos\bar{\beta} - \cos\bar{\alpha}\sin\bar{\beta} = \sin(\bar{\alpha} - \bar{\beta}) = 0 \tag{3.13}$$

or

$$\bar{\alpha} - \bar{\beta} = n\pi, \quad n \in \mathbb{N} \tag{3.14}$$

is inferred. Substituting this condition into Eq.(3.4)

$$\cos(n\pi + \bar{\beta})\sin\bar{\beta}\ (\bar{\kappa}^2 - \bar{\beta}^2)^2 + \sin(n\pi + \bar{\beta})\cos\bar{\beta}\ 4\bar{\alpha}\bar{\beta}\bar{\kappa}^2 = 0 \tag{3.15}$$

yields

$$\cos\bar{\beta}\sin\bar{\beta}\ (\bar{\kappa}^2 - \bar{\beta}^2)^2 + \sin\bar{\beta}\cos\bar{\beta}\ 4\bar{\alpha}\bar{\beta}\bar{\kappa}^2 = 0, \tag{3.16}$$

hence one concludes

$$\bar{\beta} = n\pi/2, \quad n \in \mathbb{N}^+. \tag{3.17}$$

Recalling Eq.(3.14), it is proved that at a crossing point either case I

$$\bar{\beta} = n_\beta \pi, \quad \bar{\alpha} = n_\alpha \pi, \quad n_\beta, n_\alpha \in \mathbb{N}^+ \tag{3.18}$$

or case II

$$\bar{\beta} = \tfrac{(2n_\beta - 1)\pi}{2}, \quad \bar{\alpha} = \tfrac{(2n_\alpha - 1)\pi}{2}, \quad n_\beta, n_\alpha \in \mathbb{N}^+ \tag{3.19}$$

must hold. Eq.(3.18) is referred to as case I and Eq.(3.19) as case II. Note that $n_\beta > n_\alpha$ by the definition of $\bar{\alpha}$ and $\bar{\beta}$. Using Eq.(2.21), these conditions allow for the computation of the corresponding frequencies as

$$\bar{\omega} = \sqrt{\frac{n}{c_\mathrm{L}^2 - c_\mathrm{T}^2}}\, c_\mathrm{L} c_\mathrm{T} \pi, \tag{3.20}$$

where $n = n_\beta^2 - n_\alpha^2$ for case I, and $n = n_\beta(n_\beta - 1) - n_\alpha(n_\alpha - 1)$ for case II.

3.2.1.2 Phase Velocity Matching

Assuming that $(\bar{\omega}, \bar{\kappa})$ is a crossing point, Eq.(3.18) or Eq.(3.19) must hold. In the case of phase matching, it is concluded for both cases with Eq.(3.2) that

$$\bar{\beta}^{(2\omega)} = \bar{n}_\beta \pi, \quad \bar{\alpha}^{(2\omega)} = \bar{n}_\alpha \pi, \quad \bar{n}_\beta, \bar{n}_\alpha \in \mathbb{N}^+, \tag{3.21}$$

at frequency $2\bar{\omega}$. For case I, $\bar{n}_\beta, \bar{n}_\alpha$ are even, and odd for case II. This fulfills Eq.(3.18) and it follows that $(\bar{\omega}^{(2\omega)}, \bar{\kappa}^{(2\omega)})$ is a crossing point of case I, which matches phase velocity with the point $(\bar{\omega}, \bar{\kappa})$. By the definition of a crossing point, it is obvious that there is phase velocity matching from the symmetric as well as from the antisymmetric mode to both the symmetric and antisymmetric mode at the double frequency.

3.2.1.3 Group Velocity Matching

To calculate the group velocities, the results from Eqs.(3.6) to (3.9) are recalled. For case I, using Eq.(3.18) the group velocity takes the form

$$c_{\mathrm{g,sym}}^{\mathrm{I}} = \frac{\bar{\kappa}(\bar{\kappa}^2 - \bar{\beta}^2)^2 + 4\bar{\beta}^2\bar{\kappa}^3}{(\bar{\omega}/c_\mathrm{T}^2)(\bar{\kappa}^2 - \bar{\beta}^2)^2 + 4\bar{\beta}^2\bar{\kappa}^2(\bar{\omega}/c_\mathrm{L}^2)}, \tag{3.22}$$

$$c_{\mathrm{g,asym}}^{\mathrm{I}} = \frac{\bar{\kappa}(\bar{\kappa}^2 - \bar{\beta}^2)^2 + 4\bar{\alpha}^2\bar{\kappa}^3}{(\bar{\omega}/c_\mathrm{L}^2)(\bar{\kappa}^2 - \bar{\beta}^2)^2 + 4\bar{\alpha}^2\bar{\kappa}^2(\bar{\omega}/c_\mathrm{T}^2)}, \tag{3.23}$$

while for case II, using Eq.(3.19) one arrives at

$$c^{\mathrm{II}}_{\mathrm{g,sym}} = \frac{\bar{\kappa}(\bar{\kappa}^2 - \bar{\beta}^2)^2 + 4\bar{\alpha}^2\bar{\kappa}^3}{(\bar{\omega}/c_{\mathrm{L}}^2)(\bar{\kappa}^2 - \bar{\beta}^2)^2 + 4\bar{\alpha}^2\bar{\kappa}^2(\bar{\omega}/c_{\mathrm{T}}^2)}, \tag{3.24}$$

$$c^{\mathrm{II}}_{\mathrm{g,asym}} = \frac{\bar{\kappa}(\bar{\kappa}^2 - \bar{\beta}^2)^2 + 4\bar{\beta}^2\bar{\kappa}^3}{(\bar{\omega}/c_{\mathrm{T}}^2)(\bar{\kappa}^2 - \bar{\beta}^2)^2 + 4\bar{\beta}^2\bar{\kappa}^2(\bar{\omega}/c_{\mathrm{L}}^2)}. \tag{3.25}$$

Note that $c^{\mathrm{I}}_{\mathrm{g,sym}} = c^{\mathrm{II}}_{\mathrm{g,asym}}$ and $c^{\mathrm{II}}_{\mathrm{g,sym}} = c^{\mathrm{I}}_{\mathrm{g,asym}}$ hold.

Regarding the crossing point at the double frequency, it was stated already that it can be only of case I. Further, as phase matching is shown, applying Eq.(3.2) to the group velocities in Eqs.(3.22) and (3.23), the factors of two cancel and it is shown that

$$c^{\mathrm{I}}_{\mathrm{g,sym}} = c^{\mathrm{I},(2\omega)}_{\mathrm{g,sym}}, \tag{3.26}$$

$$c^{\mathrm{I}}_{\mathrm{g,asym}} = c^{\mathrm{I},(2\omega)}_{\mathrm{g,asym}}. \tag{3.27}$$

From the statements above, the following conclusions are made:

- If the crossing point $(\bar{\omega}, \bar{\kappa})$ is case I, there is group velocity matching from the symmetric mode at $(\bar{\omega}, \bar{\kappa})$ to the symmetric mode at $(2\bar{\omega}, 2\bar{\kappa})$, i.e. $c^{\mathrm{I}}_{\mathrm{g,sym}} = c^{\mathrm{I},(2\omega)}_{\mathrm{g,sym}}$, as well as from the antisymmetric mode at $(\bar{\omega}, \bar{\kappa})$ to the antisymmetric mode at $(2\bar{\omega}, 2\bar{\kappa})$, i.e. $c^{\mathrm{I}}_{\mathrm{g,asym}} = c^{\mathrm{I},(2\omega)}_{\mathrm{g,asym}}$.

- If the crossing point $(\bar{\omega}, \bar{\kappa})$ is case II, there is group velocity matching from the symmetric mode at $(\bar{\omega}, \bar{\kappa})$ to the antisymmetric mode at $(2\bar{\omega}, 2\bar{\kappa})$, i.e. $c^{\mathrm{II}}_{\mathrm{g,sym}} = c^{\mathrm{I},(2\omega)}_{\mathrm{g,asym}}$, as well as from the antisymmetric mode at $(\bar{\omega}, \bar{\kappa})$ to the symmetric mode at $(2\bar{\omega}, 2\bar{\kappa})$, i.e. $c^{\mathrm{II}}_{\mathrm{g,asym}} = c^{\mathrm{I},(2\omega)}_{\mathrm{g,sym}}$.

Table 3.1 shows each possible combination along with the results about the displacements at the surface presented in the following subsection.

3.2.1.4 Displacements at the Surface

Looking at case I crossing points, the displacements at the surface follow by substitution of Eq.(3.18) into Eqs.(2.18) and (2.20), setting $y = h$. For symmetric modes,

one obtains

$$\tilde{u}_y^{\mathrm{I}}(h) = 0, \tag{3.28a}$$

$$\tilde{u}_z^{\mathrm{I}}(h) = Dh\bar{\beta}\,\frac{\bar{\kappa}^2+\bar{\beta}^2}{\bar{\kappa}^2-\bar{\beta}^2}\cos\bar{\beta}, \tag{3.28b}$$

where the frequency equation Eq.(2.17) is applied to simplify the expression. The displacements at the surface for the antisymmetric modes take the form

$$\tilde{u}_y^{\mathrm{I}}(h) = iCh\,\frac{\bar{\kappa}^2+\bar{\beta}^2}{2\bar{\kappa}}\cos\bar{\beta}, \tag{3.29a}$$

$$\tilde{u}_z^{\mathrm{I}}(h) = 0, \tag{3.29b}$$

where the frequency equation Eq.(2.19) is used.

Regarding case II crossing points, Eq.(3.19), and (2.17) to (2.20) yield

$$\tilde{u}_y^{\mathrm{II}}(h) = iDh\,\frac{\bar{\kappa}^2+\bar{\beta}^2}{2\bar{\kappa}}\sin\bar{\beta}, \tag{3.30a}$$

$$\tilde{u}_z^{\mathrm{II}}(h) = 0 \tag{3.30b}$$

for symmetric modes, and

$$\tilde{u}_y^{\mathrm{II}}(h) = 0, \tag{3.31a}$$

$$\tilde{u}_z^{\mathrm{II}}(h) = -Ch\bar{\beta}\,\frac{\bar{\kappa}^2+\bar{\beta}^2}{\bar{\kappa}^2-\bar{\beta}^2}\sin\bar{\beta} \tag{3.31b}$$

for antisymmetric modes.

3.2.1.5 Summary

Table 3.1 summarizes the results obtained in this section. Two observations deserve special mention. First, only the first two entries in Table 3.1 satisfy all the conditions required for practical applications. The other entries have either an antisymmetric secondary mode making the power flux from the primary wave zero, or do not match group velocity. Secondly, for all the relevant pairs, the normal displacements at the surface are identically zero, which displays a disadvantage for experiments where transducers excite and measure mainly out-of-plane displacements or particle velocities at the surface.

Table 3.1: Phase Matching Pairs at Crossing Points

FROM MODE AT $\bar{\omega}$				TO MODE AT $2\bar{\omega}$				Group-
Sym.	Case	$\tilde{u}_y(h)$	$\tilde{u}_z(h)$	Sym.	Case	$\tilde{u}_y(h)$	$\tilde{u}_z(h)$	match
sym	I	0	$\neq 0$	sym	I	0	$\neq 0$	yes
asym	II	0	$\neq 0$	sym	I	0	$\neq 0$	yes
sym	II	$\neq 0$	0	sym	I	0	$\neq 0$	no
asym	I	$\neq 0$	0	sym	I	0	$\neq 0$	no
asym	I	$\neq 0$	0	asym	I	$\neq 0$	0	yes
sym	II	$\neq 0$	0	asym	I	$\neq 0$	0	yes
asym	II	0	$\neq 0$	asym	I	$\neq 0$	0	no
sym	I	0	$\neq 0$	asym	I	$\neq 0$	0	no

3.2.2 Symmetric Modes at the Longitudinal Velocity

An investigation of symmetric Lamb modes at the longitudinal phase velocity c_L with regard to normal displacement at the free surface and group velocity was presented by Pilarski et al. [18]. They provide frequency-thickness products, where phase velocity equals longitudinal velocity. Then, they prove that the normal displacement at the surface vanishes and that all modes have the same group velocity at these frequencies, where the group velocity depends only on the linear material properties. In this section, these results are summarized and related to the concepts of phase matching and group matching as defined in Section 3.1.

3.2.2.1 General Conditions

From the condition $c_\mathrm{ph} = c_\mathrm{L}$ and Eq.(2.21), it is inferred that

$$\bar{\alpha} = 0, \tag{3.32}$$

and with the frequency equation for symmetric modes Eq.(3.4)

$$\bar{\beta} = n\pi, \quad n \in \mathbb{N}^+ \tag{3.33}$$

follows. These are the two equations characterizing all the points in the dispersion curve where the phase velocity of symmetric modes equals the longitudinal velocity.

The corresponding frequencies

$$\bar{\omega} = \frac{n\pi c_{\mathrm{T}}}{\sqrt{1-(c_{\mathrm{T}}/c_{\mathrm{L}})^2}}, \quad n \in \mathbb{N}^+ \tag{3.34}$$

are obtained from Eq.(3.32), Eq.(3.33), and the basic relations between $\bar{\omega}$, $\bar{\kappa}$ and $\bar{\beta}$.

3.2.2.2 Phase Velocity Matching

Assuming phase matching, Eq.(3.2) yields

$$\bar{\alpha}^{(2\omega)} = 0 \quad \text{and} \quad \bar{\beta}^{(2\omega)} = 2n\pi, \quad n \in \mathbb{N}^+, \tag{3.35}$$

which satisfies Eqs.(3.32) and (3.33). Thus, there is phase matching from each symmetric mode at frequencies described in Eq.(3.34) to another symmetric mode at double frequency, both having longitudinal phase velocity.

3.2.2.3 Group Velocity Matching

Substitution of Eqs.(3.32) and (3.33) into the relation for the group velocity Eq.(3.6) results in

$$c_{\mathrm{g}} = \frac{\bar{\kappa}(\bar{\kappa}^2-\bar{\beta}^2)^2 + 8\bar{\beta}^2\bar{\kappa}^3}{(\bar{\omega}/c_{\mathrm{T}}^2)(\bar{\kappa}^2-\bar{\beta}^2)^2 + 8\bar{\beta}^2\bar{\kappa}^2(\bar{\omega}/c_{\mathrm{L}}^2)}. \tag{3.36}$$

where the limit $\sin(\bar{\alpha}) \approx \bar{\alpha}$ is used, since $\bar{\alpha}$ is very small. This is simplified as

$$c_{\mathrm{g}} = \frac{c_{\mathrm{L}}c_{\mathrm{T}}^2(c_{\mathrm{L}}^4 + 4c_{\mathrm{L}}^2c_{\mathrm{T}}^2 - 4c_{\mathrm{T}}^4)}{12c_{\mathrm{L}}^2c_{\mathrm{T}}^4 - 4c_{\mathrm{L}}^4c_{\mathrm{T}}^2 + c_{\mathrm{L}}^6 - 8c_{\mathrm{T}}^6} \tag{3.37}$$

and thus, depends only on the material's properties. Consequently, the group velocity is constant for all symmetric modes at the frequencies according to Eq.(3.34). Furthermore, for each phase matching pair, group matching is fulfilled as well. Note that Pilarski et al. [18] obtain another value for the group velocity. Confidence in the value presented here is gained by comparison to numerical results from the software Disperse [17].

3.2.2.4 Displacements at the Surface

By looking at the displacement field in Eq.(2.18) it is seen immediately that

$$\tilde{u}_y(h) = 0, \tag{3.38}$$

i.e. the normal displacement is zero at the surface. Using the frequency Eq.(2.17), the in-plane displacement at the surface becomes

$$\tilde{u}_z(h) = Dh\,\bar{\beta}\,\frac{\bar{\kappa}^2 + \bar{\beta}^2}{\bar{\kappa}^2 - \bar{\beta}^2}\cos\bar{\beta}, \tag{3.39}$$

which is nonzero.

3.2.2.5 Summary

In summary, each symmetric mode at the longitudinal phase velocity shows phase and group matching with another symmetric mode at the double frequency. The respective frequencies and the common group velocity are given above. As in Section 3.2.1 for crossing points, the out-of-plane displacement at the surface is zero, while the in-plane displacement at the surface is nonzero. The lowest pair (S1,S2) has been used by Bermes et al. [3] and Pruell et al. [19].

3.2.3 Nonzero Order Modes at Cutoff Frequencies

Graff [10] provides a concise introduction on cutoff frequencies, which are obtained for the low wave number limit $\bar{\kappa} \to 0$. Besides presenting the basic conditions that result naturally from the linear theory, this section relates the results to phase and group matching.

3.2.3.1 General Conditions

In the low wave number limit $\bar{\kappa} \to 0$,

$$\bar{\alpha} \to \frac{\bar{\omega}}{c_{\mathrm{L}}}, \quad \bar{\beta} \to \frac{\bar{\omega}}{c_{\mathrm{T}}}, \tag{3.40}$$

hold, hence

$$\bar{\alpha} c_{\mathrm{L}} \to \bar{\beta} c_{\mathrm{T}} \tag{3.41}$$

follows. For $\bar{\kappa} \to 0$, the frequency equations Eqs.(3.4) and (3.5) become

$$\Phi_{\mathrm{sym}}(\bar{\omega}, \bar{\kappa}) \to \cos \frac{\bar{\omega}}{c_{\mathrm{L}}} \sin \frac{\bar{\omega}}{c_{\mathrm{T}}} \left(\frac{\bar{\omega}}{c_{\mathrm{T}}} \right)^4 = 0, \tag{3.42}$$

and

$$\Phi_{\mathrm{asym}}(\bar{\omega}, \bar{\kappa}) \to \sin \frac{\bar{\omega}}{c_{\mathrm{L}}} \cos \frac{\bar{\omega}}{c_{\mathrm{T}}} \left(\frac{\bar{\omega}}{c_{\mathrm{T}}} \right)^4 = 0. \tag{3.43}$$

The choice $\bar{\omega} \to 0$ leads to the fundamental modes S0 and A0. For the nonzero modes, however, it is required that

$$\text{case SI:} \qquad \bar{\alpha} \to \frac{(2n-1)\pi}{2}, \qquad n \in \mathbb{N}^+, \quad \text{or} \tag{3.44}$$

$$\text{case SII:} \qquad \bar{\beta} \to n\pi, \qquad n \in \mathbb{N}^+, \tag{3.45}$$

for symmetric modes, or

$$\text{case AI:} \qquad \bar{\alpha} \to n\pi, \qquad n \in \mathbb{N}^+, \quad \text{or} \tag{3.46}$$

$$\text{case AII:} \qquad \bar{\beta} \to \frac{(2n-1)\pi}{2}, \qquad n \in \mathbb{N}^+, \tag{3.47}$$

for antisymmetric modes. From Eqs.(3.40) and (3.44) to (3.47), the respective cutoff frequencies are obtained as

$$\text{case SI:} \qquad \bar{\omega} \to \frac{(2n-1)\pi}{2} c_{\mathrm{L}}, \qquad n \in \mathbb{N}^+, \tag{3.48}$$

$$\text{case SII:} \qquad \bar{\omega} \to n\pi c_{\mathrm{T}}, \qquad n \in \mathbb{N}^+, \tag{3.49}$$

$$\text{case AI:} \qquad \bar{\omega} \to n\pi c_{\mathrm{L}}, \qquad n \in \mathbb{N}^+, \tag{3.50}$$

$$\text{case AII:} \qquad \bar{\omega} \to \frac{(2n-1)\pi}{2} c_{\mathrm{T}}, \qquad n \in \mathbb{N}^+. \tag{3.51}$$

Depending on the ratio $c_{\mathrm{L}}/c_{\mathrm{T}}$, the cutoff frequencies can be similar for different modes. However, it is assumed in this work that the cutoff frequencies of all modes are distinct.

3.2.3.2 Phase Velocity Matching

To show phase matching for a case SI mode in the limit $\bar{\kappa} \to 0$, the conditions Eq.(3.2) are applied to Eq.(3.44). One obtains

$$\bar{\alpha}_{\mathrm{SI}}^{(2\omega)} = (2n-1)\pi \quad \in \text{ case AI}, \tag{3.52}$$

where the subindex indicates the type of the mode at frequency $\bar{\omega}$. This means that there is phase matching from every case SI mode to the case AI mode at double frequency. Similarly, the phase matching conditions for the other cases

$$\bar{\beta}_{\mathrm{SII}}^{(2\omega)} = 2n\pi \quad \in \text{ case SII}, \tag{3.53}$$

$$\bar{\alpha}_{\mathrm{AI}}^{(2\omega)} = 2n\pi \quad \in \text{ case AI}, \tag{3.54}$$

$$\bar{\beta}_{\mathrm{AII}}^{(2\omega)} = (2n-1)\pi \quad \in \text{ case SII} \tag{3.55}$$

are obtained. In other words, in the limit $\bar{\kappa} \to 0$ there is phase velocity matching

- from every case SI symmetric mode to a case AI antisymmetric mode,
- from every case SII symmetric mode to a case SII symmetric mode,
- from every case AI antisymmetric mode to a case AI antisymmetric mode,
- from every case AII antisymmetric mode to a case SII symmetric mode.

Note that

$$c_{\mathrm{ph}} \to \infty \tag{3.56}$$

as $\bar{\kappa} \to 0$, and thus, phase matching in this limit case means that both phase velocities of the mode pair approach infinity.

3.2.3.3 Group Velocity Matching

The group velocities for all the modes described above converge to zero, i.e.

$$c_{\mathrm{g}}^{i} \to 0, \quad i = \mathrm{SI}, \mathrm{SII}, \mathrm{AI}, \mathrm{AII} \tag{3.57}$$

as $\bar{\kappa} \to 0$, which can be seen by Eqs.(3.6) and (3.7): Using the relations above, all the terms in the nominator tend to zero, while there is always a term in the denominator that does not vanish. Hence, each phase matching pair shows group matching with group velocity tending to zero.

3.2.3.4 Displacements at the Surface

For the discussion on the displacements at the surface, it is noted that both $\bar{\alpha}$ and $\bar{\beta}$ have finite values, as is concluded by Eq.(3.41) and Eqs.(3.44) to (3.47).

As $\bar{\kappa} \to 0$, Eqs.(A.27) yield

$$\tilde{u}_y(y) \to -\tfrac{A}{h}\bar{\alpha}\sin\bar{\alpha}\tfrac{y}{h}, \tag{3.58a}$$

$$\tilde{u}_z(y) \to -\tfrac{D}{h}\bar{\beta}\cos\bar{\beta}\tfrac{y}{h}, \tag{3.58b}$$

for the displacements of symmetric modes. For case SI according to Eq.(3.44), the boundary condition Eq.(A.17b) requires $D = 0$, and thus,

$$\tilde{u}_y^{\mathrm{SI}}(h) \to -\tfrac{A}{h}\bar{\alpha}\sin\bar{\alpha}, \tag{3.59a}$$

$$\tilde{u}_z^{\mathrm{SI}}(h) \to 0, \tag{3.59b}$$

with $\bar{\alpha} \to (2n-1)\pi/2$. For case SII on the other hand, Eqs.(3.45) and (A.17c) require $A = 0$, resulting in

$$\tilde{u}_y^{\mathrm{SII}}(h) \to 0, \tag{3.60a}$$

$$\tilde{u}_z^{\mathrm{SII}}(h) \to -\tfrac{D}{h}\bar{\beta}\cos\bar{\beta}, \tag{3.60b}$$

with $\bar{\beta} \to n\pi$.

Using Eqs.(A.30), the displacement field for antisymmetric modes reduces to

$$\tilde{u}_y(y) \to \tfrac{B}{h}\bar{\alpha}\cos\bar{\alpha}\tfrac{y}{h}, \tag{3.61a}$$

$$\tilde{u}_z(y) \to \tfrac{C}{h}\bar{\beta}\sin\bar{\beta}\tfrac{y}{h}. \tag{3.61b}$$

Specifically, Eq.(3.46) for case AI and Eq.(A.17b) yield $C = 0$, or

$$\tilde{u}_y^{\mathrm{AI}}(h) \to \tfrac{B}{h}\bar{\alpha}\cos\bar{\alpha}, \tag{3.62a}$$

$$\tilde{u}_z^{\mathrm{AI}}(h) \to 0. \tag{3.62b}$$

with $\bar{\alpha} \to n\pi$, while Eqs.(3.47) and (A.17c) require $B = 0$, and thus,

$$\tilde{u}_y^{\mathrm{AII}}(h) \to 0 \tag{3.63a}$$

$$\tilde{u}_z^{\mathrm{AII}}(h) \to \tfrac{C}{h}\bar{\beta}\sin\bar{\beta}, \tag{3.63b}$$

for case AII modes, where $\bar{\beta} \to (2n-1)\pi/2$.

3.2.3.5 Summary

Table 3.2 shows all possible combinations with their displacements at the surface. Again, only symmetric modes at double frequencies are useful for second harmonic generation, i.e. the first two entries in the table. One observes that the out-of-plane displacement at the surface for these modes is zero, while the in-plane component is nonzero.

For $\bar{\kappa} = 0$, the group velocity is zero, meaning that no energy is carried and the wave does not propagate. For that reason, these modes are practically relevant only in the approximation where $\bar{\kappa}$ is small but nonzero. Then, phase matching holds approximately, and the group velocity and the normal displacement at the surface are small but nonzero.

Table 3.2: Phase Matching Pairs at Cutoff Frequencies

FROM MODE AT $\bar{\omega}$				TO MODE AT $2\bar{\omega}$			
Case	$\bar{\alpha}$, $\bar{\beta}$	$\tilde{u}_y(h)$	$\tilde{u}_z(h)$	Case	$\bar{\alpha}$, $\bar{\beta}$	$\tilde{u}_y(h)$	$\tilde{u}_z(h)$
SII	$\bar{\beta} = n\pi$	0	$\neq 0$	SII	$\bar{\beta} = 2n\pi$	0	$\neq 0$
AII	$\bar{\beta} = (2n-1)\pi/2$	0	$\neq 0$	SII	$\bar{\beta} = (2n-1)\pi$	0	$\neq 0$
SI	$\bar{\alpha} = (2n-1)\pi/2$	$\neq 0$	0	AI	$\bar{\alpha} = (2n-1)\pi$	$\neq 0$	0
AI	$\bar{\alpha} = n\pi$	$\neq 0$	0	AI	$\bar{\alpha} = 2n\pi$	$\neq 0$	0

3.2.4 Nonzero Order Modes with High Wave Number

For high wave numbers, i.e. $\bar{\kappa} \to \infty$, nonzero order modes show nondispersive behavior. It will be shown that both the phase and the group velocity converge to the shear wave speed c_{T} for all nonzero order modes, and thus satisfy approximately the matching conditions when both wave number and frequency become large.

3.2.4.1 General Conditions

In this section, the region $c_{\mathrm{T}} < c_{\mathrm{ph}} < c_{\mathrm{L}}$ is considered. It follows that $\bar{\alpha} = \bar{\alpha}' i$, where

$$\bar{\alpha}' = \sqrt{\bar{\kappa}^2 - \left(\frac{\bar{\omega}}{c_{\mathrm{L}}}\right)^2}, \tag{3.64}$$

and thus, the frequency equations read as

$$\Phi_{\mathrm{sym}}(\bar{\omega}, \bar{\kappa}) = \sin\bar{\beta}\,\left[1 - \left(\frac{\bar{\beta}}{\bar{\kappa}}\right)^2\right]^2 - 4\tanh\bar{\alpha}'\cos\bar{\beta}\,\frac{\bar{\alpha}'\bar{\beta}}{\bar{\kappa}^2} = 0 \tag{3.65}$$

and

$$\Phi_{\mathrm{asym}}(\bar{\omega}, \bar{\kappa}) = \cos\bar{\beta}\,\left[1 - \left(\frac{\bar{\beta}}{\bar{\kappa}}\right)^2\right]^2 + 4\coth\bar{\alpha}'\sin\bar{\beta}\,\frac{\bar{\alpha}'\bar{\beta}}{\bar{\kappa}^2} = 0. \tag{3.66}$$

In the high wave number limit $\bar{\kappa} \to \infty$, requiring

$$\bar{\beta} \to n\pi, \quad n \in \mathbb{N}^+ \tag{3.67}$$

satisfies Eq.(3.65) for symmetric modes. Similarly, Eq.(3.66) for antisymmetric modes holds for

$$\bar{\beta} \to \frac{(2n-1)\pi}{2}, \quad n \in \mathbb{N}^+. \tag{3.68}$$

In these cases, since

$$\frac{\bar{\beta}}{\bar{\kappa}} = \sqrt{\left(\frac{c_{\mathrm{ph}}}{c_{\mathrm{T}}}\right)^2 - 1} \to 0, \tag{3.69}$$

one concludes

$$c_{\mathrm{ph}} \to c_{\mathrm{T}}, \tag{3.70}$$

and

$$\bar{\alpha}' = \bar{\kappa}\sqrt{1 - \left(\frac{c_{\mathrm{ph}}}{c_{\mathrm{L}}}\right)^2} \to \bar{\kappa}\gamma \to \infty, \tag{3.71}$$

where

$$\gamma = \sqrt{1 - \left(\frac{c_{\mathrm{T}}}{c_{\mathrm{L}}}\right)^2}. \tag{3.72}$$

That is, the phase velocity of all the nonzero order modes converges to the shear velocity for $\bar{\kappa} \to \infty$. Furthermore, since

$$\bar{\omega} \to c_{\mathrm{T}}\bar{\kappa} \to \infty, \tag{3.73}$$

frequency increases with wave number. As to the fundamental modes, it will be shown in Section 3.2.5 that they converge to the Rayleigh wave speed for high frequencies and wave numbers.

3.2.4.2 Phase Velocity Matching

Since all the nonzero order modes converge to the same phase velocity, there is phase matching from each to every nonzero order mode in the high wave number limit $\bar{\kappa} \to \infty$. For a large but finite wave number, there are mode pairs satisfying approximate phase matching. The number of matching pairs depends on the wave number and the approximation tolerance that is applied.

3.2.4.3 Group Velocity Matching

Application of the limits obtained in Section 3.2.4.1 on the expressions for the group velocities Eqs.(3.6) and (3.7) yields

$$c_{\mathrm{g,sym}} \to \frac{\cosh \bar{\alpha}'\, \gamma\bar{\kappa}^2\left(\bar{\kappa}^2 - (n\pi)^2\right)^2}{\cosh \bar{\alpha}'\, \gamma\frac{\bar{\kappa}^2}{c_{\mathrm{T}}}\left(\bar{\kappa}^2 - (n\pi)^2\right)^2} \to c_{\mathrm{T}} \tag{3.74}$$

for symmetric modes, and

$$c_{\mathrm{g,asym}} \to \frac{\sinh \bar{\alpha}'\, \gamma\bar{\kappa}^2\left(\bar{\kappa}^2 - \left(\frac{(2n-1)\pi}{2}\right)^2\right)^2}{\sinh \bar{\alpha}'\, \gamma\frac{\bar{\kappa}^2}{c_{\mathrm{T}}}\left(\bar{\kappa}^2 - \left(\frac{(2n-1)\pi}{2}\right)^2\right)^2} \to c_{\mathrm{T}} \tag{3.75}$$

for antisymmetric modes, i.e. the group velocities of all the nonzero order modes converge to the shear velocity. Thus, group matching from each to every nonzero

order mode is concluded for the limit $\bar{\kappa} \to \infty$. Again, for a large and finite wave number, group matching holds approximately.

3.2.4.4 Displacements at the Surface

For the subsequent investigation of the displacements, the limits

$$\frac{(\bar{\kappa}^2 - \bar{\beta}^2)}{\bar{\kappa}} = \bar{\kappa}\Big[1 - \big(\frac{\bar{\beta}}{\bar{\kappa}}\big)^2\Big] \to \bar{\kappa} \tag{3.76}$$

and

$$\frac{(\bar{\kappa}^2 - \bar{\beta}^2)}{\bar{\alpha}} = \frac{1}{\gamma}\,\bar{\kappa}\Big[1 - \big(\frac{\bar{\beta}}{\bar{\kappa}}\big)^2\Big] \to \frac{\bar{\kappa}}{\gamma} \tag{3.77}$$

will be helpful. Another limit for symmetric modes is obtained using the frequency equation Eq.(3.65) and the limits presented in Section 3.2.4.1,

$$\begin{aligned} \bar{\kappa}\sin\bar{\beta} &\to 4\tanh\bar{\alpha}'\cos\bar{\beta}\;\frac{\bar{\alpha}'\bar{\beta}}{\bar{\kappa}} \\ &\to 4\gamma\bar{\beta}\cos\bar{\beta} < \infty, \end{aligned} \tag{3.78}$$

which is used to calculate the displacements at the surface from Eqs.(2.18) as follows:

$$\begin{aligned} \tilde{u}_y^{\mathrm{sym}}(h) &\to iDh(-\tfrac{1}{2}\bar{\kappa}\sin\bar{\beta} + \bar{\kappa}\sin\bar{\beta}) \\ &= \tfrac{1}{2}iDh\bar{\kappa}\sin\bar{\beta} \\ &\to 2iDh\gamma\bar{\beta}\cos\bar{\beta} < \infty, \end{aligned} \tag{3.79a}$$

$$\begin{aligned} \tilde{u}_z^{\mathrm{sym}}(h) &\to -Dh(-\tfrac{1}{2\gamma}\coth\bar{\alpha}'\,\bar{\kappa}\sin\bar{\beta} + \bar{\beta}\cos\bar{\beta}) \\ &\to -Dh(-2\bar{\beta}\coth\bar{\alpha}' + \bar{\beta})\cos\bar{\beta} \\ &\to Dh\bar{\beta}\cos\bar{\beta} < \infty. \end{aligned} \tag{3.79b}$$

Note that tanh(.) and coth(.) converge to 1 as the argument becomes large.

Eqs.(3.79) indicate that the displacements at the surface are nonzero. Yet, if for example the depth $y^* = h/(2n)$ is considered, one term in the normal displacement of Eqs.(2.18) approaches infinity, since

$$\bar{\kappa}\sin(\bar{\beta}y^*/h) \to \bar{\kappa}\sin(\pi/2) = \bar{\kappa} \to \infty. \tag{3.80}$$

In order to interprete this correctly, it is noted that the displacements in Eqs.(2.18) and (2.20) are of a relative nature. This means that as long as D and C are not specified, these terms express only the shape of the displacement field. The absolute magnitude is defined by D or C, respectively, which is determined physically by the external excitation of the mode. In the case above, this means that D has to approach zero in order to obtain a physically reasonable, finite displacement field. Thus, the out-of-plane displacement at the surface $u_y(h)$ becomes infinitesimally small compared to the displacement $u_y(h/(2n))$, and

$$\tilde{u}_y^{\mathrm{sym}}(h) \to 0. \tag{3.81}$$

For the in-plane displacement $u_z(y)$, there is no depth y to make any term unbounded, so that

$$\tilde{u}_z^{\mathrm{sym}}(y) \to 0, \quad \text{for all } y \tag{3.82}$$

follows, i.e. the wave tends to become a pure shear wave as $\bar{\kappa} \to \infty$, propagating with shear wave speed.

Regarding antisymmetric modes, Eqs.(3.66) and (3.68) yield the limit

$$\begin{aligned} \bar{\kappa}\cos\bar{\beta} &\to -4\coth\bar{\alpha}'\sin\bar{\beta}\ \frac{\bar{\alpha}'\bar{\beta}}{\bar{\kappa}} \\ &\to -4\gamma\bar{\beta}\sin\bar{\beta} < \infty, \end{aligned} \tag{3.83}$$

which is used to calculate the displacements of Eqs.(2.20) at the surface

$$\begin{aligned} \tilde{u}_y^{\mathrm{asym}}(h) &\to iCh(-\tfrac{1}{2}\bar{\kappa}\cos\bar{\beta} + \bar{\kappa}\cos\bar{\beta}) \\ &= \tfrac{1}{2}iCh\bar{\kappa}\cos\bar{\beta} \\ &\to -2iCh\gamma\bar{\beta}\sin\bar{\beta} < \infty, \end{aligned} \tag{3.84a}$$

$$\begin{aligned} \tilde{u}_z^{\mathrm{asym}}(h) &\to Ch(\tfrac{1}{2\gamma}\tanh\bar{\alpha}'\,\bar{\kappa}\cos\bar{\beta} + \bar{\beta}\sin\bar{\beta}) \\ &\to Ch(-2\bar{\beta}\tanh\bar{\alpha}' + \bar{\beta})\sin\bar{\beta} \\ &\to -Ch\bar{\beta}\sin\bar{\beta} < \infty. \end{aligned} \tag{3.84b}$$

If the middle layer $y^* = 0$ is considered in Eqs.(2.20), the normal displacement tends to infinity, because

$$\bar{\kappa}\cos(\bar{\beta}y^*/h) \to \bar{\kappa}\cos(0) = \bar{\kappa} \to \infty, \tag{3.85}$$

while there is no y that makes the in-plane displacement unbounded. Hence, with the same argumentation as above,

$$\tilde{u}_y^{\text{asym}}(h) \to 0. \tag{3.86}$$

and

$$\tilde{u}_z^{\text{asym}}(y) \to 0, \quad \text{for all } y. \tag{3.87}$$

Thus, as $\bar{\kappa} \to \infty$, both symmetric and antisymmetric modes tend to become pure shear waves at the shear velocity with zero normal displacement at the surface.

3.2.4.5 Summary

As $\bar{\kappa} \to \infty$ in the region $c_{\text{T}} < c_{\text{ph}} < c_{\text{L}}$, it is shown that all nonzero order modes approach the shear velocity c_{T} in both phase and group velocity, whence phase and group matching is concluded from each to every mode in the high wave number limit. Furthermore, the out-of-plane displacement at the surface and the in-plane displacement over the whole cross section converge to zero, so that motion becomes pure shear.

In a practical view, the results may be applied approximately, i.e. as $\bar{\kappa}$ being large but not infinity. Then, dependent on the wave number and the approximation tolerance applied, the results hold up to a certain number of modes.

3.2.5 Fundamental Modes with High Wave Number (Quasi-Rayleigh Surface Wave)

In the region $c_{\text{ph}} < c_{\text{T}} < c_{\text{L}}$ for $\bar{\kappa} \to \infty$, the wave length becomes very small compared to the thickness of the plate, so that the fundamental modes take the form of a Rayleigh surface wave, whose characteristics are presented for example in Graff [10].

3.2.5.1 General Conditions

The condition $c_{\mathrm{ph}} < c_{\mathrm{T}}$ implies that $\bar{\alpha}$ and $\bar{\beta}$ are complex and written as $\bar{\alpha} = i\bar{\alpha}'$ and $\bar{\beta} = i\bar{\beta}'$, where $\bar{\alpha}'$ as in Eq.(3.64) and

$$\bar{\beta}' = \sqrt{\bar{\kappa}^2 - \left(\frac{\bar{\omega}}{c_{\mathrm{T}}}\right)^2}. \tag{3.88}$$

The frequency Eqs.(3.4) and (3.5) then reduce to the Rayleigh wave equation

$$(\bar{\kappa}^2 + \bar{\beta}'^2)^2 - 4\bar{\alpha}'\bar{\beta}'\bar{\kappa}^2 = 0, \tag{3.89}$$

whose solution is the Rayleigh wave speed c_{R} with the property $c_{\mathrm{R}} < c_{\mathrm{T}}$. Hence, the limits

$$\bar{\alpha}' = \bar{\kappa}\sqrt{1 - \left(\frac{c_{\mathrm{R}}}{c_{\mathrm{L}}}\right)^2} \to \bar{\kappa}\gamma_\alpha \to \infty, \tag{3.90}$$

$$\bar{\beta}' = \bar{\kappa}\sqrt{1 - \left(\frac{c_{\mathrm{R}}}{c_{\mathrm{T}}}\right)^2} \to \bar{\kappa}\gamma_\beta \to \infty \tag{3.91}$$

are concluded, where

$$\gamma_\alpha = \sqrt{1 - \left(\frac{c_{\mathrm{R}}}{c_{\mathrm{L}}}\right)^2}, \tag{3.92}$$

$$\gamma_\beta = \sqrt{1 - \left(\frac{c_{\mathrm{R}}}{c_{\mathrm{T}}}\right)^2}. \tag{3.93}$$

The term quasi-Rayleigh wave is used for these kind of modes because in the high wave number and frequency limit, these Lamb modes behave approximately like a Rayleigh wave. As the wave length becomes much smaller than the plate thickness, the plate appears to be an infinite half space for the propagating wave as in the Rayleigh surface wave problem. The additional term *quasi* indicates that not the original Rayleigh wave – as defined for an infinite half space – is meant, but the Lamb modes that behave like a Rayleigh wave in the high frequency domain.

3.2.5.2 Phase Velocity Matching

Since the fundamental modes S0 and A0 converge to the Rayleigh wave speed in the high wave number limit $\bar{\kappa} \to \infty$, there is phase matching from each fundamental mode

to itself and to the other one. For a large but finite wave number, phase matching holds approximately.

3.2.5.3 Group Velocity Matching

Due to the nondispersive behavior, group velocity equals phase velocity, i.e.

$$c_{\mathrm{g}} \rightarrow c_{\mathrm{ph}} \rightarrow c_{\mathrm{R}} \tag{3.94}$$

as can be inferred from Eq.(3.10). Hence, group matching for the fundamental modes is concluded.

3.2.5.4 Displacements at the Surface

Substituting the limits obtained in Section 3.2.5.1 in the displacement fields Eqs.(2.18) and (2.20) results in

$$\tilde{u}_y^{\mathrm{S0}}(y) = \tfrac{D\bar{\kappa}}{h}\Big(\frac{(1+\gamma_\beta^2)\sinh\bar{\beta}'}{2\sinh\bar{\alpha}'}\sinh\bar{\alpha}'\tfrac{y}{h} - \sinh\bar{\beta}'\tfrac{y}{h}\Big) \tag{3.95a}$$

$$\tilde{u}_z^{\mathrm{S0}}(y) = \tfrac{iD\bar{\kappa}}{h}\Big(\frac{(1+\gamma_\beta^2)\sinh\bar{\beta}'}{2\gamma_\alpha\sinh\bar{\alpha}'}\cosh\bar{\alpha}'\tfrac{y}{h} - \gamma_\beta\cosh\bar{\beta}'\tfrac{y}{h}\Big) \tag{3.95b}$$

for the symmetric fundamental mode S0, and

$$\tilde{u}_y^{\mathrm{A0}}(y) = \tfrac{iC\bar{\kappa}}{h}\Big(-\frac{(1+\gamma_\beta^2)\cosh\bar{\beta}'}{2\cosh\bar{\alpha}'}\cosh\bar{\alpha}'\tfrac{y}{h} + \cosh\bar{\beta}'\tfrac{y}{h}\Big) \tag{3.96a}$$

$$\tilde{u}_z^{\mathrm{A0}}(y) = \tfrac{C\bar{\kappa}}{h}\Big(\frac{(1+\gamma_\beta^2)\cosh\bar{\beta}'}{2\gamma_\alpha\cosh\bar{\alpha}'}\sinh\bar{\alpha}'\tfrac{y}{h} - \gamma_\beta\sinh\bar{\beta}'\tfrac{y}{h}\Big) \tag{3.96b}$$

for the antisymmetric fundamental mode A0. These equations show – according to the theory of Rayleigh waves – that the energy is concentrated at the surface and that displacements vanish exponentially with depth: As $\bar{\alpha}'$ and $\bar{\beta}'$ become large, the sinh(.) and cosh(.) terms grow with a faster exponential rate as y approaches h. In the very limit $\bar{\alpha}', \bar{\beta}' \rightarrow \infty$, the displacement is concentrated entirely in an infinitesimally small layer beneath the surface. At the surface, Eqs.(3.95) and (3.96) take the form

$$\tilde{u}_y^{\mathrm{S0}}(h) = \tfrac{D\bar{\kappa}}{h}\,\tfrac{\gamma_\beta^2}{2}\cosh\bar{\beta}' \tag{3.97a}$$

$$\tilde{u}_z^{\mathrm{S0}}(h) = \tfrac{iD\bar{\kappa}}{h}\,\tfrac{1-2\gamma_\alpha\gamma_\beta+\gamma_\beta^2}{2\gamma_\alpha}\cosh\bar{\beta}' \tag{3.97b}$$

and

$$\tilde{u}_y^{\mathrm{A0}}(h) = -\frac{iC\bar{\kappa}}{h}\,\frac{\gamma_\beta^2}{2}\cosh\bar{\beta}' \tag{3.98a}$$

$$\tilde{u}_z^{\mathrm{A0}}(h) = \frac{C\bar{\kappa}}{h}\,\frac{1-2\gamma_\alpha\gamma_\beta+\gamma_\beta^2}{2\gamma_\alpha}\cosh\bar{\beta}' \tag{3.98b}$$

as $\cosh(.) \to \sinh(.)$ for large arguments.

3.2.5.5 Summary

In summary, for large wave numbers and frequencies, both the phase and the group velocity of the fundamental modes S0 and A0 converge to the Rayleigh surface wave speed $c_{\mathrm{R}} < c_{\mathrm{T}}$. Due to the nondispersive behavior phase and group matching is concluded. The displacements at the surface are large compared to the ones in the inner part of the plate, since energy is concentrated in a thin layer beneath the surface.

Herrmann et al. [11] and Shui et al. [23] use this mode in their experiments.

CHAPTER IV

EVALUATION OF MATCHING PAIRS FOR AN ALUMINUM PLATE

The statements concerning frequencies where phase and group matching can occur – as provided in Chapter 3 – are general and can be applied to any homogeneous, isotropic, elastic plate. The objective of this work, however, is not only to give possible excitation frequencies, but also to evaluate them with regard to practical issues related to excitation and measurement. With the investigation of the displacements at the surface in Chapter 3, a first step in this direction is made already. However, other factors, most importantly the rate of second harmonic generation, have not been addressed yet. Also, for some modes in Chapter 3, the wave number is assumed to converge to zero or infinity, respectively, which is practically impossible. Therefore, how to determine deviation tolerances from exact phase matching and how the approximation influences the second harmonic wave, are questions of importance.

One of the most important factors, the rate of second harmonic generation, among others, cannot be analyzed conveniently in a general framework. In order to obtain comparable numbers and ratios, and descriptive plots of dispersion curves, the material properties must be known. For this reason, the calculations in this chapter are performed for an aluminum plate, whose material properties are given in Table 4.1. The same procedure can be carried out easily for other materials as well. Even though the absolute numbers may be different for different materials, a similar qualitative behavior is expected.

The following section summarizes previously mentioned and newly introduced factors that are critical as to the evaluation and comparison of modes and excitation

Table 4.1: Material Properties of Aluminum. [1)] Disperse [17]. [2)] Landau and Lifshitz [13].

ρ_0 [1)]	c_L [1)]	c_T [1)]	μ [1)]	λ [1)]	$\mathcal{A}$ [2)]	$\mathcal{B}$ [2)]	$\mathcal{C}$ [2)]
2700 kg/m^3	6320 m/s	3130 m/s	26.5 GPa	54.9 GPa	-320 GPa	-200 GPa	-190 GPa

frequencies. Section 4.2 then evaluates the matching pairs found for the aluminum plate up to a frequency-thickness-product of $fd_\mathrm{max} = 20\,\mathrm{MHz\,mm}$ with regard to these influencing factors. Pros and cons for each type of matching pair are given and then compared to other types.

4.1 Influencing Factors

Displacements at the Surface. Measurements using wedge transducers mainly detect the out-of-plane displacement at the surface since they are mostly liquid-coupled to the structure. A large normal displacement at the surface is therefore advantageous. For the investigation of displacements in this chapter, the normalization

$$\bar{\boldsymbol{u}} = \frac{\boldsymbol{u}}{h} \tag{4.1}$$

is introduced so that further calculations will be independent of the plate's thickness. As to crossing points and symmetric modes at the longitudinal phase velocity, it is shown in Sections 3.2.1 and 3.2.2 that only the in-plane displacement at the surface is nonzero. For the other three types, however, there is a nonzero normal displacement at the surface since only approximations are considered. That is, while the derivations in Chapter 3 are carried out for the wave number converging to zero or infinity, this chapter deals with high finite or low nonzero wave numbers, which results in small deviations from the theory presented before. In order to quantify the normal displacement of a mode, the ratio

$$r_y = \frac{\tilde{\bar{u}}_y(h)}{\tilde{\bar{u}}_{y,\mathrm{max}}} \tag{4.2}$$

is introduced, where

$$\tilde{\bar{u}}_{y,\max} = \max_{y\in[-h,h]} |\tilde{\bar{u}}_y(y)|. \tag{4.3}$$

is the maximum normal displacement in the cross section of the plate. A high value for r_y indicates a high out-of-plane displacement at the surface, making excitation and measurement of this mode easier.

Rate of Second Harmonic Generation. While the discussion above deals only with the mode shape of the modes involved in second harmonic generation – either as primary mode or as one of the secondary modes – the actual rate of second harmonic generation is important with regard to the measurement of the second harmonic mode: The stronger the secondary mode gets excited, the bigger are its amplitude and signal-to-noise ratio. The amplitude ratio

$$r_s = \left| \frac{\bar{A}_{(2)}}{\bar{A}^2_{(1)}} \right| \tag{4.4}$$

quantifies the rate of second harmonic generation. $\bar{A}_{(1)}$ and $\bar{A}_{(2)}$ represent the amplitude of the primary and secondary mode, respectively. Further explanations on how the amplitude of a Lamb mode is defined, are given in Section 4.2. It is noted here that r_s normalizes the secondary amplitude by the squared amplitude of the primary mode. This is due to the fact that the primary mode enters the calculation of the secondary mode quadratically, as one can see in Eqs.(2.14) and Eqs.(2.37). Moreover, in the theory of second harmonic bulk waves in an infinite medium, as for example presented by Norris [16], r_s is proportional to the nonlinear parameter $\tilde{\beta}$ and the propagation distance. While it is true for Lamb waves according to Eq.(2.41) that r_s is proportinal to the propagation distance if phase matching is satisfied, the dependency on the nonlinear parameter has not been shown yet. Nevertheless, experiments such as those by Bermes et al. [3] and Pruell et al. [19, 20] employ r_s to show a correlation between the material's nonlinearity and the second harmonic amplitude.

Dispersion Length. For approximate phase matching pairs, the dispersion length

L as defined in Eq.(2.58) determines those values of propagation distance for which measurements are reasonable. As stated in Section 2.2.4, the useful propagation distance is one fourth of the dispersion length where a linear increase of the amplitude holds approximately. If the dispersion length is normalized as

$$\bar{L} = \frac{L}{h}, \tag{4.5}$$

the normalized useful propagation length is obtained by

$$\bar{L}^{\text{use}} = \frac{\bar{L}}{4} = \frac{\pi}{2|\bar{\kappa}_{\text{d}}|}. \tag{4.6}$$

In the following section, $\bar{L}^{\text{use}}$ is required to be at least

$$\bar{L}^{\text{use}} > 400, \tag{4.7}$$

which means that measurements can be performed along a propagation distance that is at least 200 times the plate thickness. Using this requirement and Eq.(4.6) yields

$$|\bar{\kappa}_{\text{d}}| < \frac{\pi}{800} \approx 4 \cdot 10^{-3} \tag{4.8}$$

for the allowed deviance from exact phase matching.

Symmetry of the Excitation Mode. A practical issue is proposed by the symmetry of the excitation mode. As shown in Chapter 2, the secondary mode can only be symmetric, so that only the symmetry of the primary mode can be selected by the experimenter. By experience, the excitation of an antisymmetric mode turns out to be easier than that of a symmetric mode. The reason for that is the y-symmetric normal displacement field of antisymmetric modes as discussed in Section 2.1.2.1 on the primary solution.

Isolated Excitation Mode. Also, for the excitation of a primary mode, the mode should be isolated in the dispersion curve. That is, no other mode should have a similar wave number at a similar frequency . Otherwise, that other mode is likely to be excited as well, and thus, complicates the signals measured.

Frequency. The excitation frequency should not be too high due to attenuation and high requirements on measurements and signal processing. The maximum frequency-thickness-product fd for the primary mode assumed in this work is $fd_{\max} = 20\,\text{MHz mm}$ based on experience. Also, modes with higher frequency are more difficult to excite.

Group Velocity. Depending on the situation, a high value for the group velocity might be helpful. Signals with high group velocity will separate from signals with lower group velocity and arrive earlier at the point of measurement, so that slower waves cannot disturb the signal being measured. However, it is noted that this requirement does not apply to all practical applications.

4.2 Evaluation

In order to evaluate the mode types presented in Section 3.2 with regard to the factors proposed above, two software tools are used. The program Disperse [17] provides numerical dispersion curves for various wave propagation problems. The numerical data for a stress free aluminum plate are exported from Disperse to Matlab and analyzed there with regard to frequencies, phase velocity, group velocity, etc. Also, the search for approximate matching pairs according to condition Eq.(4.8) is performed with numerical results from Disperse.

Concerning the computation of the second harmonic amplitude, the term a_n for the secondary mode n as in Eq.(2.43) needs to be obtained. Referring to the derivations in Section 2.1, it is observed that the computation requires derivatives as well as integrations. In this work, the symbolic toolbox of Matlab is employed to perform these calculations analytically. Matlab offers a variety of symbolic operations and possibilities to create new functions, which makes the computer-based symbolic calculation convenient and comprehensible. Also, as opposed to numerical methods, convergence issues need not to be addressed.

The following sections present the results obtained for the five mode types from Section 3.2. The dispersion curves in Figure 4.1 overview the points of phase velocity and group velocity matching that are investigated in the following.

4.2.1 Crossing Points of Symmetric and Antisymmetric Modes

The investigation of matching pairs at crossing points, which are listed as 'C' in Figure 4.1, for the frequency range up to $fd_{\max} = 20\,\mathrm{MHz\,mm}$ of the primary mode results in the mode pairs that are presented in Table 4.2. The table itemizes the reference tag, the mode pairs involved, the frequency-thickness product of the primary mode, and the conditions on $\bar{\alpha}$ and $\bar{\beta}$ for the primary mode. The phase velocity c_{ph} and the group velocity c_{g}, respectively, are the same for both the primary and the secondary mode as shown in Chapter 3. The group velocity $c_{\mathrm{g}}^{\mathrm{u}}$ of the mode at the primary crossing point, which does not satisfy group velocity matching to the secondary symmetric mode, is given as well. The latter mode is referred to as non-matching mode.

Regarding the rate of second harmonic generation r_s for exact phase matching, Eq.(2.41) yields

$$\left|\frac{\bar{u}_z^{(2)}(h)}{\left(\bar{u}_z^{(1)}(h)\right)^2}\right|(z) = \left|\frac{a_n\,\tilde{\bar{u}}_z^{(2)}(h)\,z}{\left(\tilde{\bar{u}}_z^{(1)}(h)\right)^2}\right| = \left|\frac{a_n\,\tilde{u}_z^{(2)}(h)}{\left(\tilde{\bar{u}}_z^{(1)}(h)\right)^2}\right|\,\frac{z}{h} = r_s\,\frac{z}{h}, \tag{4.9}$$

where

$$r_s = \left|\frac{a_n\,\tilde{u}_z^{(2)}(h)}{\left(\tilde{\bar{u}}_z^{(1)}(h)\right)^2}\right|. \tag{4.10}$$

In words, the rate of second harmonic generation r_s represents the slope of the amplitude of the secondary in-plane displacement at the surface normalized by the primary mode squared. The in-plane component at the surface is chosen for this definition because the normal component vanishes at the surface as shown in Chapter 3, so that the in-plane component displays the only measurable quantity.

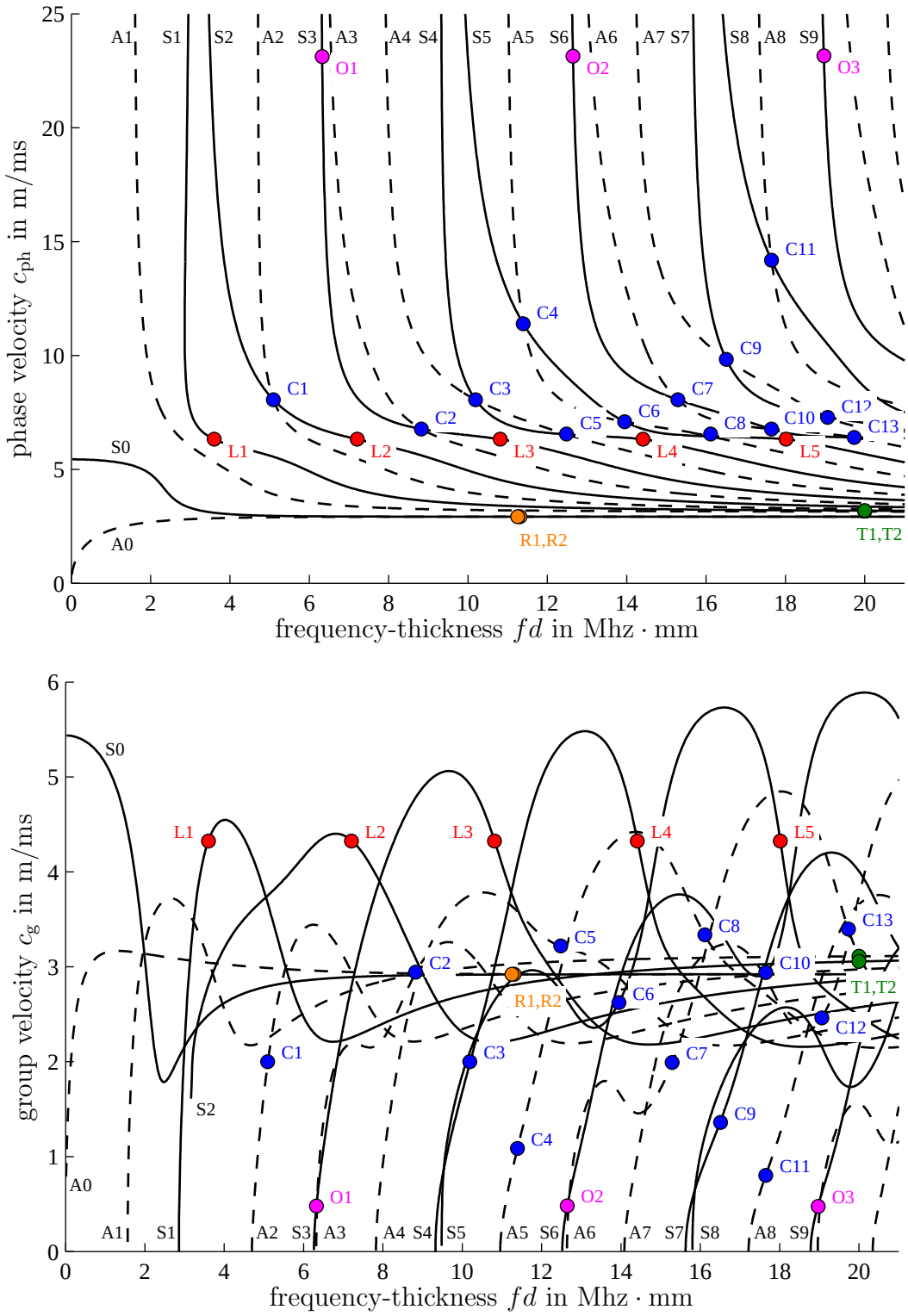

Figure 4.1: Dispersion Curves for an Aluminum Plate with Matching Pairs: C - Crossing, L - Sym. Modes at Long. Velocity, O - Cutoff Frequency, T - Nonzero Order Modes at Transversal/Shear Velocity, R - Fundamental Modes at Rayleigh Wave Speed

Table 4.2: Evaluation of Matching Pairs at Crossing Points. fd in Mhz $\cdot$ mm.

Ref.	Modes	fd	$\bar{\alpha}$, $\bar{\beta}$	c_{ph} [m/s]	c_{g} [m/s]	$c_{\mathrm{g}}^{\mathrm{u}}$ [m/s]	r_s
C1	A2→S4	5.095	$\pi/2$, $3\pi/2$	8057	2000	3752	2.49
C2	A3→S6	8.825	$\pi/2$, $5\pi/2$	6769	2943	4779	6.98
C3	S4→S8	10.190	π, 3π	8057	2000	3749	9.97
C4	A5→S10	11.390	$3\pi/2$, $7\pi/2$	11394	1086	2913	4.83
C5	A4→S8	12.480	$\pi/2$, $7\pi/2$	6533	3220	5368	14.68
C6	S5→S10	13.950	π, 4π	7089	2622	4355	16.29
C7	A6→S12	15.290	$3\pi/2$, $9\pi/2$	8057	1992	3750	22.43
C8	A5→S10	16.113	$\pi/2$, $9\pi/2$	6554	3337	5660	24.93
C9	S7→S14	16.510	2π, 5π	9824	1360	3230	13.25
C10	S6→S12	17.650	π, 5π	6769	2940	4784	27.91
C11	A8→S16	17.650	$5\pi/2$, $11\pi/2$	14179	802	2475	7.70
C12	A7→S14	19.065	$3\pi/2$, $11\pi/2$	7284	2462	4180	29.16
C13	A6→S12	19.734	$\pi/2$, $11\pi/2$	6403	3398	5848	37.74

Analyzing the results of Table 4.2 with regard to the factors mentioned in Section 4.1 reveals the following features of modes at crossing points. The major advantage of crossing points is marked by the fact that a variety of antisymmetric primary modes can be selected, first of all C1 with the lowest frequency. Even though the rate of second harmonic generation appears to be smaller for antisymmetric modes compared to symmetric primary modes, the benefit from choosing an antisymmetric primary mode might outweigh this factor. Furthermore, the fact that exact phase matching occurs at crossing points, removes any concerns about approximation tolerances on phase matching.

As will be seen later on, the absolute value of the rate of second harmonic generation is rather small compared to the other mode types, except the nonzero order modes at high wave number. Also, zero out-of-plane displacement at the surface presents a disadvantage as to measurements and excitation.

For low frequencies, crossing points are isolated very well as is seen in Figure 4.1. Even though second harmonic generation seems to be higher for high frequencies, the disadvantages of high frequencies stated in section 4.1 are likely to favor the choice of low frequencies. As crossing points are distributed all over the frequency range, they

offer the opportunity to investigate the dependency on frequency experimentally.

By the definition of a crossing point, both a symmetric and an antisymmetric primary mode simultaneously get excited, only one of which matches group velocity with the secondary mode. As seen in Table 4.2, the group velocity of the non-matching mode is much bigger than that of the matching mode. This means that the undesired non-matching mode propagates ahead of the matching mode pair. Since the non-matching mode generates secondary components as well, the measured signal can be disturbed by these waves. This problem might be moderated by exciting the mode shape of the matching primary mode as precisely as possible, so that the amplitude of the non-matching mode becomes small. This is complicated by the fact that the non-matching mode has nonzero normal displacement at the surface. An in-plane excitation approach might be needed, therefore, to excite only the matching primary mode.

4.2.2 Symmetric Modes at the Longitudinal Velocity

Table 4.3 presents the quantitative results for symmetric modes at the longitudinal phase velocity abbreviated with 'L' in Figure 4.1. The rate of second harmonic generation is defined as in Eq.(4.10) because the normal displacement at the surface is shown to be zero in this case as well.

Compared to crossing points at similar frequencies, these mode pairs allow a

Table 4.3: Evaluation of Matching Pairs at the Longitudinal Phase Velocity. fd in Mhz $\cdot$ mm.

Ref.	Modes	fd	c_{ph} [m/s]	c_{g} [m/s]	r_s
L1	S1→S2	3.603	6320	4326	3.76
L2	S2→S4	7.206	6320	4326	15.05
L3	S3→S6	10.809	6320	4326	33.87
L4	S4→S8	14.412	6320	4326	60.22
L5	S5→S10	18.015	6320	4326	94.09

higher rate of second harmonic generation. Figure 4.2 compares the second harmonic amplitude for the first two mode pairs of each type. It is pointed out that this figure only expresses the rate of second harmonic generation, and does not allow for any conclusions on the excitability of the primary wave. That is, for Figure 4.2, it is assumed that all primary modes of the mode pairs C1, C2, L1, and L2 are excited with the same in-plane displacement at the surface. Since modes at higher frequencies are usually more difficult to excite, modes with lower frequencies might be preferred, even though mode pairs with higher frequencies show larger second harmonic generation. Or in other words, a high rate of second harmonic generation is useless if the primary mode cannot be excited strongly enough, since the secondary amplitude is proportional to the primary amplitude squared.

Regarding the other factors, the primary mode is well isolated in the dispersion curve for lower frequencies. Moreover, L1 represents the matching pair with the lowest frequency. A last advantage is presented by the comparably high group velocity of

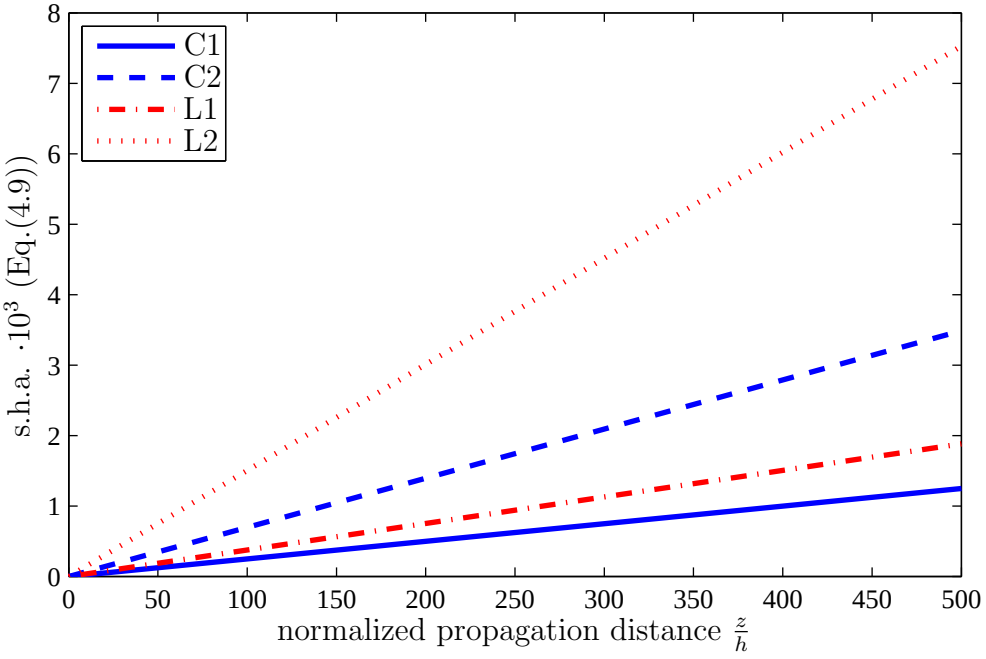

Figure 4.2: Second Harmonic Amplitude (s.h.a.) for Crossing Points and Symmetric Modes at Longitudinal Velocity

the modes involved.

Yet, two disadvantages stand out. First, only symmetric modes can be excited, which might speak in favor for crossing points with an antisymmetric primary mode, and secondly, the normal displacement at the surface vanishes as for crossing points. Again, an in-plane excitation method might help to excite a strong primary mode.

4.2.3 Nonzero Order Modes at Cutoff Frequencies

For nonzero order modes at cutoff frequencies, which are tagged 'O' in Figure 4.1, phase and group matching hold only approximately. For this reason, Table 4.4 shows not only the phase and group velocity for the primary but also for the secondary mode. The frequency of evaluation is chosen to be at one percent deviation from the exact cutoff frequency, i.e.

$$fd = 1.01\, fd_{\text{cutoff}}. \tag{4.11}$$

By analyzing all the modes at these frequencies, it is found that only three mode pairs are close to condition Eq.(4.8), while only one mode pair, O1, satisfies the condition. Due to the high rate of second harmonic generation, however, a smaller value for $\bar{L}$ than required above might still be sufficient.

As the approximation for low but nonzero wave numbers is considered, the normal displacement at the surface does not vanish identically as suggested by Chapter 3. The rate of the normal displacements r_y is given in Table 4.4 for the primary and the secondary mode, respectively.

Also, the rate of second harmonic generation is derived in a slightly different way than before. Since approximate phase matching holds, Eqs.(2.41) and (2.57) yield

$$\begin{aligned}\left|\frac{\bar{u}_y^{(2)}(h)}{\left(\bar{u}_y^{(1)}(h)\right)^2}\right|(z) &= \left|\frac{a_n\,\tilde{\bar{u}}_y^{(2)}(h)}{\left(\tilde{\bar{u}}_y^{(1)}(h)\right)^2}\,\frac{2\sin\left(\frac{1}{2}\kappa_{\mathrm{d}}\,z\right)}{\kappa_{\mathrm{d}}}\right| = \left|\frac{a_n\,\tilde{u}_y^{(2)}(h)}{\left(\tilde{\bar{u}}_y^{(1)}(h)\right)^2}\right|\left|\frac{2}{\bar{\kappa}_{\mathrm{d}}}\sin\left(\tfrac{1}{2}\bar{\kappa}_{\mathrm{d}}\,\tfrac{z}{h}\right)\right| \\ &= r_s\left|\frac{2}{\bar{\kappa}_{\mathrm{d}}}\sin\left(\tfrac{1}{2}\bar{\kappa}_{\mathrm{d}}\,\tfrac{z}{h}\right)\right|,\end{aligned} \tag{4.12}$$

where

$$r_s = \left| \frac{a_n \, \tilde{u}_y^{(2)}(h)}{\left(\tilde{u}_y^{(1)}(h)\right)^2} \right|. \tag{4.13}$$

Note that the rate of second harmonic generation reads in terms of the normal displacement at the surface as opposed to the in-plane component above. Furthermore, one observes that for small $\bar{\kappa}_\mathrm{d}\, z/h$

$$r_s \left| \frac{2}{\bar{\kappa}_\mathrm{d}} \sin\left(\tfrac{1}{2}\bar{\kappa}_\mathrm{d}\, \tfrac{z}{h}\right) \right| \approx r_s \frac{z}{h}, \tag{4.14}$$

which shows that approximate phase matching results in an approximately linear increase of the second harmonic amplitude over a long distance, if the deviation $\bar{\kappa}_\mathrm{d}$ from exact phase matching is small enough.

The critical observation in Table 4.4 is the big rate of second harmonic generation for these modes. This is explained by the wave propagation of the partial waves comprising the Lamb mode. Since the wave number $\bar{\kappa}$ of the mode is small, the partial waves propagate at an angle almost perpendicular to the plate's surface, bouncing back and forth between the surfaces at a sharp angle. In this way, the partial waves pass a long distance in the material while proceeding only little in the propagation direction. The long travel distance in the material leads then to a high second harmonic generation due to nonlinearities.

Besides this big advantage, there are a couple of issues that need to be addressed. Since the phase velocity and the wave number are very sensitive to changes in frequency, the modes are highly dispersive, meaning that it will be hard to excite a mode

Table 4.4: Evaluation of Matching Pairs at Cutoff Frequencies. fd in Mhz $\cdot$ mm. Velocities in m/s.

Ref.	Modes	fd	$c_\mathrm{ph}^{(1)}$	$c_\mathrm{ph}^{(2)}$	$c_\mathrm{g}^{(1)}$	$c_\mathrm{g}^{(2)}$	r_s	$\bar{L}$	$r_y^{(1)}$	$r_y^{(2)}$
O1	S3→S6	6.323	23125	23135	480	482	261.10	1960	0.07	0.14
O2	S6→S12	12.645	23136	23182	482	478	568.27	228	0.14	0.26
O3	S9→S18	18.969	23154	23272	475	499	989.99	60	0.20	0.38

with specific frequency and wave number. Also, only symmetric primary modes show sufficient approximation precision, and the ratios of normal displacements at the surface $r_y^{(1)}$ and $r_y^{(2)}$ tend to be small, especially for the mode pair O1 with the lowest frequency.

Low group velocity displays another remarkable feature of these modes. Depending on the application this might lead to problems as reflexions from the boundaries of faster modes might influence measurements. On the other hand, this feature might be used to obtain a signal that is well separated from other modes in the time domain.

4.2.4 Nonzero Order Modes with High Wave Number

Table 4.5 shows the evalution of nonzero order modes for high wave numbers, which are abbreviated with 'T' in Figure 4.1. It is found that no mode pair can satisfy Eq.(4.8) for a primary frequency smaller than $fd = 20\,\mathrm{MHz\,mm}$. The two best mode pairs in terms of a long dispersion length at frequency $fd = 20\,\mathrm{MHz\,mm}$ are presented, nevertheless, in order to evaluate them with regard to other factors. The items in Table 4.5 are defined in the same way as those of Table 4.4 in Section 4.2.3.

In short, the only positive feature of these modes turns out to be the antisymmetry of the primary mode of mode pair T1, which offers an advantage in the excitation of the primary mode. For most of the other factors, however, these modes perform worse than other mode pairs.

First, even at very high frequencies, the dispersion length is fairly small. For the mode pair T1 and a plate of thickness 1 mm, measurements are useful along a distance

Table 4.5: Evaluation of Matching Pairs for Nonzero Order Modes with High Wave Number. fd in Mhz $\cdot$ mm. Velocities in m/s.

Ref.	Modes	fd	$c_{\mathrm{ph}}^{(1)}$	$c_{\mathrm{ph}}^{(2)}$	$c_{\mathrm{g}}^{(1)}$	$c_{\mathrm{g}}^{(2)}$	r_s	$\bar{L}$	$r_y^{(1)}$	$r_y^{(2)}$
T1	A1 $\rightarrow$ S1	20.000	3144.0	3141.5	3111	3116	0.6684	49.4	0.16	0.14
T2	S1 $\rightarrow$ S2	20.000	3186.3	3176.6	3056	3077	2.3354	13.0	0.29	0.28

of about 5 cm from the source, for example. Besides the small normal displacement at the surface, the rate of second harmonic generation remains small as well. Also, the nonzero order modes are barely isolated from each other for high frequencies, which makes the excitation of a single mode difficult. The group velocity at the shear wave speed is neither particularly high nor low.

4.2.5 Quasi-Rayleigh Surface Wave

The quasi-Rayleigh wave, which is marked as 'R' in Figure 4.1, is evaluated at the lowest frequency where the condition on $|\bar{\kappa}_\mathrm{d}|$ in Eq.(4.8) is satisfied. All items of Table 4.6 are defined in the same way as in the two sections on approximate matching pairs above.

Table 4.6 reveals several advantages for quasi-Rayleigh waves. While all other mode pairs have zero or near zero normal displacement at the surface, the quasi-Rayleigh wave shows by far the largest normal displacement component at the surface, making it much easier to excite and detect. Also, the rate of second harmonic generation is exceeded only by modes at cutoff frequencies. Figure 4.3 compares the rates of second harmonic generation for the approximate matching pairs O1, T1, and R1 according to Eq.(4.12). Returning to the quasi-Rayleigh wave, the fact that the quasi-Rayleigh wave is approximately nondispersive displays another advantage, making the excitation less sensitive to shifts of the excitation frequency. Thus, there is much freedom in the choice of the excitation frequency.

The major disadvantage is presented by the fact that quasi-Rayleigh waves are

Table 4.6: Evaluation of Matching Pairs for the Quasi-Rayleigh Wave. fd in Mhz $\cdot$ mm. Velocities in m/s.

Ref.	Modes	fd	$c_\mathrm{ph}^{(1)}$	$c_\mathrm{ph}^{(2)}$	$c_\mathrm{g}^{(1)}$	$c_\mathrm{g}^{(2)}$	r_s	$\bar{L}$	$r_y^{(1)}$	$r_y^{(2)}$
R1	S0 $\rightarrow$ S0	10.288	2921.3	2920.8	2917	2921	54.4327	400	0.91	0.91
R2	A0 $\rightarrow$ S0	10.264	2920.2	2920.8	2924	2921	54.2234	400	0.91	0.91

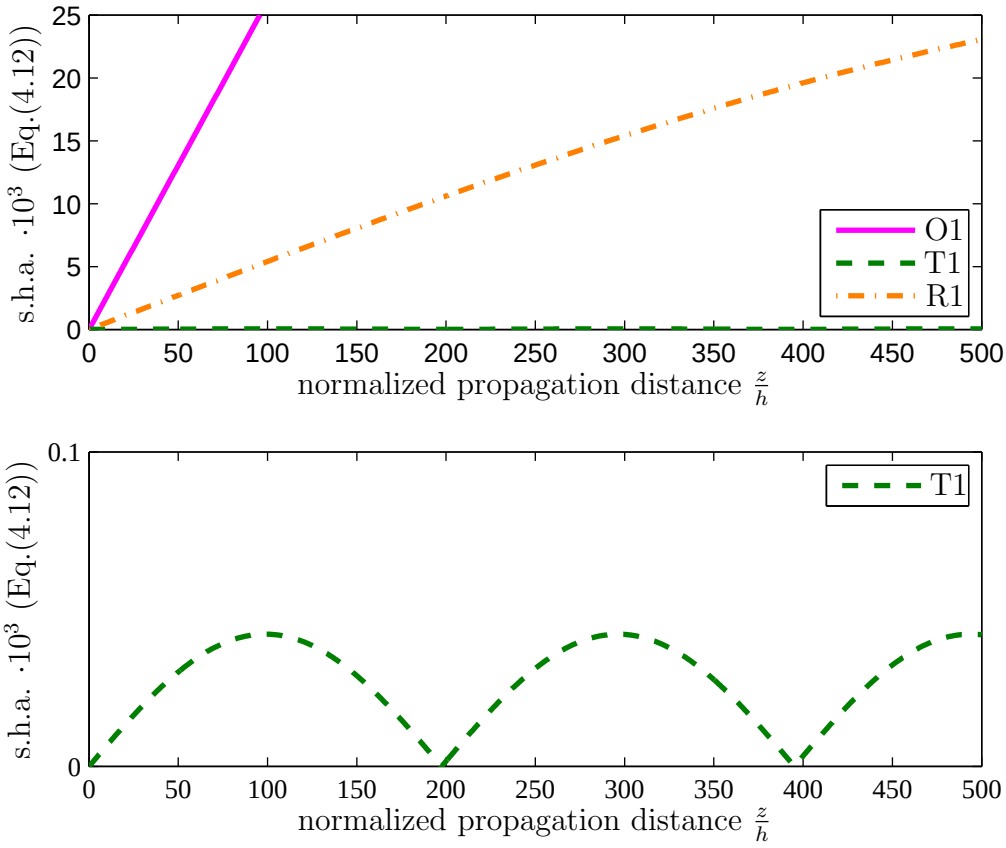

Figure 4.3: Second Harmonic Amplitude (s.h.a.) for Approximate Matching Pairs (O1, T1, and R1)

basically surface waves, meaning that the energy is concentrated within a thin layer with the thickness of one wavelength beneath the surface. Thus, with regard to material's characterization methods that are intended to evaluate properties of the whole volume of a plate, the quasi-Rayleigh wave is useless. Applications of quasi-Rayleigh waves are common, however, where the surface of the plate is of interest, as for example in Herrmann et al. [11].

Rather low group velocity and the proximity to nonzero order modes in the dispersion curve are minor disadvantages. The discussion on the symmetry of the primary mode is unessential as the symmetric and the antisymmetric primary mode comprise the quasi-Rayleigh wave together. In this context, it is noted that the theory

presented here suggests that the secondary wave will differ in shape from the primary wave, since only symmetric second harmonic modes are generated according to Chapter 2. This means that both surfaces of the plate have to show the same normal displacement for the second harmonic wave, while for the primary wave, the superposition of the symmetric and the antisymmetric fundamental mode can cancel out the displacement at one surface.

4.2.6 Summary

The pros and cons for the different types of matching pairs, as presented above, are listed in Table 4.7 for quick reference. It remains to summarize the most important observations from the above evaluation.

First, all modes satisfying phase and group velocity matching show zero or small normal displacement at the surface except the quasi-Rayleigh wave. The latter has the crucial disadavantage of not being an actual Lamb mode since the quasi-Rayleigh wave does not penetrate the whole plate but only the region beneath the surface. As to the other modes, an in-plane excitation approach is suggested to increase the excitation of the primary wave.

In terms of second harmonic generation, the modes at cutoff frequencies dominate the other mode pair types. However, due to several disadvantages mentioned in Table 4.7, the practicability of these modes needs to be investigated experimentally. Besides quasi-Rayleigh waves, which could be useless for some material's characterization methods because of their surface wave character, crossing points and symmetric waves at longitudinal velocity represent the set of modes to choose from. Crossing points offer the advantage of allowing an antisymmetric mode as a primary mode, while the excitation of the other, non-matching primary mode at the crossing point might cause problems as discussed in Section 4.2.1. The nonzero order modes with

high wave number appear to have no crucial advantage over other mode pairs, probably making them useless for practical applications.

Table 4.7: Pros and Cons of Matching Pairs

Crossing Points – C	
+ antisymmetric primary wave possible	– zero normal displacement at surface
+ exact phase and group velocity matching	– rather low rate of second harmonic generation
+ low excitation frequency possible	– excitation of non-matching primary mode
Symmetric Modes at Longitudinal Velocity – L	
+ exact phase and group velocity matching	– zero normal displacement at surface
+ high group velocity	– no antisymmetric primary mode
+ low excitation frequency possible	
Modes at Cutoff Frequencies – O	
+ very high rate of second harmonic generation	– approximate phase and group velocity matching
	– highly dispersive
	– low normal displacement at the surface
	– very low group velocity
Nonzero Order Modes with High Wave Number – T	
+ antisymmetric primary wave possible	– very low rate of second harmonic generation
+ approximately non-dispersive	– low normal displacement at the surface
	– fairly short dispersion length even for very high frequencies
	– modes not well isolated
Quasi-Rayleigh Surface Wave – R	
+ high normal displacement at the surface	– energy of the mode concentrated at the surface
+ Good rate of second harmonic generation	– high frequencies
+ approximately non-dispersive	

CHAPTER V

CONCLUSION

Recalling the objectives in Chapter 1, the solution of second harmonic Lamb wave generation is derived in Section 2.1 following De Lima [5]. The major result is the amplitude coefficient $A_n(z)$ for each secondary mode n in the modal expansion of the secondary wave. It is concluded that a secondary mode shows internal resonance if the power flux from the primary to the secondary mode is nonzero, and exact or approximate phase velocity matching occurs. While internal resonance is favorable to measurements due to the linear increase in the secondary amplitude, the nonresonant solution proves to be unfeasible for applications in material's characterization, because the amplitudes of the second harmonic wave remain small in this case.

With regard to the symmetry properties it is shown in Section 2.2.2 that both a symmetric and an antisymmetric primary mode have nonzero power flux to a secondary mode, but zero power flux to an antisymmetric secondary mode. This confirms Deng's statement [8] that the secondary wave is purely symmetric, and extends it to the conclusion that the cross-modal generation from an antisymmetric primary to a symmetric secondary mode is possible.

The above result is necessary as to the search for phase velocity matching pairs in the dispersion curve of Lamb modes, as performed in Chapter 3. The analysis shows that there are five types of modes that satisfy phase and group velocity matching:

1. Modes at crossing points

2. Symmetric modes at the longitudinal phase velocity

3. Nonzero order modes at cutoff frequencies

4. Nonzero order modes with high wave number

5. Fundamental modes with high wave number (quasi-Rayleigh Wave).

Each of these mode types is evaluated in Chapter 4 with regard to a strong measurable second harmonic amplitude as summarized in Table 4.7. The investigation shows that modes at cutoff frequencies display a very high second harmonic generation. Yet, they suffer from several disadavantages, whose impact on real experiments needs to be investigated in practice. Quasi-Rayleigh waves turn out to be most useful when the plate's surface is of interest. While nonzero order modes with high wave numbers appear to be unfavorable in some respects, the pros and cons of modes at crossing points and symmetric modes at the longitudinal velocity do not clearly allow for a general conclusion as to which of these two mode types should be preferred. Instead, the information provided in this work can be used to decide the answer to this choice for a specific application.

As to limitations of the results presented in this work, it is pointed out that the solution in Section 2.1 employs a perturbation method which requires the secondary mode to be much smaller than the primary mode. If this condition is violated, the perturbation solution does not hold. Moreover, the results presented in Chapter 4 are evaluated for the example of an aluminum plate, so that only qualitative conclusions for other materials are possible. Finally, it should be noted that the analysis applies only to elastic, isotropic, and homogeneous plates. Most metals meet these conditions, while composites, concrete or rock, for instance, do not.

"Knowing is not enough; we must apply.
Willing is not enough; we must do."

J. W. von Goethe

... describes in the most appropriate way which future work is needed and suggested. As a first step, the results presented in this thesis should be confirmed experimentally. Especially, the modes at cutoff frequencies present a good opportunity to achieve high second harmonic amplitudes. Also, results from crossing points and symmetric modes at longitudinal velocity should be compared experimentally, since the pros and cons cannot identify without doubt, which mode is to be preferred.

As a second step, the information provided should be used to improve existing methods for material's characterization and NDE by obtaining stronger signals for the second harmonic amplitude.

Further theoretical work might be needed as to the influence of damage and fatigue on the material's properties, and consequently on the second harmonic amplitude. Also, the extension to materials that do not satisfy homogeneity or isotropy might be of interest for future applications. Concerning different geometries, De Lima's work [5] provides tools for cylindrical rods and shells, which could be investigated for practical issues in a similar way. Also, a theory for plates with varying thickness or for wave guides with surrounding materials could be of interest in the future.

APPENDIX A

LINEAR PLATE THEORY

In this appendix, the solution for a linear plate is presented following Graff's [10] derivation. Waves propagate in the positive z-direction. Furthermore, plane strain is assumed in x and the surface of the plate is stress free.

The linear, homogeneous equations of motion in displacement formulation

$$(\lambda + 2\mu)\boldsymbol{\nabla}(\boldsymbol{\nabla} \cdot \boldsymbol{u}) - \mu\boldsymbol{\nabla} \times (\boldsymbol{\nabla} \times \boldsymbol{u}) = \rho\frac{\partial^2 \boldsymbol{u}}{\partial t^2} \tag{A.1}$$

in combination with the stress free boundary conditions

$$\sigma_{yx} = 0 \tag{A.2a}$$

$$\sigma_{yy} = 0 \tag{A.2b}$$

$$\sigma_{yz} = 0 \tag{A.2c}$$

at the surface $y = \pm h$, is the linear boundary value problem to be solved. Lamé's constant λ, the shear modulus μ and the density ρ are constant material properties. A common solution approach is the use of Helmholtz potentials. In terms of the scalar potential ϕ and the vector potential $\boldsymbol{\psi}$, the displacement field reads as

$$\boldsymbol{u} = \boldsymbol{\nabla}\phi + \boldsymbol{\nabla} \times \boldsymbol{\psi}, \tag{A.3}$$

where the divergence condition

$$\boldsymbol{\nabla} \cdot \boldsymbol{\psi} = 0 \tag{A.4}$$

on $\boldsymbol{\psi}$ is required. The equation of motion Eq.(A.1) is then rewritten as two wave

equations

$$\boldsymbol{\nabla}^2\phi = \frac{1}{c_{\mathrm{L}}^2}\frac{\partial^2\phi}{\partial t^2}, \tag{A.5a}$$

$$\boldsymbol{\nabla}^2\boldsymbol{\psi} = \frac{1}{c_{\mathrm{T}}^2}\frac{\partial^2\boldsymbol{\psi}}{\partial t^2} \tag{A.5b}$$

for the potentials, where

$$c_{\mathrm{L}} = \sqrt{\frac{\lambda + 2\mu}{\rho}} \tag{A.6}$$

is the longitudinal velocity and

$$c_{\mathrm{T}} = \sqrt{\frac{\mu}{\rho}} \tag{A.7}$$

the shear velocity in an unbounded medium. If the potentials are assumed to have the form

$$\phi(y,z,t) = \tilde{\phi}(y)\, e^{i(\kappa z - \omega t)}, \tag{A.8a}$$

$$\boldsymbol{\psi}(y,z,t) = \tilde{\boldsymbol{\psi}}(y)\, e^{i(\kappa z - \omega t)}, \tag{A.8b}$$

where κ is the wave number and ω the angular frequency, solving for Eqs.(A.5) yields

$$\phi(y,z) = (A\cos\alpha y + B\sin\alpha y)\, e^{i(\kappa z - \omega t)}, \tag{A.9a}$$

$$\psi_x(y,z) = (C\cos\beta y + D\sin\beta y)\, e^{i(\kappa z - \omega t)}, \tag{A.9b}$$

$$\psi_y(y,z) = (E\cos\beta y + F\sin\beta y)\, e^{i(\kappa z - \omega t)}, \tag{A.9c}$$

$$\psi_z(y,z) = (G\cos\beta y + H\sin\beta y)\, e^{i(\kappa z - \omega t)}, \tag{A.9d}$$

where

$$\alpha = \sqrt{(\omega/c_{\mathrm{L}})^2 - \kappa^2}, \quad \beta = \sqrt{(\omega/c_{\mathrm{T}})^2 - \kappa^2}. \tag{A.10}$$

Writing the displacement field as

$$\boldsymbol{u}(y,z,t) = \tilde{\boldsymbol{u}}(y)\, e^{i(\kappa z - \omega t)}, \tag{A.11}$$

one obtains

$$\tilde{u}_x = -Ei\kappa\cos\beta y - Fi\kappa\sin\beta y - G\beta\sin\beta y + H\beta\cos\beta y, \tag{A.12a}$$

$$\tilde{u}_y = -A\alpha\sin\alpha y + B\alpha\cos\alpha y + Ci\kappa\cos\beta y + Di\kappa\sin\beta y, \tag{A.12b}$$

$$\tilde{u}_z = Ai\kappa\cos\alpha y + Bi\kappa\sin\alpha y + C\beta\sin\beta y - D\beta\cos\beta y \tag{A.12c}$$

by the use of Eq.(A.3). In order to get the stress field from the displacement field, the constitutive relation

$$\sigma_{ij} = \lambda\varepsilon_{kk}\delta_{ij} + 2\mu\varepsilon_{ij} \tag{A.13}$$

in index notation is employed, where the linear strain is defined by

$$\varepsilon_{ij} = \tfrac{1}{2}\left(u_{i,j} + u_{j,i}\right). \tag{A.14}$$

In this case, Eqs.(A.12) yield

$$\varepsilon_{xx} = 0 \tag{A.15a}$$

$$\begin{aligned}\varepsilon_{yy} = \big(&\alpha^2(-A\cos\alpha y - B\sin\alpha y) + \\ &+ i\kappa\beta(-C\sin\beta y + D\cos\beta y)\big)\, e^{i(\kappa z-\omega t)}\end{aligned} \tag{A.15b}$$

$$\begin{aligned}\varepsilon_{zz} = \big(&\kappa^2(-A\cos\alpha y - B\sin\alpha y) + \\ &+ i\kappa\beta(C\sin\beta y - D\cos\beta y)\big)\, e^{i(\kappa z-\omega t)}\end{aligned} \tag{A.15c}$$

$$\begin{aligned}\varepsilon_{yx} = \frac{1}{2}\big(&i\kappa\beta(E\sin\beta y - F\cos\beta y) + \\ &+ \beta^2(-G\cos\beta y - H\sin\beta y)\big)\, e^{i(\kappa z-\omega t)}\end{aligned} \tag{A.15d}$$

$$\begin{aligned}\varepsilon_{yz} = \frac{1}{2}\big(&2i\kappa\alpha(-A\sin\alpha y + B\cos\alpha y) + \\ &+ (\beta^2-\kappa^2)(C\cos\beta y + D\sin\beta y)\big)\, e^{i(\kappa z-\omega t)}\end{aligned} \tag{A.15e}$$

for the strain components needed in the boundary conditions. The convergence condition Eq.(A.4)

$$\left(-E\beta\sin\beta y + F\beta\cos\beta y + Gi\kappa\cos\beta y + Hi\kappa\sin\beta y\right) e^{i(\kappa z-\omega t)} = 0 \tag{A.16}$$

and the boundary conditions Eqs.(A.2)

$$\sigma_{yx} = 2\mu\varepsilon_{yx} = 0 \tag{A.17a}$$

$$\sigma_{yy} = (\lambda + 2\mu)\varepsilon_{yy} + \lambda(\varepsilon_{xx} + \varepsilon_{zz}) = 0 \tag{A.17b}$$

$$\sigma_{yz} = 2\mu\varepsilon_{yz} = 0 \tag{A.17c}$$

evaluated at the surface, yield eight independent equations for the unknown variables A to G in Eqs.(A.9). These equations can be simplified as

$$\begin{bmatrix} i\kappa\cos\beta h & \beta\cos\beta h & 0 & 0 & 0 & 0 & 0 & 0 \\ \beta^2\cos\beta h & h\cos\beta h & 0 & 0 & 0 & 0 & 0 & 0 \\ 0 & 0 & -\beta\sin\beta h & i\kappa\sin\beta h & 0 & 0 & 0 & 0 \\ 0 & 0 & -h\sin\beta h & \beta^2\sin\beta h & 0 & 0 & 0 & 0 \\ 0 & 0 & 0 & 0 & -c\cos\alpha h & f\cos\beta h & 0 & 0 \\ 0 & 0 & 0 & 0 & d\sin\alpha h & g\sin\beta h & 0 & 0 \\ 0 & 0 & 0 & 0 & 0 & 0 & -g\cos\beta h & d\cos\alpha h \\ 0 & 0 & 0 & 0 & 0 & 0 & f\sin\beta h & c\sin\alpha h \end{bmatrix} \begin{bmatrix} G \\ F \\ E \\ H \\ A \\ D \\ C \\ B \end{bmatrix} = \mathbf{0}, \tag{A.18}$$

where

$$c = (\lambda + 2\mu)\alpha^2 + \lambda\kappa^2, \quad d = 2i\kappa\alpha$$

$$f = 2i\mu\kappa\beta, \quad g = \kappa^2 - \beta^2, \quad h = i\kappa\beta. \tag{A.19}$$

For a non-trivial solution, the determinant of the matrix has to be zero. Note that every two unknowns are decoupled by a two-by-two submatrix. Thus, setting to zero the determinant of one submatrix and the unknwons which are not associated with this submatrix, results in four different types of solutions, called mode types. The condition on the respective submatrix will yield a frequency condition, also called dispersion relation, for each mode type, while the ratio of the two associated unknowns is given by Eq.(A.18). The results for the mode types are presented below.

- *Symmetric SH modes* $(E, H \neq 0)$

  Frequency Equation

$$\left(\frac{\omega h}{c_{\mathrm{T}}}\right)^2 = (n\pi)^2 + (\kappa h)^2, \quad n = 0, 1, 2, 3, ... \tag{A.20}$$

Displacement Field

$$\tilde{u}_x = -Ei\kappa \cos \beta y + H\beta \cos \beta y \tag{A.21a}$$

$$\tilde{u}_y = \tilde{u}_z = 0 \tag{A.21b}$$

Simplified Displacement Field

$$\tilde{u}_x = H \, \frac{\kappa^2 + \beta^2}{\beta} \cos \beta y \tag{A.22a}$$

$$\tilde{u}_y = \tilde{u}_z = 0 \tag{A.22b}$$

- *Antisymmetric SH modes* $(G, F \neq 0)$

  Frequency Equation

$$\left(\frac{\omega h}{c_{\mathrm{T}}}\right)^2 = \left(\frac{(2n+1)\pi}{2}\right)^2 + (\kappa h)^2, \quad n = 0, 1, 2, 3, ... \tag{A.23}$$

  Displacement Field

$$\tilde{u}_x = -Fi\kappa \sin \beta y - G\beta \sin \beta y \tag{A.24a}$$

$$\tilde{u}_y = \tilde{u}_z = 0 \tag{A.24b}$$

  Simplified Displacement Field

$$\tilde{u}_x = -G \, \frac{\kappa^2 + \beta^2}{\beta} \sin \beta y \tag{A.25a}$$

$$\tilde{u}_y = \tilde{u}_z = 0 \tag{A.25b}$$

- *Symmetric Rayleigh-Lamb modes* $(A, D \neq 0)$

  Frequency Equation

$$\frac{\tan \beta h}{\tan \alpha h} = -\frac{4\alpha\beta\kappa^2}{(\kappa^2 - \beta^2)^2} \tag{A.26}$$

  Displacement Field

$$\tilde{u}_x = 0 \tag{A.27a}$$

$$\tilde{u}_y = -A\alpha \sin \alpha y + Di\kappa \sin \beta y \tag{A.27b}$$

$$\tilde{u}_z = Ai\kappa \cos \alpha y - D\beta \cos \beta y \tag{A.27c}$$

Simplified Displacement Field

$$\tilde{u}_x = 0 \tag{A.28a}$$

$$\tilde{u}_y = iD\Big(-\frac{(\kappa^2-\beta^2)\sin\beta h}{2\kappa\sin\alpha h}\sin\alpha y + \kappa\sin\beta y\Big) \tag{A.28b}$$

$$\tilde{u}_z = -D\Big(\frac{(\kappa^2-\beta^2)\sin\beta h}{2\alpha\sin\alpha h}\cos\alpha y + \beta\cos\beta y\Big) \tag{A.28c}$$

- *Antisymmetric Rayleigh-Lamb modes* $(B, C \neq 0)$

  Frequency Equation

$$\frac{\tan\beta h}{\tan\alpha h} = -\frac{(\kappa^2-\beta^2)^2}{4\alpha\beta\kappa^2} \tag{A.29}$$

  Displacement Field

$$\tilde{u}_x = 0 \tag{A.30a}$$

$$\tilde{u}_y = B\alpha\cos\alpha y + Ci\kappa\cos\beta y \tag{A.30b}$$

$$\tilde{u}_z = Bi\kappa\sin\alpha y + C\beta\sin\beta y \tag{A.30c}$$

  Simplified Displacement Field

$$\tilde{u}_x = 0 \tag{A.31a}$$

$$\tilde{u}_y = iC\Big(-\frac{(\kappa^2-\beta^2)\cos\beta h}{2\kappa\cos\alpha h}\cos\alpha y + \kappa\cos\beta y\Big) \tag{A.31b}$$

$$\tilde{u}_z = C\Big(\frac{(\kappa^2-\beta^2)\cos\beta h}{2\alpha\cos\alpha h}\sin\alpha y + \beta\sin\beta y\Big) \tag{A.31c}$$

APPENDIX B

SYMMETRY PROPERTIES OF FORCING TERMS

In order to investigate the symmetry properties of $\bar{\boldsymbol{S}}$ in Eq.(2.14b), all terms are analyzed as shown exemplarily in Section 2.2.2.

B.1 Symmetric Primary Wave

For a symmetric primary mode, one obtains the following terms in $\bar{\boldsymbol{S}}$:

- Entry i=j=2

$$\begin{aligned}\frac{\partial u_k}{\partial a_l}\frac{\partial u_k}{\partial a_l} &= \frac{\partial u_y}{\partial y}\frac{\partial u_y}{\partial y} + \frac{\partial u_y}{\partial z}\frac{\partial u_y}{\partial z} + \frac{\partial u_z}{\partial y}\frac{\partial u_z}{\partial y} + \frac{\partial u_z}{\partial z}\frac{\partial u_z}{\partial z} = \\ &= \mathcal{S}^2(y) + \mathcal{A}^2(y) + \mathcal{A}^2(y) + \mathcal{S}^2(y) = \\ &= \mathcal{S}(y) + \mathcal{S}(y) + \mathcal{S}(y) + \mathcal{S}(y) = \mathcal{S}(y), \qquad \text{(B.1a)}\\ \frac{\partial u_k}{\partial a_k}\frac{\partial u_l}{\partial a_l} &= \frac{\partial u_y}{\partial y}\frac{\partial u_y}{\partial y} + \frac{\partial u_y}{\partial z}\frac{\partial u_z}{\partial z} + \frac{\partial u_z}{\partial z}\frac{\partial u_y}{\partial y} + \frac{\partial u_z}{\partial z}\frac{\partial u_z}{\partial z} = \\ &= \mathcal{S}^2(y) + \mathcal{S}^2(y) + \mathcal{S}^2(y) + \mathcal{S}^2(y) = \\ &= \mathcal{S}(y) + \mathcal{S}(y) + \mathcal{S}(y) + \mathcal{S}(y) = \mathcal{S}(y), \qquad \text{(B.1b)}\\ \frac{\partial u_k}{\partial a_l}\frac{\partial u_l}{\partial a_k} &= \frac{\partial u_y}{\partial y}\frac{\partial u_y}{\partial y} + \frac{\partial u_y}{\partial z}\frac{\partial u_z}{\partial y} + \frac{\partial u_z}{\partial y}\frac{\partial u_y}{\partial z} + \frac{\partial u_z}{\partial z}\frac{\partial u_z}{\partial z} = \\ &= \mathcal{S}^2(y) + \mathcal{A}^2(y) + \mathcal{A}^2(y) + \mathcal{S}^2(y) = \\ &= \mathcal{S}(y) + \mathcal{S}(y) + \mathcal{S}(y) + \mathcal{S}(y) = \mathcal{S}(y), \qquad \text{(B.1c)}\end{aligned}$$

$$\frac{\partial u_k}{\partial a_k}\frac{\partial u_2}{\partial a_2} = \frac{\partial u_y}{\partial y}\frac{\partial u_y}{\partial y} + \frac{\partial u_z}{\partial z}\frac{\partial u_y}{\partial y} =$$

$$= \mathcal{S}^2(y) + \mathcal{S}^2(y) = \mathcal{S}(y) + \mathcal{S}(y) = \mathcal{S}(y), \tag{B.1d}$$

$$\frac{\partial u_2}{\partial a_k}\frac{\partial u_k}{\partial a_2} = \frac{\partial u_y}{\partial y}\frac{\partial u_y}{\partial y} + \frac{\partial u_y}{\partial z}\frac{\partial u_z}{\partial y} =$$

$$= \mathcal{S}^2(y) + \mathcal{A}^2(y) = \mathcal{S}(y) + \mathcal{S}(y) = \mathcal{S}(y), \tag{B.1e}$$

$$\frac{\partial u_2}{\partial a_k}\frac{\partial u_2}{\partial a_k} = \frac{\partial u_y}{\partial y}\frac{\partial u_y}{\partial y} + \frac{\partial u_y}{\partial z}\frac{\partial u_y}{\partial z} =$$

$$= \mathcal{S}^2(y) + \mathcal{A}^2(y) = \mathcal{S}(y) + \mathcal{S}(y) = \mathcal{S}(y), \tag{B.1f}$$

$$\frac{\partial u_k}{\partial a_2}\frac{\partial u_k}{\partial a_2} = \frac{\partial u_y}{\partial y}\frac{\partial u_y}{\partial y} + \frac{\partial u_z}{\partial y}\frac{\partial u_z}{\partial y} =$$

$$= \mathcal{S}^2(y) + \mathcal{A}^2(y) = \mathcal{S}(y) + \mathcal{S}(y) = \mathcal{S}(y). \tag{B.1g}$$

- Entry i=j=3

$$\frac{\partial u_k}{\partial a_k}\frac{\partial u_3}{\partial a_3} = \frac{\partial u_y}{\partial y}\frac{\partial u_z}{\partial z} + \frac{\partial u_z}{\partial z}\frac{\partial u_z}{\partial z} =$$

$$= \mathcal{S}^2(y) + \mathcal{S}^2(y) = \mathcal{S}(y) + \mathcal{S}(y) = \mathcal{S}(y), \tag{B.2a}$$

$$\frac{\partial u_3}{\partial a_k}\frac{\partial u_k}{\partial a_3} = \frac{\partial u_z}{\partial y}\frac{\partial u_y}{\partial z} + \frac{\partial u_z}{\partial z}\frac{\partial u_z}{\partial z} =$$

$$= \mathcal{A}^2(y) + \mathcal{S}^2(y) = \mathcal{S}(y) + \mathcal{S}(y) = \mathcal{S}(y), \tag{B.2b}$$

$$\frac{\partial u_3}{\partial a_k}\frac{\partial u_3}{\partial a_k} = \frac{\partial u_z}{\partial y}\frac{\partial u_z}{\partial y} + \frac{\partial u_z}{\partial z}\frac{\partial u_z}{\partial z} =$$

$$= \mathcal{A}^2(y) + \mathcal{S}^2(y) = \mathcal{S}(y) + \mathcal{S}(y) = \mathcal{S}(y), \tag{B.2c}$$

$$\frac{\partial u_k}{\partial a_3}\frac{\partial u_k}{\partial a_3} = \frac{\partial u_y}{\partial z}\frac{\partial u_y}{\partial z} + \frac{\partial u_z}{\partial z}\frac{\partial u_z}{\partial z} =$$

$$= \mathcal{A}^2(y) + \mathcal{S}^2(y) = \mathcal{S}(y) + \mathcal{S}(y) = \mathcal{S}(y), \tag{B.2d}$$

plus Eqs.(B.1a) to (B.1c) shown above.

- Entry i=2, j=3

$$\frac{\partial u_k}{\partial a_k}\frac{\partial u_2}{\partial a_3} = \frac{\partial u_y}{\partial y}\frac{\partial u_y}{\partial z} + \frac{\partial u_z}{\partial z}\frac{\partial u_y}{\partial z} =$$

$$= \mathcal{S}(y)\cdot\mathcal{A}(y) + \mathcal{S}(y)\cdot\mathcal{A}(y) = \mathcal{A}(y) + \mathcal{A}(y) = \mathcal{A}(y), \tag{B.3a}$$

$$\frac{\partial u_2}{\partial a_k}\frac{\partial u_k}{\partial a_3} = \frac{\partial u_y}{\partial y}\frac{\partial u_y}{\partial z} + \frac{\partial u_y}{\partial z}\frac{\partial u_z}{\partial z} =$$

$$= \mathcal{S}(y)\cdot\mathcal{A}(y) + \mathcal{A}(y)\cdot\mathcal{S}(y) = \mathcal{A}(y) + \mathcal{A}(y) = \mathcal{A}(y), \tag{B.3b}$$

$$\frac{\partial u_k}{\partial a_k}\frac{\partial u_3}{\partial a_2} = \frac{\partial u_y}{\partial y}\frac{\partial u_z}{\partial y} + \frac{\partial u_z}{\partial z}\frac{\partial u_z}{\partial y} =$$

$$= \mathcal{S}(y)\cdot\mathcal{A}(y) + \mathcal{S}(y)\cdot\mathcal{A}(y) = \mathcal{A}(y) + \mathcal{A}(y) = \mathcal{A}(y), \tag{B.3c}$$

$$\frac{\partial u_3}{\partial a_k}\frac{\partial u_2}{\partial a_k} = \frac{\partial u_z}{\partial y}\frac{\partial u_y}{\partial y} + \frac{\partial u_z}{\partial z}\frac{\partial u_y}{\partial z} =$$

$$= \mathcal{A}(y)\cdot\mathcal{S}(y) + \mathcal{S}(y)\cdot\mathcal{A}(y) = \mathcal{A}(y) + \mathcal{A}(y) = \mathcal{A}(y), \tag{B.3d}$$

$$\frac{\partial u_k}{\partial a_3}\frac{\partial u_k}{\partial a_2} = \frac{\partial u_y}{\partial z}\frac{\partial u_y}{\partial y} + \frac{\partial u_z}{\partial z}\frac{\partial u_z}{\partial y} =$$

$$= \mathcal{A}(y)\cdot\mathcal{S}(y) + \mathcal{S}(y)\cdot\mathcal{A}(y) = \mathcal{A}(y) + \mathcal{A}(y) = \mathcal{A}(y), \tag{B.3e}$$

$$\frac{\partial u_3}{\partial a_k}\frac{\partial u_k}{\partial a_2} = \frac{\partial u_z}{\partial y}\frac{\partial u_y}{\partial y} + \frac{\partial u_z}{\partial z}\frac{\partial u_z}{\partial y} =$$

$$= \mathcal{A}(y)\cdot\mathcal{S}(y) + \mathcal{S}(y)\cdot\mathcal{A}(y) = \mathcal{A}(y) + \mathcal{A}(y) = \mathcal{A}(y). \tag{B.3f}$$

- Entry i=3, j=2

$$\frac{\partial u_2}{\partial a_k}\frac{\partial u_3}{\partial a_k} = \frac{\partial u_y}{\partial y}\frac{\partial u_z}{\partial y} + \frac{\partial u_y}{\partial z}\frac{\partial u_z}{\partial z} =$$

$$= \mathcal{S}(y)\cdot\mathcal{A}(y) + \mathcal{A}(y)\cdot\mathcal{S}(y) = \mathcal{A}(y) + \mathcal{A}(y) = \mathcal{A}(y), \tag{B.4a}$$

$$\frac{\partial u_k}{\partial a_2}\frac{\partial u_k}{\partial a_3} = \frac{\partial u_y}{\partial y}\frac{\partial u_y}{\partial z} + \frac{\partial u_z}{\partial y}\frac{\partial u_z}{\partial z} =$$

$$= \mathcal{S}(y)\cdot\mathcal{A}(y) + \mathcal{A}(y)\cdot\mathcal{S}(y) = \mathcal{A}(y) + \mathcal{A}(y) = \mathcal{A}(y), \tag{B.4b}$$

plus, Eqs.(B.3a) to (B.3c) and Eq.(B.3f) shown above.

B.2 Antisymmetric Primary Wave

For an antisymmetric primary mode, one obtains the following terms in $\bar{\boldsymbol{S}}$:

- Entry i=j=2

$$\frac{\partial u_k}{\partial a_l}\frac{\partial u_k}{\partial a_l} = \frac{\partial u_y}{\partial y}\frac{\partial u_y}{\partial y} + \frac{\partial u_y}{\partial z}\frac{\partial u_y}{\partial z} + \frac{\partial u_z}{\partial y}\frac{\partial u_z}{\partial y} + \frac{\partial u_z}{\partial z}\frac{\partial u_z}{\partial z} =$$
$$= \mathcal{A}^2(y) + \mathcal{S}^2(y) + \mathcal{S}^2(y) + \mathcal{A}^2(y) =$$
$$= \mathcal{S}(y) + \mathcal{S}(y) + \mathcal{S}(y) + \mathcal{S}(y) = \mathcal{S}(y), \tag{B.5a}$$
$$\frac{\partial u_k}{\partial a_k}\frac{\partial u_l}{\partial a_l} = \frac{\partial u_y}{\partial y}\frac{\partial u_y}{\partial y} + \frac{\partial u_y}{\partial z}\frac{\partial u_z}{\partial z} + \frac{\partial u_z}{\partial z}\frac{\partial u_y}{\partial y} + \frac{\partial u_z}{\partial z}\frac{\partial u_z}{\partial z} =$$
$$= \mathcal{A}^2(y) + \mathcal{A}^2(y) + \mathcal{A}^2(y) + \mathcal{A}^2(y) =$$
$$= \mathcal{S}(y) + \mathcal{S}(y) + \mathcal{S}(y) + \mathcal{S}(y) = \mathcal{S}(y), \tag{B.5b}$$
$$\frac{\partial u_k}{\partial a_l}\frac{\partial u_l}{\partial a_k} = \frac{\partial u_y}{\partial y}\frac{\partial u_y}{\partial y} + \frac{\partial u_y}{\partial z}\frac{\partial u_z}{\partial y} + \frac{\partial u_z}{\partial y}\frac{\partial u_y}{\partial z} + \frac{\partial u_z}{\partial z}\frac{\partial u_z}{\partial z} =$$
$$= \mathcal{A}^2(y) + \mathcal{S}^2(y) + \mathcal{S}^2(y) + \mathcal{A}^2(y) =$$
$$= \mathcal{S}(y) + \mathcal{S}(y) + \mathcal{S}(y) + \mathcal{S}(y) = \mathcal{S}(y), \tag{B.5c}$$

$$\frac{\partial u_k}{\partial a_k}\frac{\partial u_2}{\partial a_2} = \frac{\partial u_y}{\partial y}\frac{\partial u_y}{\partial y} + \frac{\partial u_z}{\partial z}\frac{\partial u_y}{\partial y} =$$
$$= \mathcal{A}^2(y) + \mathcal{A}^2(y) = \mathcal{S}(y) + \mathcal{S}(y) = \mathcal{S}(y), \tag{B.5d}$$
$$\frac{\partial u_2}{\partial a_k}\frac{\partial u_k}{\partial a_2} = \frac{\partial u_y}{\partial y}\frac{\partial u_y}{\partial y} + \frac{\partial u_y}{\partial z}\frac{\partial u_z}{\partial y} =$$
$$= \mathcal{A}^2(y) + \mathcal{S}^2(y) = \mathcal{S}(y) + \mathcal{S}(y) = \mathcal{S}(y), \tag{B.5e}$$
$$\frac{\partial u_2}{\partial a_k}\frac{\partial u_2}{\partial a_k} = \frac{\partial u_y}{\partial y}\frac{\partial u_y}{\partial y} + \frac{\partial u_y}{\partial z}\frac{\partial u_y}{\partial z} =$$
$$= \mathcal{A}^2(y) + \mathcal{S}^2(y) = \mathcal{S}(y) + \mathcal{S}(y) = \mathcal{S}(y), \tag{B.5f}$$
$$\frac{\partial u_k}{\partial a_2}\frac{\partial u_k}{\partial a_2} = \frac{\partial u_y}{\partial y}\frac{\partial u_y}{\partial y} + \frac{\partial u_z}{\partial y}\frac{\partial u_z}{\partial y} =$$
$$= \mathcal{A}^2(y) + \mathcal{S}^2(y) = \mathcal{S}(y) + \mathcal{S}(y) = \mathcal{S}(y). \tag{B.5g}$$

- Entry i=j=3

$$\frac{\partial u_k}{\partial a_k}\frac{\partial u_3}{\partial a_3} = \frac{\partial u_y}{\partial y}\frac{\partial u_z}{\partial z} + \frac{\partial u_z}{\partial z}\frac{\partial u_z}{\partial z} =$$

$$= \mathcal{A}^2(y) + \mathcal{A}^2(y) = \mathcal{S}(y) + \mathcal{S}(y) = \mathcal{S}(y), \tag{B.6a}$$

$$\frac{\partial u_3}{\partial a_k}\frac{\partial u_k}{\partial a_3} = \frac{\partial u_z}{\partial y}\frac{\partial u_y}{\partial z} + \frac{\partial u_z}{\partial z}\frac{\partial u_z}{\partial z} =$$

$$= \mathcal{S}^2(y) + \mathcal{A}^2(y) = \mathcal{S}(y) + \mathcal{S}(y) = \mathcal{S}(y), \tag{B.6b}$$

$$\frac{\partial u_3}{\partial a_k}\frac{\partial u_3}{\partial a_k} = \frac{\partial u_z}{\partial y}\frac{\partial u_z}{\partial y} + \frac{\partial u_z}{\partial z}\frac{\partial u_z}{\partial z} =$$

$$= \mathcal{S}^2(y) + \mathcal{A}^2(y) = \mathcal{S}(y) + \mathcal{S}(y) = \mathcal{S}(y), \tag{B.6c}$$

$$\frac{\partial u_k}{\partial a_3}\frac{\partial u_k}{\partial a_3} = \frac{\partial u_y}{\partial z}\frac{\partial u_y}{\partial z} + \frac{\partial u_z}{\partial z}\frac{\partial u_z}{\partial z} =$$

$$= \mathcal{S}^2(y) + \mathcal{A}^2(y) = \mathcal{S}(y) + \mathcal{S}(y) = \mathcal{S}(y), \tag{B.6d}$$

plus Eqs.(B.5a) to (B.5c) shown above.

- Entry i=2, j=3

$$\frac{\partial u_k}{\partial a_k}\frac{\partial u_2}{\partial a_3} = \frac{\partial u_y}{\partial y}\frac{\partial u_y}{\partial z} + \frac{\partial u_z}{\partial z}\frac{\partial u_y}{\partial z} =$$

$$= \mathcal{A}(y)\cdot\mathcal{S}(y) + \mathcal{A}(y)\cdot\mathcal{S}(y) = \mathcal{A}(y) + \mathcal{A}(y) = \mathcal{A}(y), \tag{B.7a}$$

$$\frac{\partial u_2}{\partial a_k}\frac{\partial u_k}{\partial a_3} = \frac{\partial u_y}{\partial y}\frac{\partial u_y}{\partial z} + \frac{\partial u_y}{\partial z}\frac{\partial u_z}{\partial z} =$$

$$= \mathcal{A}(y)\cdot\mathcal{S}(y) + \mathcal{S}(y)\cdot\mathcal{A}(y) = \mathcal{A}(y) + \mathcal{A}(y) = \mathcal{A}(y), \tag{B.7b}$$

$$\frac{\partial u_k}{\partial a_k}\frac{\partial u_3}{\partial a_2} = \frac{\partial u_y}{\partial y}\frac{\partial u_z}{\partial y} + \frac{\partial u_z}{\partial z}\frac{\partial u_z}{\partial y} =$$

$$= \mathcal{A}(y)\cdot\mathcal{S}(y) + \mathcal{A}(y)\cdot\mathcal{S}(y) = \mathcal{A}(y) + \mathcal{A}(y) = \mathcal{A}(y), \tag{B.7c}$$

$$\frac{\partial u_3}{\partial a_k}\frac{\partial u_2}{\partial a_k} = \frac{\partial u_z}{\partial y}\frac{\partial u_y}{\partial y} + \frac{\partial u_z}{\partial z}\frac{\partial u_y}{\partial z} =$$

$$= \mathcal{S}(y)\cdot\mathcal{A}(y) + \mathcal{A}(y)\cdot\mathcal{S}(y) = \mathcal{A}(y) + \mathcal{A}(y) = \mathcal{A}(y), \tag{B.7d}$$

$$\frac{\partial u_k}{\partial a_3}\frac{\partial u_k}{\partial a_2} = \frac{\partial u_y}{\partial z}\frac{\partial u_y}{\partial y} + \frac{\partial u_z}{\partial z}\frac{\partial u_z}{\partial y} =$$

$$= \mathcal{S}(y)\cdot\mathcal{A}(y) + \mathcal{A}(y)\cdot\mathcal{S}(y) = \mathcal{A}(y) + \mathcal{A}(y) = \mathcal{A}(y), \tag{B.7e}$$

$$\frac{\partial u_3}{\partial a_k}\frac{\partial u_k}{\partial a_2} = \frac{\partial u_z}{\partial y}\frac{\partial u_y}{\partial y} + \frac{\partial u_z}{\partial z}\frac{\partial u_z}{\partial y} =$$

$$= \mathcal{S}(y)\cdot\mathcal{A}(y) + \mathcal{A}(y)\cdot\mathcal{S}(y) = \mathcal{A}(y) + \mathcal{A}(y) = \mathcal{A}(y). \tag{B.7f}$$

- Entry i=3, j=2

$$\frac{\partial u_2}{\partial a_k}\frac{\partial u_3}{\partial a_k} = \frac{\partial u_y}{\partial y}\frac{\partial u_z}{\partial y} + \frac{\partial u_y}{\partial z}\frac{\partial u_z}{\partial z} =$$

$$= \mathcal{A}(y)\cdot\mathcal{S}(y) + \mathcal{S}(y)\cdot\mathcal{A}(y) = \mathcal{A}(y) + \mathcal{A}(y) = \mathcal{A}(y), \tag{B.8a}$$

$$\frac{\partial u_k}{\partial a_2}\frac{\partial u_k}{\partial a_3} = \frac{\partial u_y}{\partial y}\frac{\partial u_y}{\partial z} + \frac{\partial u_z}{\partial y}\frac{\partial u_z}{\partial z} =$$

$$= \mathcal{A}(y)\cdot\mathcal{S}(y) + \mathcal{S}(y)\cdot\mathcal{A}(y) = \mathcal{A}(y) + \mathcal{A}(y) = \mathcal{A}(y), \tag{B.8b}$$

plus, Eqs.(B.7a) to (B.7c) and Eq.(B.7f) shown above.

REFERENCES

[1] Achenbach, J. D., *Wave Propagation in Elastic Solids*. Elsevier Science Publishers B.V., Amsterdam, 1975.

[2] Auld, B. A., *Acoustic Fields and Waves in Solids*, vol. II. Robert E. Krieger Publishing Company, Malabar, 2 ed., 1990.

[3] Bermes, C., Kim, J.-Y., Qu, J., and Jacobs, L. J., "Experimental characterization of material nonlinearity using lamb waves," *Applied Physics Letters*, vol. 90, no. 2, p. 021901, 2007.

[4] Bray, D. E. and Stanley, R. K., *Nondestructive Evaluation - A Tool in Design, Manufacturing, and Service*. CRC Press, Boca Raton, 1997.

[5] De Lima, W. J., *Harmonic Generation in Isotropic Elastic Waveguides*. PhD thesis, University of Texas at Austin, 2000.

[6] De Lima, W. J. and Hamilton, M. F., "Finite-amplitude waves in isotropic elastic plates," *Journal of Sound and Vibration*, vol. 265, pp. 819–839, 2003.

[7] Deng, M., "Cumulative second-harmonic generation of lamb-mode propagation in a solid plate," *Journal of Applied Physics*, vol. 85, no. 6, pp. 3051–3058, 1999.

[8] Deng, M., "Analysis of second-harmonic generation of lamb modes using a modal analysis approach," *Journal of Applied Physics*, vol. 94, no. 6, pp. 4152–4159, 2003.

[9] Deng, M., Wang, P., and Lv, X., "Experimental observation of cumulative second-harmonic generation of lamb-wave propagation in an elastic plate," *Journal of Physics D: Applied Physics*, vol. 38, pp. 344–353, 2005.

[10] Graff, K. F., *Wave Motion in Elastic Solids*. Oxford University Press, London, 1975.

[11] Herrmann, J., Kim, J.-Y., Jacobs, L. J., Qu, J., Littles, J. W., and Savage, M. F., "Assessment of material damage in a nickel-base superalloy using nonlinear rayleigh surface waves," *Journal of Applied Physics*, vol. 99, no. 12, p. 124913, 2006.

[12] Kim, J.-Y., Jacobs, L. J., Qu, J., and Littles, J. W., "Experimental characterization of fatigue damage in a nickel-base superalloy using nonlinear ultrasonic waves," *Journal of the Acoustical Society of America*, vol. 120, no. 3, pp. 1266–1273, 2006.

[13] Landau, L. D. and Lifshitz, E. M., *Theory of Elasticity*. Pergamon Press, New York, 1986.

[14] Lee, T.-H., Choi, I.-H., and Jhang, K.-Y., "The nonlinearity of guided wave in an elastic plate," *Modern Physics Letters B*, vol. 22, no. 11, pp. 1135–1140, 2008.

[15] Malvern, L. E., *Introduction to the Mechanics of a Continuous Medium*. Prentice-Hall Inc., Upper Saddle River, 1969.

[16] Norris, A. N., "Finite-amplitude waves in solids," in *Nonlinear Acoustics*, Academic Press, San Diego.

[17] Pavlakovic, B. and Lowe, M., "Disperse," 1996-1999. Software Version 2.0.6.

[18] Pilarski, A., Ditri, J. J., and Rose, J. L., "Remarks on symmetric lamb waves with dominant longitudinal displacements," *Journal of the Acoustical Society of America*, vol. 93, no. 4, pp. 2228–2230, 1993.

[19] Pruell, C., Kim, J.-Y., Qu, J., and Jacobs, L. J., "Evaluation of plasticity driven material damage using lamb waves," *Applied Physics Letters*, vol. 91, no. 23, p. 231911, 2007.

[20] Pruell, C., Kim, J.-Y., Qu, J., and Jacobs, L. J., "Evaluation of fatigue damage using nonlinear guided waves," in *Review of Progress in Quantitative Nondestructive Evaluation* (Thompson, D. O. and Chimenti, D. E., eds.), pp. 201–208, AIP Conference Proceedings vol. 1096, American Institute of Physics, Melville, NY, March 2009.

[21] Renton, J. D., *Applied Elasticity: Matrix and Tensor Analysis of Elastic Continua*. Ellis Horwood Limited, Chichester, 1987.

[22] Rose, J. L., *Ultrasonic Waves in Solid Media*. Cambridge University Press, Cambridge, 1999.

[23] Shui, G., Kim, J.-Y., Qu, J., Wang, Y.-S., and Jacobs, L. J., "A new technique for measuring the acoustic nonlinearity of materials using rayleigh waves," *NDT & E International*, vol. 41, pp. 326–329, 2008.

[24] Shui, Y. and Solodov, I. Y., "Nonlinear properties of rayleigh and stoneley waves in solids," *Journal of Applied Physics*, vol. 64, no. 11, pp. 6155–6165, 1988.

[25] Srivastava, A. and di Scalea, F. L., "On the existence of antisymmetric or symmetric lamb waves at nonlinear higher harmonics," *Journal of Sound and Vibration*, 2009.